E.O. Paton Electric Welding Institute of the National Academy of Sciences of Ukraine

International Scientific-Technical and Production Journal

The Paton WELDING JOURNAL

September 2016
No. 9

Published since 2000

English translation of the monthly «Avtomaticheskaya Svarka» (Automatic Welding) journal published in Russian since 1948

Address
E.O. Paton Electric Welding Institute,
International Association «Welding»
11 Kazimir Malevich Str. (former Bozhenko Str.),
03680, Kiev, Ukraine
Tel.: (38044) 200 60 16, 200 82 77
Fax: (38044) 200 82 77, 200 81 45
E-mail: journal@paton.kiev.ua
www.patonpublishinghouse.com

State Registration Certificate
KV 4790 of 09.01.2001
ISSN 0957-798X

Subscriptions
$348, 12 issues per year,
air postage and packaging included.
Back issues available.

CONTENTS

doi.org/10.15407/tpwj2016.09.01

BRITTLE FRACTURE RESISTANCE OF HAZ METAL IN ARC-WELDED JOINTS OF HIGH-STRENGTH STEELS WITH CARBON CONTENT OF 0.55–0.65 %

A.A. GAJVORONSKY, V.D. POZNYAKOV, L.I. MARKASHOVA, E.N. BERDNIKOVA and **V.Ya. YASHCHUK**
E.O. Paton Electric Welding Institute, NASU
11 Kazimir Malevich Str., 03680, Kiev, Ukraine. E-mail: office@paton.kiev.ua

Modeling methods were used to study the influence of structural-phase composition and diffusible hydrogen on brittle fracture resistance of HAZ metal of high-strength steel with carbon content of 0.55–0.65 %. It is shown that to achieve comparatively high resistance of the joints to crack propagation, it is necessary to ensure formation in the HAZ metal of bainitic-martensitic structure, in which upper bainite is absent, and martensite volume fraction does not exceed lower bainite fraction. At saturation of HAZ metal with hydrogen, which diffuses from deposited metal during arc welding or surfacing, its brittle fracture susceptibility increases markedly. To reduce metal embrittlement, it is necessary to apply special welding techniques, at which hydrogen saturation is minimum (less than 0.2 ml/100 g), or special technological methods, allowing improvement of ductile properties of HAZ metal. 14 Ref., 1 Table, 10 Figures.

Keywords: *high-strength carbon steel, arc welding, HAZ, structure, diffusible hydrogen, brittle fracture, fracture surface*

One of the main factors, determining the level of brittle fracture resistance of welded joints of high-strength steels, is structural state of steel and HAZ metal, formed during the thermodeformational welding cycle (TDWC). This condition greatly depends on carbon content in steel and cooling rate of welded joint HAZ metal [1, 2]. It is also known that diffusible hydrogen has a significant impact on metal embrittlement. Accumulating in structural discontinuities, it promotes increase of local stresses and, as a consequence, brittle fracture resistance of the metal decreases. Hydrogen influence becomes stronger with increase of carbon content that leads to a more abrupt lowering of plastic properties of metal, resulting in more intensive crack initiation and propagation [3–5].

In arc welding and surfacing of high-strength steels, carbon content in which is higher than 0.50 %, a hardened bainitic-martensitic structure with higher dislocation density forms in HAZ overheated zone. Ultimate rupture strength of such metal is more than 1060 MPa, and relative elongation is not higher than 9.3 % [6, 7]. It can be assumed that in welding high-strength carbon steels even slight local concentrations of hydrogen will lead to significant changes in brittle fracture resistance of HAZ metal.

Objective of this work was determination of the influence of structural-phase composition and diffusible hydrogen on brittle fracture resistance of HAZ metal of welded joints in high-strength carbon steels.

Used as material for investigations were high-strength carbon steels of the following compositions, wt.%: wheel steel of grade 2 (DSTU GOST 10791) — 0.58 C; 0.44 Si; 0.77 Mn; 0.10 Ni; 0.05 Cr; 0.012 S; 0.11 P; and structural carbon steel 65G (GOST 1050) — 0.65 C; 0.19 Si; 0.91 Mn; 0.18 Ni; 0.16 Cr; 0.017 S; 0.010 P.

Methods of investigation. Assessment of brittle fracture resistance of the metal was performed in keeping with standard method of three-point bending [8–10]. Samples of studied steels of 100×20×10 mm size with 7 mm deep notch in the center were used. Before testing, 3 mm long fatigue crack was grown in the notch tip by loading by cyclic bending (cycle stress of 120 MPa, frequency of 35 Hz). Sample loading rate at static bending was equal to 1 mm/min. Critical stress intensity factor K_{1C} was taken as the criterion of assessment of brittle fracture resistance of the metal.

HAZ metal resistance to brittle fracture was assessed using a sample of similar dimensions, treated by TDWC, followed by growing a fatigue crack in it. For TDWC simulation, rigidly-restrained samples were heated by passing current up to 1250 ºC (heating rate of 150 ºC/s), and then cooled by specified cycle. Sample cooling rate in the temperature range of 600–500 ºC was selected from the conditions of formation of characteristic structures in welded joint HAZ metal. For wheel steel of grade 2 cooling rate was $w_{6/5}$ = 6 ºC/s, when a structure of bainite forms in HAZ

metal overheated zone, 13.5 ºC/s for bainitic-martensitic structure and 20 ºC/s for martensitic-bainitic structure. Investigations on steel 65G were performed at $w_{6/5}$ = 6 and 13.5 ºC/s, when bainitic-martensitic and martensitic structures form, respectively.

Saturation of samples with a fatigue crack by diffusible hydrogen $[H]_{dif}$ was performed electrolytically (current density of 10 A/cm^2) just before their static loading. Electrolytic solution of sulphuric acid H_2SO_4 in distilled water with addition of sodium thiosulphate $Na_2S_2O_2$ in the proportion of 0.05 g per 1 l was used for this purpose. $[H]_{dif}$ quantity was varied in the range of 0.2–1.5 ml per 100 g of metal by changing the time of samples soaking in electrolytic solution. This was performed in keeping with the data of [11], which showed that diffusible hydrogen content in the HAZ can reach 1.5 ml/100 g at its initial amount in the deposited metal of up to 10 ml/100 g.

HAZ metal structure was studied by the methods of optical metallography. Sample fractures after testing were studied by the methods of scanning electron microscopy in Philips scanning electron microscope SEM-515, fitted with energy-dispersive spectrometer of LINK system.

Investigation results and their discussion. At the initial stage of investigations, facture mechanics approaches and criteria were used to determine the influence of steel structural state on critical stress intensity factor. Figure 1 gives generalized results of testing performed at the temperature of 20 ºC. As is seen from the given data, brittle fracture resistance of steel in the initial state significantly depends on its structure and carbon content. For steel 65G critical SIF is approximately 1.4 times higher than for wheel steel of grade 2 (72 and 52 MPa√m, respectively). This difference is, most probably, associated with the features of metal phase composition and structure parameters. Metallographic studies showed that structure of grade 2 wheel steel is presented by pearlite-ferrite mixture (Figure 2, *a*) with grain size between 16 and 32 μm. Microhardness of structural components is in the range of *HV*0.1-1990–2450 MPa, and total integral hardness of metal is equal to *HV*10-2300 MPa. Ferrite fringes 5–10 μm wide are located along grain boundaries. Structure of as-delivered steel 65G is represented predominantly by bainite (Figure 2, *b*), grain size is 16–24 μm, microhardness of structural components is 2570–2730 MPa, and integral hardness of metal is 2760 MPa.

One can see that high-carbon steel with bainitic structure has higher resistance to brittle fracture at three-point bending than steel with pearlitic-ferritic structure. It should be also noted that similar results were obtained by authors of [12] at testing high-carbon steel under cyclic loading.

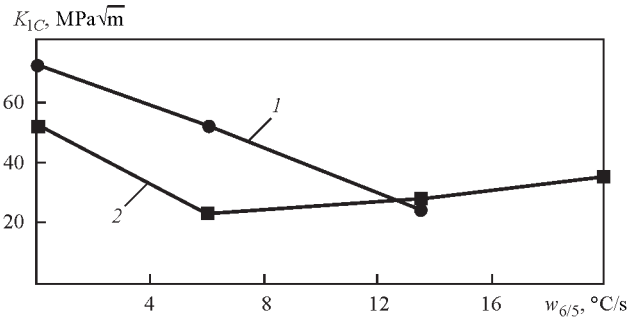

Figure 1. Brittle fracture resistance of HAZ metal of steel 65G (*1*) and wheel steel of grade 2 (*2*)

Further studies showed that structural changes in the metal, induced by the TDWC, also have a significant impact on its brittle fracture resistance. Carbon content in steel plays a determinant role here. Figure 3 gives the diagrams of supercooled austenite transformation in HAZ metal of studied steels, and Figure 4 shows the characteristic microstructure of metal [13, 14]. Let us analyze these data in comparison with changes of K_{1C} value.

Under the conditions of welding, when $w_{6/5}$ = 6 ºC/s, HAZ metal of grade 2 steel forms a structure of upper bainite (Figure 3, *a*) with coarse grain (63–94 μm) and microhardness of 2640–3090 MPa (Figure 4, *a*). Integral hardness of metal with such a structure is equal to 3140 MPa. It is known that upper bainite, formed by diffusion mechanism, has lower ductility, unlike other metal structures [1]. Therefore, brittle fracture resistance of such metal drops markedly. This is confirmed by the results of testing samples with a crack for three-point bending. Testing showed

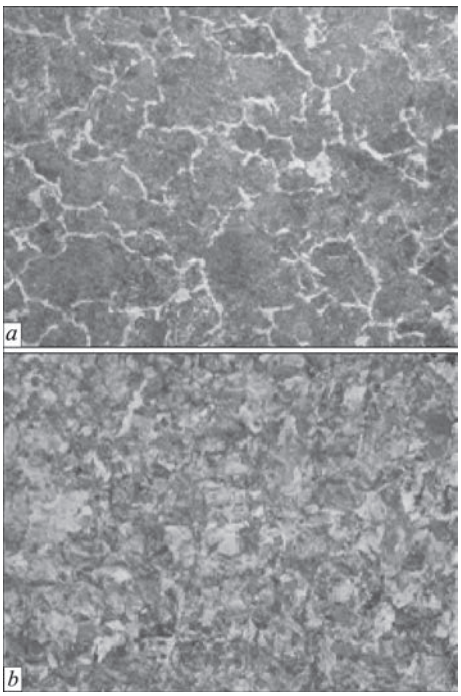

Figure 2. Microstructure of as-delivered grade 2 wheel steel (*a* — ×500) and 65G steel (*b* — ×200)

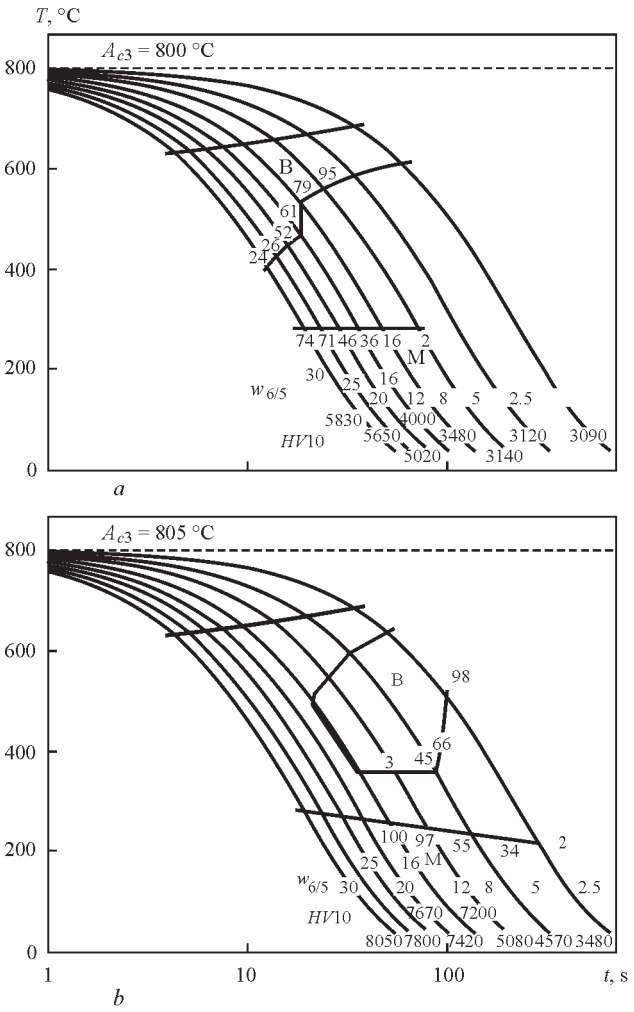

Figure 3. Supercooled austenite transformation diagram in HAZ metal of grade 2 wheel steel (*a*) and 65G steel (*b*) in arc welding (T_{max} = 1250 ºC, t_h = 6 s) [13, 14]

that compared to as-delivered steel K_{1C} value for HAZ metal decreases 2.3 times (from 52 to 23 MPa√m — see Figure 1, curve *2*).

At $w_{6/5}$ = 13.5 ºC/s, HAZ metal of grade 2 wheel steel forms a bainitic-martensitic structure with microhardness of 3340–4320 MPa, in which lower bainite prevails (80 %) (Figure 4, *b*). Such changes in the structure, compared to metal with upper bainite structure, promoted its brittle fracture resistance rising by 22 % (up to 28 MPa√m).

At 20 ºC/s a structure with approximately equal quantity of martensite and lower bainite (46 and 54 %, respectively) forms in overheated zone of HAZ metal. Microhardness of metal structural components rises up to 3780–4560 MPa (integral hardness of 3920 MPa), and grain size decreases to 32.0–47.5 μm (Figure 4, *c*). With such a structure, K_{1C} value is the largest, and is equal to 35 MPa√m. But even under such conditions brittle fracture resistance of HAZ metal is approximately 1.5 times lower, compared to initial condition of wheel steel.

Unlike grade 2 wheel steel, in 65G steel (0.65 % C) bainitic-martensitic structure forms at $w_{6/5}$ = 6 ºC/s, which contains 70 % lower bainite and 30 % martensite (Figure 3, *b*). Microhardness of lower bainite is 3220–3800 MPa, and that of martensite is 5600–6130 MPa, grain size varies from 63 to 94 μm (Figure 5, *a*). As shown by mechanical testing, K_{1C} value of HAZ metal with bainitic-martensitic structure decreases by 28 % (from 72 to 52 MPa√m — see Figure 1, curve *1*) relative to steel initial state.

At increase of cooling rate to 13.5 ºC/s, the metal mainly forms a martensitic structure (98 %) with more than 6130 MPa microhardness (Figures 5, *b*). At this cooling rate, lower bainite (2 %) is locally distributed along the grain boundaries. Grain size here did not significantly change. At formation of predominantly martensitic structure ($w_{6/5}$ = 13.5 ºC/s) K_{1C} value drops markedly to 23 MPa√m. Compared to initial state of steel, brittle fracture resistance of HAZ metal at this cooling rate is lower by approximately 3.1 times.

Comparing the given test results, we can state that in order to improve brittle fracture resistance of HAZ metal in high-strength steel at carbon content of

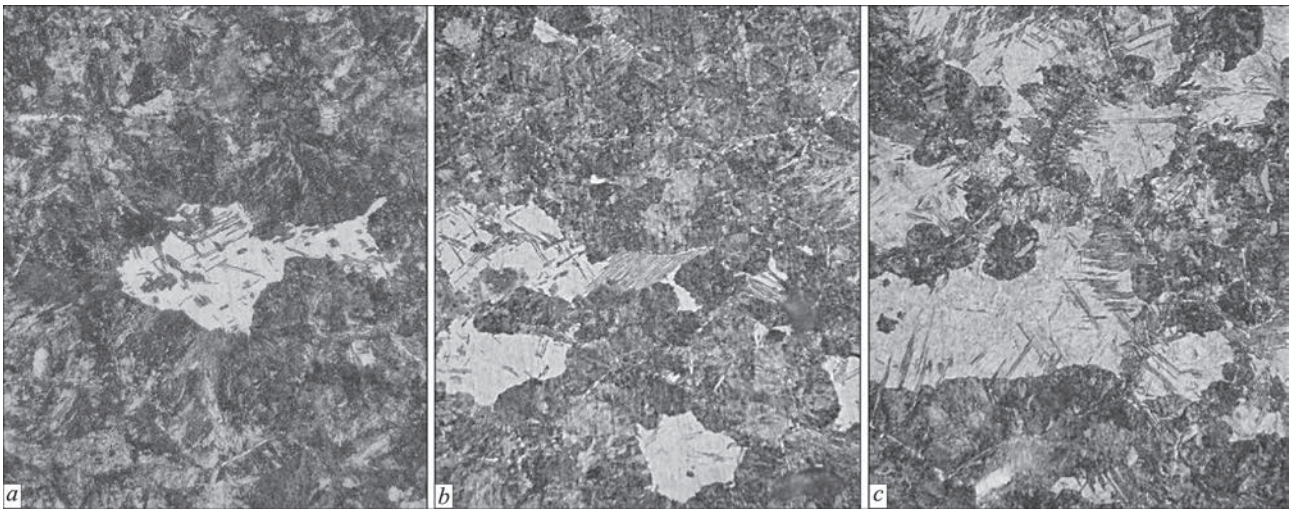

Figure 4. Microstructure of metal (×500) in HAZ overheated zone of grade 2 wheel steel: *a* — $w_{6/5}$ = 6; *b* — 13.5; *c* — 20 ºC/s

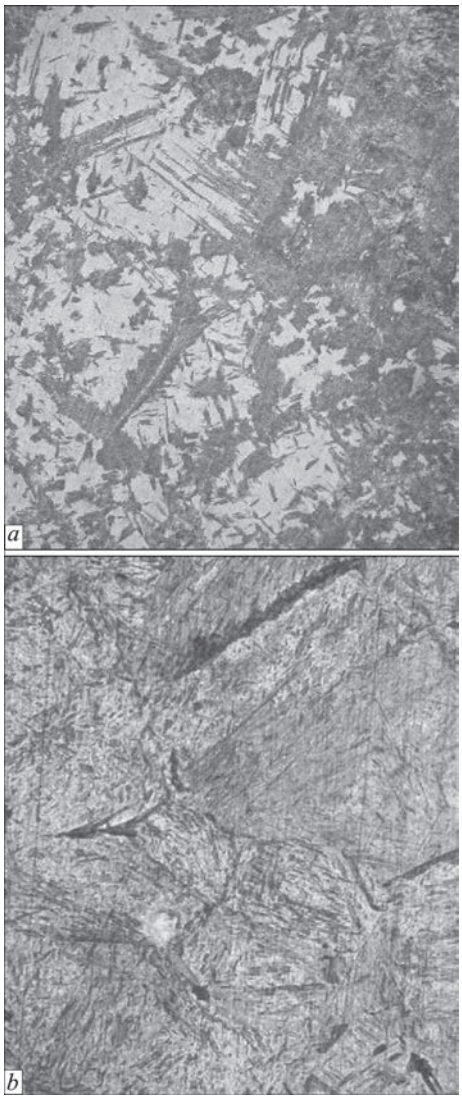

Figure 5. Microstructure (×500) of metal in HAZ overheated zone of 65G steel: *a* — $w_{6/5}$ = 6; *b* — 13.5 ºC/s

0.55–0.65 %, it is necessary to provide the conditions, at which a structure, consisting of lower bainite and martensite, will form in it. Volume fraction of martensite should not be higher than 50 %. At formation of prevailing structure of upper bainite or martensite in the HAZ, brittle fracture susceptibility of metal rises markedly.

Diffusible hydrogen has a significant impact on brittle fracture resistance of high-carbon steel. At hydrogen saturation of samples of as-delivered steels, K_{1C} value decreases (Figure 6). Degree of K_{1C} value lowering depends on carbon content in steel. For grade 2 wheel steel with carbon content of 0.58 %, presence of hydrogen in the metal on the level of 0.2 ml/100 g leads to K_{1C} lowering by 23 % (from 52 to 40 MPa√m — see curve *2*). At increase of hydrogen concentration up to 1.5 ml/100 g, SIF drops to 30 MPa√m. Thus, wheel steel resistance to crack propagation decreases approximately 1.7 times in the presence of diffusible hydrogen in the metal.

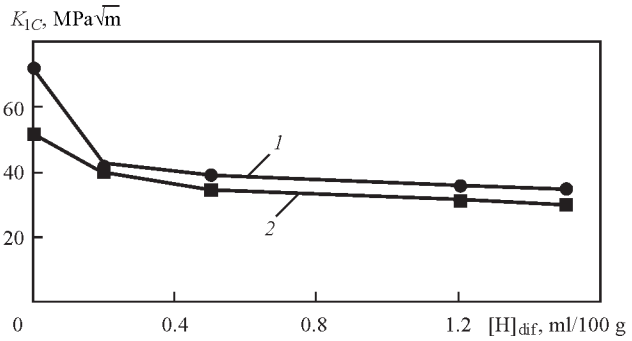

Figure 6. Hydrogen influence on brittle fracture resistance of 65G steel (*1*) and grade 2 wheel steel (*2*)

A more abrupt embrittlement in the presence of hydrogen proceeds in steel, in which hydrogen content is equal to 0.65 %. At minimum saturation of steel 65G with hydrogen, K_{1C} value decreases by 42 % (from 72 to 42 MPa√m — see curve *1* in Figure 6), and at its maximum content — by 2.1 times (up to 35 MPa√m).

In the presence of diffusible hydrogen in HAZ metal of studied steels its brittle fracture resistance also decreases (Figure 7). Level of this decrease depends on carbon content, which determines the degree of metal hardening under TDWC impact. More marked changes of properties are characteristic for HAZ metal of 65G steel. Hydrogen presence in it on the level of 0.2 ml/100 g leads to lowering of K_{1C} value by 2.4–3.2 times (Figure 7, *a*). For HAZ metal of wheel steel it is 1.1–1.2 times (Figure 7, *b*). At subsequent increase of $[H]_{dif}$ in the metal up to 1.5 ml/100g, K_{1C} value for HAZ metal of 65G steel gradually decreases up to 2 times, and by 40 % — for wheel steel of grade

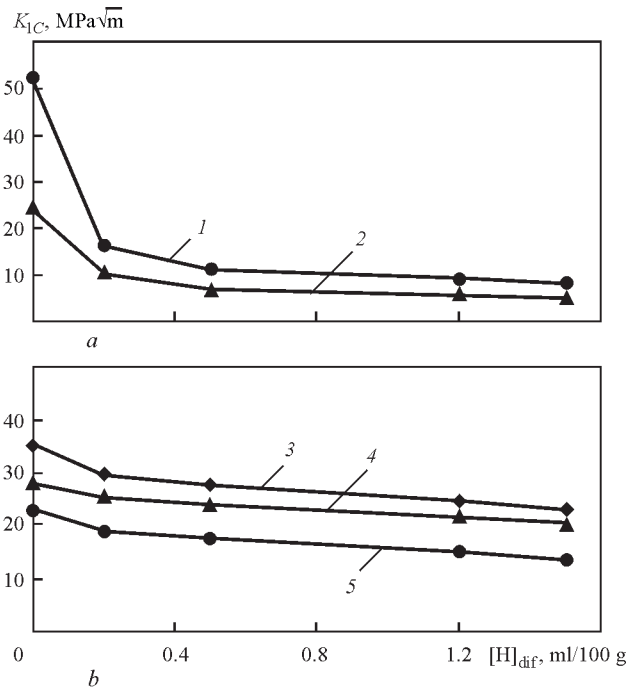

Figure 7. Influence of cooling rate and diffusible hydrogen on brittle fracture resistance of HAZ metal of 65G steel (*a*) and grade 2 wheel steel (*b*): *1*, *5* — $w_{6/5}$ = 6; *2*, *4* — 13.5; *3* — 20 ºC/s

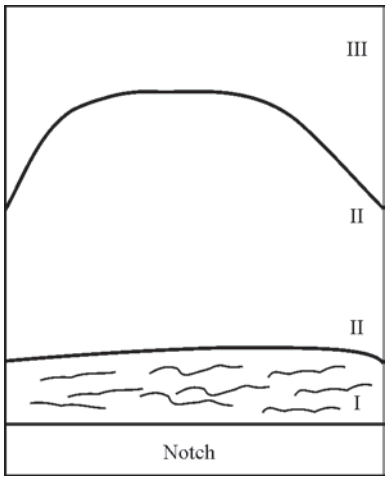

Figure 8. Zones of sample fracture after testing: I — fatigue crack; II — main crack; III — final fracture zone

2. Thus, hydrogen presence in the structure leads to overall lowering of brittle fracture resistance of HAZ metal by 6.5 times for 65G steel (52 and 8 MPa√m at $w_{6/5}$ = 6 ºC/s — see Figure 7, *a*, curve *1*), and by 1.5 times for wheel steel of grade 2 (35 and 23 MPa√m at 20 ºC/s — Figure 7, *b*, curve *3*).

As shown by factographic studies, not only K_{1C} values, but also the mode of sample failure change under the TDWC impact and in the presence of diffusible hydrogen. Characteristic fracture zones (Figure 8) are observed on sample fracture surface: I — zone of initiation and propagation of a fatigue crack, formed as a result of loading by cyclic bending; II — zone of main crack propagation; and final fracture zone III at three-point bending. Characteristic fractures of HAZ metal samples, not saturated by hydrogen, are given in Figure 9.

Fatigue crack initiation in HAZ metal of high-carbon steel, irrespective of its structural state, proceeds in the brittle mode along grain boundaries (Figure 9, *a*). Fatigue crack propagates also in the brittle mode, but predominantly across the grain body (Figure 9, *b*). The features of fatigue crack propagation, depending on steel composition and structural state of the metal, are as follows. In HAZ metal of wheel steel with upper bainitic structure ($w_{6/5}$ = 6 ºC/s) the size of brittle fracture facets is equal to 300–100 μm, and in metal with bainitic-martensitic structure (13.5 ºC/s) it is 30–70 μm. This fracture zone is characterized by presence of secondary cracks along grain boundaries. In grade 2 wheel steel with upper bainite structure these cracks have the size of 50–100 μm, and at formation of the structure of lower bainite and martensite in the HAZ their extent decreases to 60 μm. Similar dimensions of the facets were observed also in fractures of 65G steel. However, the length of secondary cracks in it increases to 200 μm.

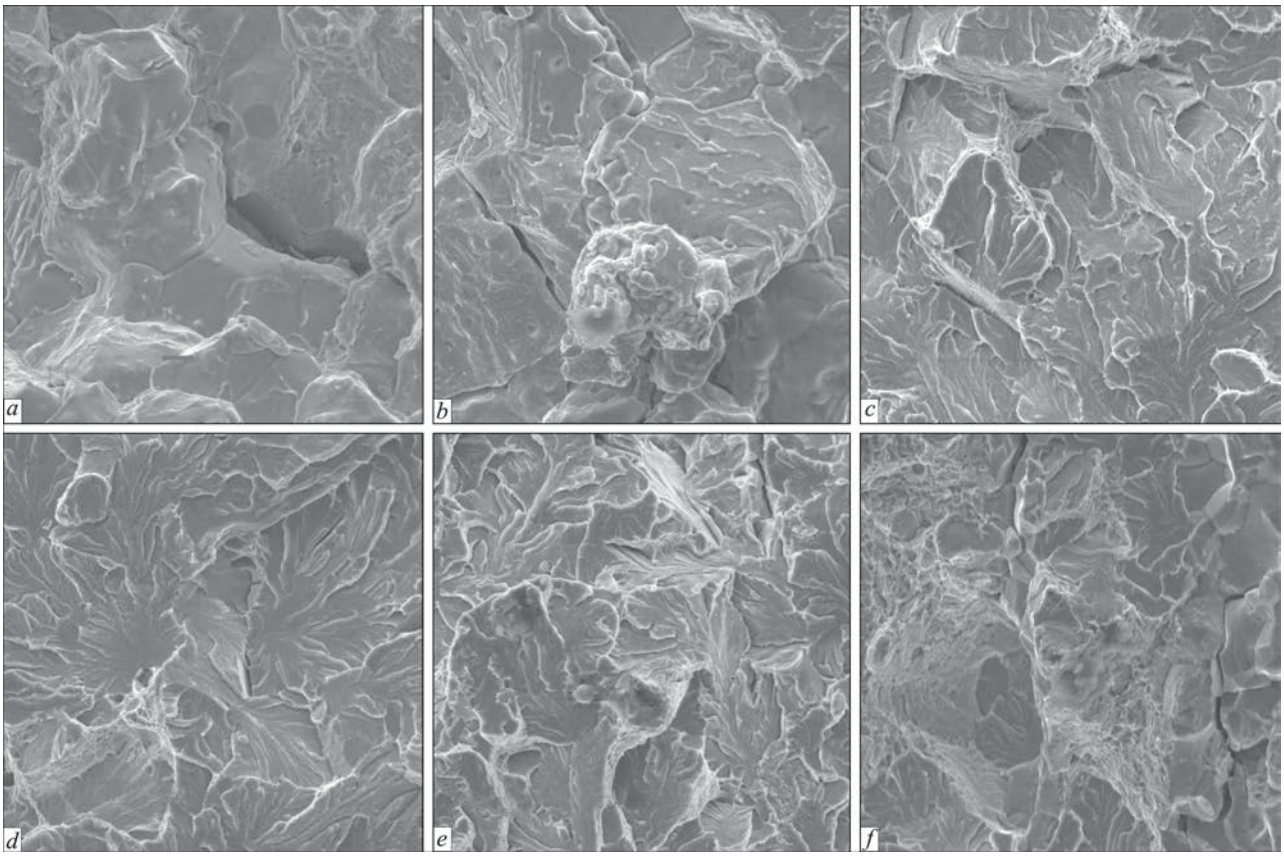

Figure 9. Characteristic fracture (×1010) of HAZ metal of grade 2 wheel steel (*a–d*) and 65G steel (*e*, *f*) without hydrogen: *a*, *b* — zone I (*a* — $w_{6/5}$ = 6; *b* — 13.5); *c*, *d* — zone II (*c* — 6; *d* — 13.5); *e*, *f* — zone II (*e* — 6; *f* — 13.5 ºC/s)

HAZ metal brittle fracture mode in main crack propagation zone

$[H]_{dif}$, ml/100 g	Grade 2 wheel steel				65G steel			
	6 °C/s		13.5 °C/s		6 °C/s		13.5 °C/s	
	Intragranular fracture, %/L_s, μm	Intergranular fracture, %/L_s, μm	Intragranular fracture, %/L_s, μm	Intergranular fracture, %/L_s, μm	Intragranular fracture, %/L_s, μm	Intergranular fracture, %/L_s, μm	Intragranular fracture, %/L_s, μm	Intergranular fracture, %/L_s, μm
0	100/40	–	100/5	–	95/30	5/30	80/60	20/60
0.2	80/100	20/100	70/40	30/40	50/150	50/150	30/220	70/220
0.5	70/120	30/120	65/60	35/60	40/170	60/170	20/250	80/250

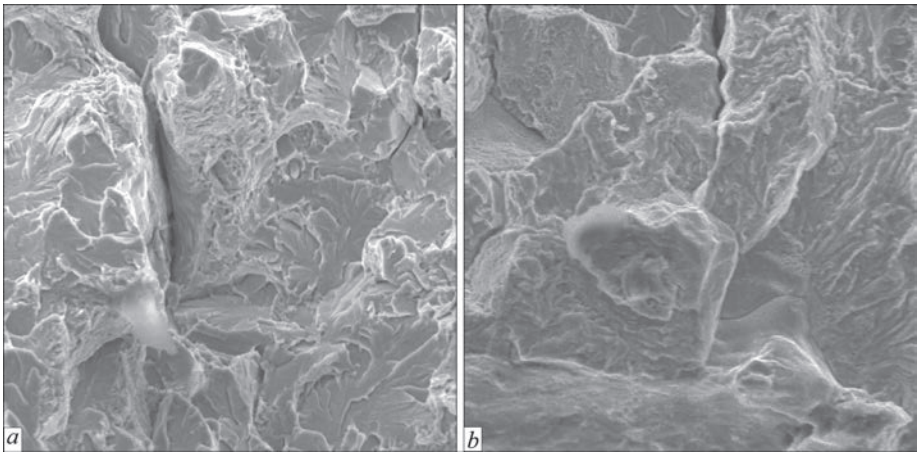

Figure 10. Fracture (×1010) at propagation of main crack (zone II) in HAZ metal of 65G steel ($w_{6/5}$ = 13.5 ºC/s) in the presence of hydrogen: *a* — $[H]_{dif}$ = 0.2; *b* — 0.5 ml/100 g

In the zone of main crack development in HAZ metal of wheel steel, the fracture is brittle intragranular one, corresponding to the structure given in Figure 9, *c*, *d*. At $w_{6/5}$ = 6 ºC/s, secondary cracks of length up to L_s = 40 μm are observed, and at 13.5 ºC/s their length does not exceed 5 μm. In HAZ metal of 65G steel the crack propagates also in the brittle mode, but fracture runs both along the boundaries (brittle intergranular), and through the grain bulk (brittle intragranular). The extent of secondary cracks in it is increased up to 60 μm (Figure 9, *e*, *f*). In final fracture zone fracture runs in the ductile mode for all the samples.

In the presence of hydrogen, brittle intergranular fraction in the fracture increases in HAZ metal at crack propagation. Generalized results of studying the fractures are given in the Table, and Figure 10 shows the characteristic fractures of hydrogenated samples.

Analysis of the given data shows that at diffusible hydrogen saturation of HAZ metal of high-strength carbon steels, the fraction of brittle intergranular fracture is significantly increased. Particularly abrupt changes of fracture structure are characteristic for 65G steel. At $w_{6/5}$ = 6 ºC/s, when HAZ metal forms a bainitic-martensitic structure (70/30), hydrogen presence on the level of 0.2 ml/100 g leads to increase of the fraction of brittle intergranular fracture up to 50 %. Here, K_{1C} value decreases 3.2 times. Increase of the fraction of brittle intergranular fracture in the presence of hydrogen is characteristic also for HAZ metal of grade 2 wheel steel. However, as a result of formation of more ductile structures, brittle fracture resistance decreases by just 20 %. With increase of hydrogen content, the extent of secondary cracks in the fracture of samples of HAZ metal of grade 2 wheel steel increases 3 times, and in 65G steel — more than 3.5–6 times.

Conducted studies showed that in welding and surfacing of high-strength carbon steels, two main conditions should be satisfied, in order to ensure comparatively high brittle fracture resistance of HAZ metal. First, bainitic-martensitic structure with more than 50 % volume fraction of martensite should form in the HAZ metal. And secondly, diffusible hydrogen concentration in the deposited metal should be not more than 1.5 ml/100 g (hydrogen saturation of HAZ metal on the level of 0.2 ml/100 g, respectively). With increase of carbon content, diffusible hydrogen impact on HAZ metal embrittlement becomes stronger.

Conclusions

1. Brittle fracture resistance of high-strength steels with carbon content of 0.55–0.65 % essentially depends on steel structural state and carbon content. Cracking resistance of steel with bainitic structure is 1.4 times higher than that of steel with pearlitic-ferritic structure.

2. At saturation of wheel steel of grade 2 (0.58 % C) by hydrogen in the amount of 1.5 ml/100 g critical stress intensity factor at crack propagation decreases 1.7 times. Brittle fracture resistance of steel with 0.65 % C decreases almost 2.1 times at similar quantity of hydrogen.

3. During welding of joints of high-strength carbon steels a hardening structure forms in HAZ overheated zone. Phase composition of this structure depends on carbon content in the metal and its cooling rate. To achieve a relatively high resistance of joints to crack propagation, it was necessary to ensure in the HAZ metal formation of bainitic-martensitic structure, in which upper bainite is absent, and volume fraction of martensite is not greater than that of lower bainite.

4. Hydrogen, diffusing from the deposited metal, promotes an abrupt embrittlement of HAZ metal in high-strength carbon steels. To increase brittle fracture resistance of HAZ metal, it is necessary to apply welding processes, which provide $[H]_{dif} \leq 1.5$ ml/100 g in the deposited metal, or special technological methods, allowing removal of diffusible hydrogen from HAZ metal.

1. Shorshorov, M.Kh. (1965) *Metals science of welding of steel and titanium alloys*. Moscow: Nauka.
2. Grabin, V.F., Denisenko, A.V. (1978) *Metals science of welding of low- and medium-alloy steels*. Kiev: Naukova Dumka.
3. Kasatkin, O.G. (1994) Peculiarities of hydrogen embrittlement of high-strength steels in welding. *Avtomatich. Svarka*, **1**, 3–7.
4. Ignatenko, A.V., Pokhodnya, I.K., Paltsevich, A.P. et al. (2012) Dislocation model of hydrogen-enhanced localizing of plasticity in metals with bcc lattice. *The Paton Welding J.*, **3**, 15–19.
5. Gajvoronsky, A.A. (2013) Influence of diffusible hydrogen on delayed cracking resistance of high-carbon steel welded joints. *Ibid.*, **5**, 14–20.
6. Sarzhevsky, V.A., Gajvoronsky, A.A., Gordonny, V.G. et al. (1996) Influence of technological factors on structure and properties of HAZ metal in repair-restoration surfacing of all-rolled wheel flanges. *Avtomatich. Svarka*, **3**, 22–27, 33.
7. Gajvoronsky, A.A., Poznyakov, V.D., Markashova, L.I. et al. (2012) Influence of deposited metal composition on structure and mechanical properties of reconditioned railway wheels. *The Paton Welding J.*, **8**, 16–22.
8. (1972) *New methods for evaluation of resistance of metals to brittle fracture*. Ed. by Yu.N. Robotnov. Moscow: Mir.
9. Shorshorov, M.Kh., Chernyshova, T.A., Krasovsky, A.I. (1972) *Weldability testing of metals*. Moscow: Metallurgiya.
10. *GOST 25.506:* Methods of mechanical tests of metals. Characterization of crack resistance (fracture toughness) in static loading.
11. Makhnenko, V.I., Korolyova, T.V., Lavrinets, I.G. (2002) Effect of microstructural transformations on redistribution of hydrogen in fusion welding of structural steels. *The Paton Welding J.*, **2**, 6–13.
12. Ostash, O.P., Andreiko, I.M., Kulyk, V.V. et al. (2009) Influence of the mode of thermal treatment and load ratio on the cyclic crack-growth resistance of wheel steels. *Materials Sci.*, 45(**2**), 211–219.
13. Gajvoronsky, A.A., Zhukov, V.V., Vasiliev, V.G. et al. (2014) Structural changes in overheating zone of HAZ metal of railway wheels in arc surfacing. *The Paton Welding J.*, **1**, 13–19.
14. Gajvoronsky, A.A., Zhukov, V.V., Shishkevich, A.S. (2014) Weldability of high-strength carbon steel 65G. *Svarka i Diagnostika*, **5**, 50–54.

Received 06.04.2016

doi.org/10.15407/tpwj2016.09.02

ARGON ARC WELDING OF TITANIUM VT22 ALLOY USING FILLER FLUX-CORED WIRE

V.P. PRILUTSKY, S.L. SHVAB, I.K. PETRICHENKO, S.V. AKHONIN, S.B. RUKHANSKY and **I.A. RADKEVICH**
E.O. Paton Electric Welding Institute, NASU
11 Kazimir Malevich Str., 03680, Kiev, Ukraine. E-mail: office@paton.kiev.ua

At the present time the use of welded assemblies and structures of high-strength titanium alloys ($\sigma_t \geq$ 1100 MPa) is widened. Moreover, the strength characteristics of welded joints should be at the level of characteristics of alloys. For load-carrying elements of aircrafts of AN type, high-strength two-phase ($\alpha + \beta$)-titanium VT22 alloy is used. The aim of the work was the investigation of the influence of reducing the degree of weld metal alloying on its strength characteristics. For this purpose a completely new filler material, namely titanium flux-cored wire, for argon arc welding of VT22 alloy was developed. Despite the decrease in the degree of alloying of weld metal, its strength reaches 1121.5 MPa after the standard heat treatment, which is higher than the level of strength of the base metal (1057.5 MPa). Moreover, the impact toughness amounts to 70–75 % of the base metal impact toughness. 15 Ref., 4 Tables, 6 Figures.

Keywords: *titanium, welding, flux-cored wire, controlled magnetic field*

One of the main technological processes in the manufacture of assemblies of aircraft engineering is welding. Weldability is an important factor determining the use of titanium alloys in the assemblies of aircraft engineering. In aircraft construction the low-alloyed titanium alloys, which are well-welded, became the most widely spread. In the operating conditions the characteristics of welded joints of these alloys are close to the corresponding characteristics of the alloys themselves. At the present time a considerable attention is paid to widening the use of welded structures and assemblies of high-strength titanium alloys with tensile strength of more than 1100 MPa.

The problem is put in the way that the mechanical characteristics of welded joints were close to the characteristics of alloys. It is connected with the appearance of such aircrafts as AN-124, AN-225, AN-70, AN-140, AN-148 and with the need to use the large-sized heavily loaded assemblies in their designs. They include chassis, frame rings, monorails, traverse beams, wing carriages and others. However, the weldability of the existing high-strength titanium alloys is significantly worse than that of the low-alloyed alloys. For load-carrying elements of aircrafts of the AN type the two-phase high-strength titanium alloy VT22 (system Ti–5Al–5Mo–5V–1Fe–1Cr) is widely used. It is applied both in annealed as well as in heat-hardened state.

The structure of annealed VT22 alloy consists of approximately equal amounts of α- and β-phases and, therefore, it belongs to the highest-strength titanium alloys in the annealed state. This property allows using VT22 alloy in the large-sized products, when the hardening heat treatment is complicated. An advantage of VT22 alloy as compared to other titanium alloys is the possibility of hardening by multi-stage annealing at the regulated cooling rate. However, its structure and properties depend much on the variation of chemical composition in the ranges established by GOST 19807–91.

This factor affects also weldability, and as far as according to the degree of alloying VT22 alloy belongs to the alloys with a critical composition, then under the influence of thermal cycle of welding the phase composition and the structure are formed in the weld metal and HAZ, having a very low ductility and impact toughness. Thus, during manufacture of welded structures of VT22 alloy using EBW the chemical composition of welds remains the same as that of the base metal, having a low ductility and impact toughness [1, 2]. When the postweld hardening heat treatment of welded joint is applied according to the modes recommended for the base metals, the ever further reduction in mechanical properties of weld metal is observed. It greatly reduces the efficiency of EBW.

For the manufacture of welded titanium structures such a universal method became rather widely applied as argon arc welding using tungsten electrode (TIG) with surface arc. This method allows applying filler wire in welding into a groove, which makes it possible to change the composition of weld metal and also to adjust the thermal cycle of welding. In one-pass arc welding of VT22 alloy the chemical composition remains the same as that of the base metal,

the weld metal has also a low ductility and impact toughness. This is connected with the heterogeneity of the structure of different areas of the joint, arising under the influence of thermal cycle of welding and, as a result, with uneven distribution, shape and sizes of the decay products of β-solid solution [3]. It is assumed that a certain role here belongs to the chemical heterogeneity arising in the process of weld formation [4]. Therefore, while selecting the modes of heat treatment of welded joints of this alloy the phase and structural peculiarities should be considered, occurring after welding.

According to the prevailing assumptions, during welding of thermally hardened alloys to decrease the forming microheterogeneity of weld metal it is recommended to reduce the degree, as well as the system of its alloying by applying filler wires with different content of elements of β-stabilizers [2, 4–6]. It helps improving the ductility of welds, but at the same time it greatly reduces their strength. Moreover, such a characteristic lack of thermally hardened two-phase alloys is revealed as the decrease in ratio of weld strength to the strength of base metal during its hardening. Therefore it is recommended to locate the welds in the thickened areas.

Till now this technique is considered as the only possibility to realize the strength characteristics in welded structures of VT22 alloy [4]. At the present time in accordance with these preconditions, high-alloyed welding wire of SP15 grade (Ti–4.5Al–2V–3Mo–3.5Nb–1.5Zr) with tensile strength of not lower than 750 MPa became widely applied [5, 7]. The total equivalent by molybdenum of this wire reaches 7.5 % and, therefore, it is recommend for application in welding of two-phase titanium alloys of a large range. The tensile strength of welds of VT22 alloy, made by this wire, does not exceed 1000 MPa.

It should be noted that the process of manufacturing of high-alloyed filler wire is characterized by a technological complexity and high power consumption (after each 0.15 mm transition an etching in acids and vacuum annealing should be carried out). In addition, the composition of SP15 wire includes a number of expensive and scarce elements such as V, Mo, Nb and Zr. After completion of the process of manufacturing wire, some small defects still remain on its surface in the form of tears, microcracks, remnants of oxide layers. The depth of occurrence of such defects is regulated and in accordance with GOST 27265–87 it is not more than 0.4 mm. In welding they can be a source of additional contamination of weld metal with interstitial impurities and also they contribute to appearance of porosity in them. The presence of porosity results in a loss of service characteristics of products, reduction of mechanical properties, static and especially fatigue strength of welded joints [8, 9]. In TIG it is possible to prevent the occurrence of such defects by using the metallurgical treatment of a weld pool with a liquid flux when it is introduced into the arc zone, thus increasing the cyclic strength of welded joints [10].

In TIG welding with edge preparation the mixing of filler and base metals occurs, as a result of which the chemical and phase composition of the weld differs both from the composition of base metal as well as from the composition of the filler wire. As a consequence, the resulting structural and chemical heterogeneity leads to anisotropy of physical and mechanical properties, and the difference in phase composition of the HAZ and the weld requires a careful selection of modes of heat treatment of welded assemblies.

The basic aim of the work was investigation of the effect of reducing the degree of the weld metal alloying without changing the composition of alloying elements on the formation of the required phase composition and the structure of weld metal and the strength characteristics during application of heat treatment of welded joint. The task of the investigations included the search for conditions and parameters of welding process, under which the chemical and physical heterogeneity developed in the layers of the deposited metal and HAZ would be minimal. Solution of this problem can significantly simplify the process of heat treatment of welded joints and obtain the desired complex of mechanical characteristics.

As far as VT22 alloy has a high sensitivity to a thermal cycle of welding, first of all, it is necessary to create such conditions of weld formation, under which it is possible to adjust the parameters of thermal cycle in order to reduce the length of HAZ. This, in its turn, will affect intragranular structure and phase composition of the weld and HAZ metal properties. For this purpose, to control the process of weld formation, the external transverse magnetic field was applied, the application of which was realized during automatic narrow-gap welding of titanium [11] and in manual welding under the site conditions [12]. It allowed controlling the spatial position of arc column and redistributing its thermal energy between the base metal, filler wire and weld metal.

The mechanical characteristics of the weld metal during welding with edge preparation can be changed by choosing an appropriate thermal cycle of welding and the mode of subsequent heat treatment of welded joint, as well as by controlling the degree of weld metal alloying. For this purpose, on the basis of previous investigations a principally new filler material was developed for welding titanium, namely titanium

Table 1. Content of alloying elements in the granules of VT22 alloy (results of spectral analysis)

Components	Chemical composition, wt.%							
	Al	V	Mo	Zr	Si	Fe	Cr	Ti
GOST 19807–91	4.4–5.7	4.0–5.5	4.0–5.5	0.3	0.15	0.5–1.5	0.5–1.5	Rest
Granules	5.6	4.8	5.0	0.05	0.12	0.72	1.0	Rest

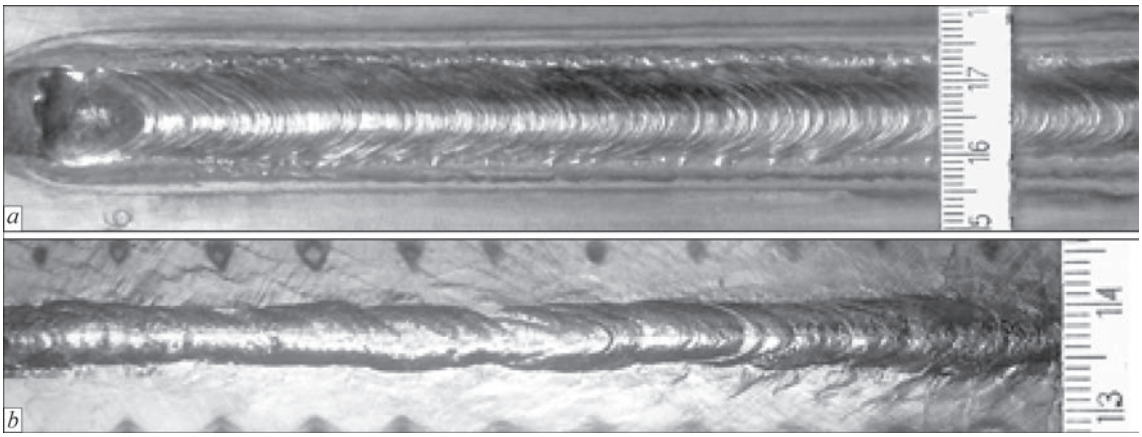

Figure 1. Specimen of welded joint of VT22 alloy 8 mm thick produced using filler flux-cored wire PPT-22: *a* — face weld surface; *b* — reverse formation

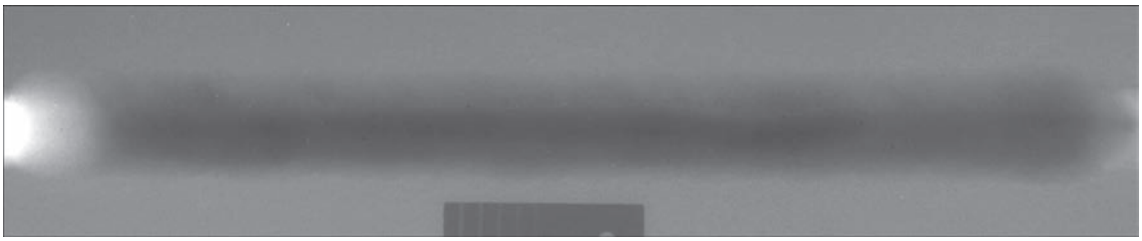

Figure 2. Radiogram of welded joint produced using filler flux-cored wire PPT-22

filler flux-cored wire [13, 14]. It represents a tubular sheath of commercial titanium of grade VT1-00, inside which there is the core composed of metal and flux components. Such a design unlike the solid wire allows introducing a flux component into the core intended to prevent the occurrence of porosity in welds and the arc constriction. The flux component of the core includes fluorides of alkaline earth metals.

As the metal component it was suggested to use granules produced by plasma centrifugal spraying from the billet of VT22 alloy (Table 1).

The experiments on the development of welding technology were carried out on the specimens of VT22 alloy of 8 mm thickness with V-shaped preparation at 90° angle of edges opening and at 1 mm root-face. As the filler material the experimental flux-cored wire PPT-22 of 3 mm diameter was used. In welding an external transverse alternating magnetic field (the frequency is 20 Hz, magnitude of magnetic induction is 4 mT) was used to move the arc column and, accordingly, the weld pool across the weld. The welding modes are given in Table 2, the appearance of welded specimen is shown in Figure 1. Figure 2 shows the radiogram of welded joint, confirming that the use of flux component in the flux-cored wire prevents the arising of pores in the weld.

The macrosection of the produced joint is shown in Figure 3. The comparison of microstructures of weld metal, produced during welding with magnetic control and without it, shows that the use of an alternating magnetic field allows adjusting not only the sizes of the weld, but also influencing the crystallization conditions of the weld pool metal by promoting the formation of a more uniform and homogeneous structure. Thus, in welding without application of magnetic field the intragranular structure is heterogeneous, the areas with intensive decay and high density of plate martensite particles are observed in it, which are alternated with the light areas, where the density of martensite particles is smaller, i.e. the decay of β-solid solution is not uniform (Figure 4, *a*). Under the influence of alternating magnetic field on the metal of the weld pool a large uniformity of decay of solid

Table 2. Parameters of the mode for welding specimens

Number of pass	Welding parameters			
	I_w, A	U_a, V	v_w, m/h	v_{feed}, m/h
1	200	13.0	9	30
2, 3	220	13.5	7	30

Table 3. Mechanical properties of as-welded weld metal of VT22 alloy with thickness of 8 mm

Sampling of test specimens	Mechanical properties				
	σ_y, MPa	σ_t, MPa	δ, %	ψ, %	*KCV*, J/cm^2
Base metal	1003.8	1039.7	9.6	19.5	32.6
Weld metal	987.7	1065.1	9.0	23.9	5.9
Note. Average values of the results of testing three specimens are given.					

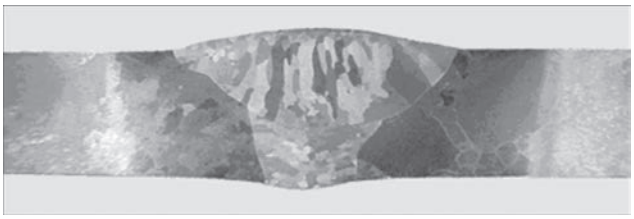

Figure 3. Macrosection of welded joint of VT22 alloy 8 mm thick in the as-welded state

solution and formation of a more homogeneous structure (Figure 4, *b*) is achieved.

The results of mechanical tests of the weld metal in the as-welded state are given in Table 3.

The obtained results show that the use of magnetic field had no effect on the value of impact toughness of the weld metal in the as-welded state.

As a rule, the welded joints after welding are subjected to annealing. An effective way to improve the ductile properties of VT22 alloy is a high-temperature annealing in the two-phase area at the temperature range of 750–800 °C followed by the furnace cooling [15]. The purpose of annealing is not only to eliminate thermal welding stresses, but also to obtain a uniform

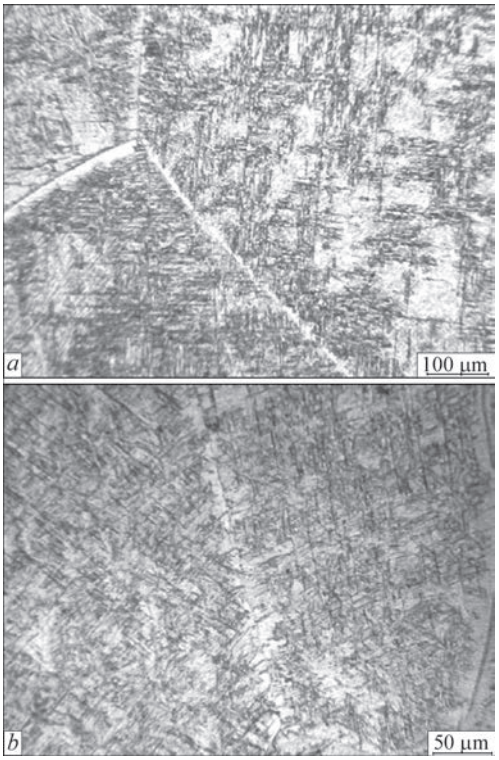

Figure 4. Microstructure of weld metal of welded joint of VT22 alloy 8 mm thick: *a* — without; *b* — with the use of magnetic field

Table 4. Mechanical properties of welded joint and base metal in the state after heat treatment

Metal	σ_y, MPa	σ_t, MPa	δ, %	ψ, %	*KCV*, J/cm^2
Welded joint	–	1121.5*	–	–	14.8
Base metal	974.1	1057.5	13.3	33.3	19.6
Notes. 1. Fracture along the weld. 2. Average values of the results of testing three specimens are given.					

equilibrium structure with a desired ratio of α- and β-phases. Based on the analysis of literature data and recommendations of the authors of [15], a rather simple technology of heat treatment process was chosen for welded joints produced using a filler flux-cored wire, namely soaking in the furnace at T = 750 °C during 1 h, cooling in the furnace.

The results of mechanical tests of welded joint and base metal in the as-treated state are given in Table 4.

The macrosection of welded joint after heat treatment is shown in Figure 5.

The investigations of microstructure of welded joints after annealing showed that in HAZ a rather uniform metastable decay of β-phase is observed with precipitation of dispersed particles of martensite α′/α′′-phase, the subgrain structure retained and the partial recrystallization of β-grain occurred (Figure 6, *b*). Along the boundaries of large β-grains the small recrystallized grains were formed.

The annealing contributed to the formation of a homogeneous and uniform metal structure in the weld height (Figure 6, *c*), at the same time a decay of metastable phases also occurred, however, the weld sizes of the decay products are larger than in the HAZ, that is associated with some disalloying of weld metal due to the sheath of flux-cored wire.

Thus, it can be concluded that the use of metal granules of VT22 alloy as the metallic component of the core of flux-cored wire in combination with the controlled magnetic field has a positive effect on the

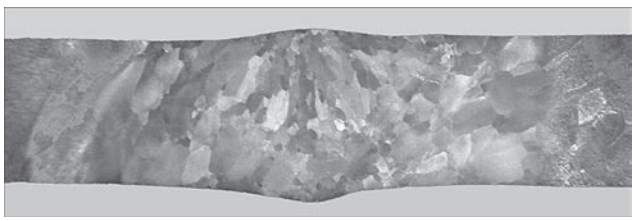

Figure 5. Macrosection of welded joint of VT22 alloy 8 mm thick in the as-treated state

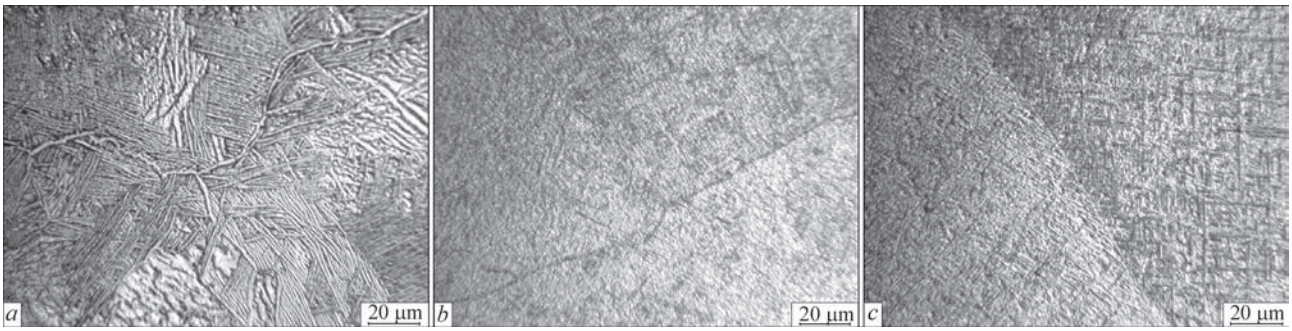

Figure 6. Macrostructure of welded joint after heat treatment: *a* — BM; *b* — HAZ; *c* — weld

properties of welded joint at the selected mode of heat treatment. The strength of weld metal is achieved being higher than the level of the base metal strength, despite the reduction in the degree of weld alloying. Here the impact toughness amounts to 70–75 % of the base metal impact toughness.

1. Zamkov, V.N., Shevelev, A.D., Arsenyuk, V.V. et al. (1984) Improvement of EBW technology of VT22 titanium alloy. *Avtomatich. Svarka*, **1**, 56–58.
2. Moiseev, V.N., Kulikov, F.R., Kirilov, Yu.G. et al. (1975) *Welded joints of titanium alloys*. Moscow: Metallurgiya.
3. Notkin, A.B., Korobov, O.S., Pertsovsky, N.Z. et al. (1982) Influence of initial structure on mode of β-solid solution in high-strength titanium alloy VT22. *Fizika Metallov i Metallovedenie*, **54**(Issue 4), 755–761.
4. Gurevich, S.M., Kulikov, F.R., Zamkov, V.N. et al. (1975) *Welding of high-strength titanium alloys*. Moscow: Mashinostroenie.
5. Gurevich, S.M., Zamkov, V.N., Kushnirenko, N.A. et al. (1980) Selection of filler material for welding of (α + β)-titanium alloys. In: *Actual problems of welding of non-ferrous metals*, 314–320. Kiev: Naukova Dumka.
6. Glazunov, S.G., Gruzdeva, L.F., Moiseev, V.N. et al. *Filler material for welding of titanium alloys with higher* β*-phase content*. USSR author's cert. 1662217. Publ. 1964.
7. *GOST 27265–87:* Technical specifications. Welding wire from titanium and titanium alloys.
8. Kulikov, F.R., Vaskin, Yu.V., Kishkina, S.I. et al. (1977) Influence of technological factors on low-cycle fatigue of VT22 alloy welded joints. *Aviats. Promyshlennost*, **6**, 65–71.
9. (1978) Low-cycle fatigue of welded joints of (α + β)-titanium alloys. In: *Proc. of 3rd Int. Conf. on Titanium*, Vol. 2, 273–281. Moscow: VILS.
10. Gurevich, S.M., Zamkov, V.N., Blashchuk, V.E. et al. (1986) *Metallurgy and technology of welding of titanium and its alloys*, 128. Kiev: Naukova Dumka.
11. Paton, B.E., Zamkov, V.N., Prilutsky, V.P. (1996) Narrow-groove welding proves its worth on thick titanium. *Welding J.*, **5**.
12. Zamkov, V.N., Prilutsky, V.P. (2005) Methods for welding titanium alloys. *The Paton Welding J.*, **8**, 41–44.
13. Gurevich, S.M., Zamkov, V.N., Prilutsky, V.P. *Flux-cored welding wire*. Pat. 4131493 US. Publ. 1978.
14. Prilutsky, V.P., Zamkov, V.N., Radkevich, I.A. et al. *Filler material based on titanium alloy*. Pat. 25333 Ukraine. Int. Cl. B23K 35/36. Fill. 08.05.1997. Publ. 30.10.1998.
15. Anisimova, L.I., Popov, A.A., Melnikova, V.I. et al. (1977) Effect of heat treatment on structure and properties of VT22 titanium alloy. *Fizika Metallov i Metallovedenie*, **44**(Issue 4), 843–845.

Received 13.04.2016

doi.org/10.15407/tpwj2016.09.03

EFFECT OF PARAMETERS OF WELDING CIRCUIT ON FORMATION OF WELDING CURRENT PULSES

G.A. TSYBULKIN
E.O. Paton Electric Welding Institute, NASU
11 Kazimir Malevich Str., 03680, Kiev, Ukraine. E-mail: office@paton.kiev.ua

This work studies a poorly investigated effect of welding arc parameters on amplitude of welding current pulses in consumable electrode gas-shielded pulsed arc welding (PAW). A welding circuit is considered as a frequency-selective system, which passes the pulses in undistorted form only in specific frequency band. The pulses out of this band are significantly suppressed, that can result in rapid decrease of PAW efficiency. The main aim of the work is to determine a width of welding circuit pass band and possibility of its increase. In scope of developed mathematical model a criterion was obtained, which sets in algebraic form one of the necessary conditions of PAW efficient application. From practical point of view, this criterion allows, using known parameters of welding circuit, carrying out a fairly simple evaluation of pass band upper boundary, inside which a set amplitude of welding current pulses is ensured. From the other side, indicated criterion can be used for solving an inverse problem, i.e. to determine the allowable values of some parameters of welding circuit using preliminary selected frequency of welding current pulse passing. Besides, due to its «analytical property» the indicated criterion can be useful for theoretical investigations of pulse-arc processes taking place in the welding circuit. 19 Ref., 5 Figures.

Keywords: *pulsed arc welding, consumable electrode, welding circuit, welding current amplitude, pulse repetition frequency, mathematical model*

One of the most efficient welding technologies, developed back in the 1960s and received further propagation in our country and abroad [1–15], is a consumable electrode gas-shielded pulsed arc welding (PAW). The rising interest to its application in the last time is to large extent related with robotization of arc welding and coming into industry of improved welding equipment, including the sources of pulsed welding current. These sources are characterized by new possibilities in welding mode regulation and, in particular, possibility of program setting of current amplitude in the pulse, pulse duration, background current and pulse setting frequency. It is well known fact that the optimum transfer of electrode metal during PAW is achieved at specific combination of indicated parameters.

A lot of publications were dedicated to the problems of stabilizing, adaptive regulation and practical realization of PAW [4, 6, 8, 9]. But, at the same time, particularly important question, related with effect of welding circuit parameters on formation of the pulses of welding current, have almost no description in the reference literature. The matter is that the welding circuit in dynamic relationship represents itself a frequency-selective system which passes the undistorted pulses only in specific frequency band [12]. Out of this band the pulses will be significantly suppressed, that can result in rapid decrease of PAW efficiency.

Meanwhile, it is difficult to say what the width of indicated frequency band is and how it depends on welding circuit parameters and what are the possibilities of its expansion. The answer on these questions is very important from practical point of view, since they can provide clear vision on real frequency limitations, caused by dynamic properties of the welding circuit, which have to be taken into account in development of pulsed welding technologies and corresponding equipment. This paper is dedicated to solution of these issues.

Mathematical model. We study the scheme of welding circuit, given in Figure 1. The dynamic processes, taking place in it, obey the equations

$$\left.\begin{aligned} (L_1 + L_2)\frac{di}{dt} + (R_1 + R_2)i = u_s(t) - u_a(i, l), \\ u_a(i, l) = u_0 + El + S_a i, \\ l = H - h, \\ h = h_0 + v_e t - M\int_0^t i dt. \end{aligned}\right\} \quad (1)$$

The following designations are taken in these equations and in Figure 1, namely $i = i(t)$ is the welding current; L_1, R_1, $u_s(t)$ are the inductance, internal resistance and pulse voltage of welding current source (WCS); L_2 is the inductance of welding circuit, formed by supply leads; R_2 is the sum resistance of electrode stick-out, supply leads and sliding contact in a nozzle tip; $u_a = u_a(l, t)$ is the arc voltage; u_0 is the sum of near electrode voltage drops; $l = l(t)$ is the arc length;

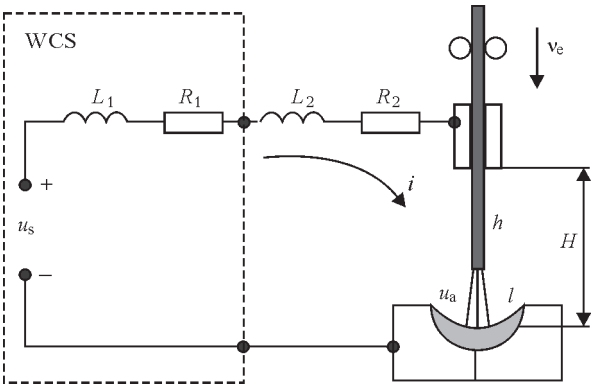

Figure 1. General scheme of welding circuit (for designations see the text)

$S_a = \partial u_a/di$ is the arc volt-ampere slope; $E = \partial u_a/\partial l$ is the intensity of electric field in the arc column; H is the distance between the end of current conducting tip and free surface of weld pool; h_0 and $h = h(t)$ are the initial and current value of electrode stick-out; v_e is the electrode feed rate; $M = \partial v_m/\partial i$ is the current slope of electrode melting; $v_m = v_m(t)$ is the rate of electrode melting; t is the current time.

Eliminating the variables $u_a(l, t)$, $l(t)$ and $h(t)$ from equation system (1) and assuming that v_e = const and H = const, one of differential equation is received:

$$L_* \frac{d^2 i}{dt^2} + R_w \frac{di}{dt} + EMi = Ev_e + \frac{du_s}{dt}, \qquad (2)$$

in which $L_* = L_1 + L_2$, $R_w = R_1 + R_2 + S_a$.

Equation (2) is the simplified mathematical model of welding circuit. It was assumed during its design that possible fluctuations of R_w and E parameters in process of arc welding are insignificant in comparison with variation of variables $u_s(t)$ and $i(t)$ and it is no need in their consideration. Besides, such called small parameters [16] were not also taken into account, since their effect in solution of this problem can also be neglected.

Equation (2) is written in operative form

$$(L_* p^2 + R_w p + EM) i = Ev_e + pu_s.$$

and for clarity this equation is compared with structural scheme, given in Figure 2.

In this scheme

$$W_1 = W_1(p) = \frac{E}{L_* p^2 + R_w p + EM}, \qquad (3)$$

$$W_2 = W_2(p) = \frac{p}{L_* p^2 + R_w p + EM} \qquad (4)$$

are the transfer function from inputs v_e and u_s to output i (p is the Laplace operator). From the scheme and expressions (3), (4) it is seen that the welding circuit in structural relationship is represented in form of sum of two elementary units, the first of which corresponds to basic frequency filter, and the second to band filter [17].

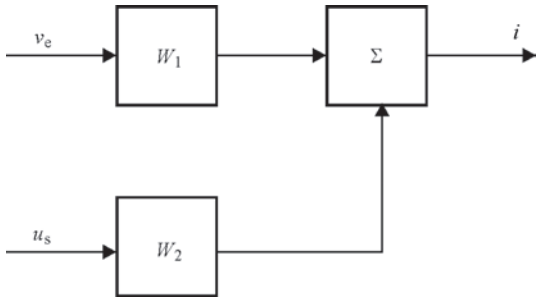

Figure 2. Structural diagram of welding circuit

The input action of unit W_1 is a rate of electrode wire feed v_e, which is constant in our case. Stationary reaction W_1 according to (3) will also be constant and equal $i_\infty(t) = v_e/M$. The input of unit W_2 receives action $u_s(t)$ in form of sequence of rectangular pulses. The amplitude of pulses at output W_2 in this case equal the amplitude of input pulses, multiplied by a value of frequency response characteristic (FRC) $A_2(\omega) = |W_2(j\omega)|$, where $j = \sqrt{-1}$, $\omega = 2\pi f$, and f is the frequency of pulse passing.

Thus, for evaluation of reaction of welding current on the action, being a periodic time function $u_s(t)$, it is necessary to have FRC of this circuit. It can be built using formula

$$A_2(\omega) = \frac{\omega}{\sqrt{(EM - L_* \omega^2)^2 + R_w^2 \omega^2}}, \qquad (5)$$

which is developed after substitution in the expression (4) of imaginary variable $j\omega$ instead of operator p [18].

Figure 3 shows a diagram of FRC of unit W_2. The same Figure includes a horizontal dashed line at the level of max $A_2/\sqrt{2}$ that corresponds –3 dB value.

Cross points of this line with the diagram $A_2(\omega)$ set the pass band $\Delta\omega = \omega_2 - \omega_1$ of welding circuit. Obviously, the wider $\Delta\omega$ is, the higher frequency of pulse passing $f = \omega/2\pi$ can be used for performance of PAW with set amplitude of these pulses.

Let's consider what are the real possibilities of expansion of band $\Delta\omega$ exist. Analysis of expression

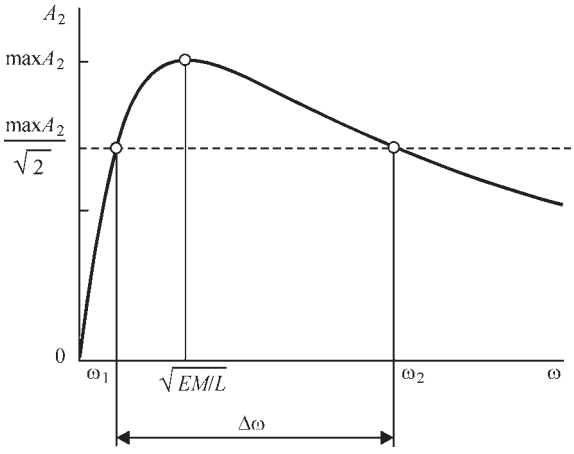

Figure 3. FRC of band filter W_2

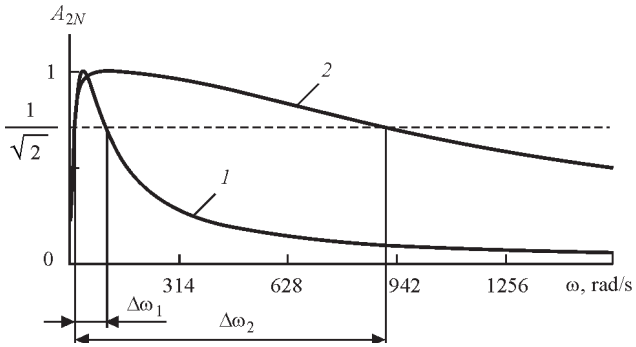

Figure 4. Normalized FRC of W_2 unit (descriptions of curves *1*, *2* see in the text)

(5) shows that parameters R_w and L_*, included in this expression, in contrast to E and M, can be used for expansion of band $\Delta\omega$. Obviously, that sum resistance $R_w = + R_1 + R_2 + S_a$ can be changed only due to change of basic summand R_1, which sets an inclination of volt-ampere characteristic of WCS. However, this characteristic can be varied randomly. Another situation is with welding circuit inductance L_*. Its variation is allowed, as is well known, in sufficiently wide range without significant deterioration of welding itself [19].

Thus, practically, it is only one possibility for significant expansion of $\Delta\omega$, namely reduction of welding circuit inductance L_*. In order to show this possibility let's plot normalized FRS (Figure 4):

$$A_{2N}(\omega) = \frac{A_2(\omega)}{\max A_2(\omega)} = \frac{R_*\omega}{\sqrt{(EM - L_*\omega^2)^2 + R_w^2\omega^2}} \qquad (6)$$

for two different cases: when $L_* = 0.5$ and when $L_* = 0.05$ mH. The values of other parameters of welding circuit, included in formula (6), are typical: $E = 2$ V/mm, $M = 0.31$ mm/(A·s) and $R_w = 0.045$ Ohm (these values are taken from work [16]). From Figure 4 it can be seen that in the first case the pass band of welding circuit $\Delta\omega_1$ is sufficiently narrow: $\Delta\omega_1 = 91$ rad/s (that corresponds to $\Delta f_1 = 14.5$ Hz). In the second case, the frequency band is significantly wider: $\Delta\omega_2 = 911$ rad/s or $\Delta f_2 = 145$ Hz. Obviously that further reduction of inductance L_* will result in more expansion of the welding circuit frequency band.

Naturally, there is a question, whether it is possible to find a dependence of pass frequency of welding current pulses f directly on inductance L_* in analytical form without using FRC graphical plotting. Let's consider equation $A_{2N}/(\omega) = 1/\sqrt{2}$, which taking into account (6), is written in the following way:

$$\frac{R_w\omega}{\sqrt{(EM - L_*\omega^2)^2 + R_w^2\omega^2}} = \frac{1}{\sqrt{2}}.$$

This equation is divided for two quadratic equations:

$$L_*\omega^2 + R_w\omega - EM = 0 \text{ if } \omega < \sqrt{\frac{EM}{L_*}},$$

$$L_*\omega^2 - R_w\omega - EM = 0 \text{ if } \omega > \sqrt{\frac{EM}{L_*}}.$$

Since we are interested in the upper boundary of pass band ω_2 (see Figure 3), i.e. the case, when $\omega > \sqrt{EM / L_*}$, then only the second from given equations is considered. The following solution satisfies this equation:

$$\omega_2 = \frac{R_w}{2L_*}\left(1 + \sqrt{1 + \frac{4L_*EM}{R_w^2}}\right). \qquad (7)$$

Taking into account that in the most of practical cases in PAW

$$L_* << \frac{R_w^2}{4EM}, \qquad (8)$$

expression (7) is significantly simplified and takes the form of

$$\omega_2 \approx \frac{R_w}{L_*}$$

or (taking into account that $\omega_2 = 2\pi f_2$)

$$f_2 \approx \frac{R_w}{2\pi L_*}.$$

Thus, if condition $f < f_2$ is fulfilled, namely if

$$f < \frac{R_w}{2\pi L_*}, \qquad (9)$$

then the pass frequency of welding circuit pulses f is within the limits of the welding circuit pass band. This means that decrease of amplitude of the pulses in this case will not exceed a set margin $\Delta A = 3$ dB.

Therefore, inequation (9) can be considered as one of the necessary conditions of efficient PAW application. This inequation due to its simplicity is very convenient for preliminary calculation of f. It is also wonderful that it due to its «analytical form» can be useful at theoretical investigations of pulse-arc processes taking place in welding circuit.

Results of calculation experiment. A calculation experiment was carried out in scope of mathematical model (2) in order to check an effect of inductance L_* on amplitude of welding current pulses. The same parameters that were used in FRS plotting were used at that. Besides, the parameters of mode of robotized PAW were set, namely $v_e = 22$ mm/s, $H = 17$ mm, pulse duration $\tau = 0.004$ s, $u_s(t) = (30 + 10z(t))$ V, where

$$z(t) = \begin{cases} 1, & nT \le t \le (nT + \tau), \\ 0, & (nT + \tau) < t < (n+1)T, \end{cases}$$
$$T = 1/f, \quad n = 0, 1, 2, 3, \ldots .$$

The frequency of pulse passing was taken equal $f = 25$ pulse/s. This choice was made is such a way

that its value was inside the pass band $\Delta f_2 \approx 145$ Hz ($\Delta\omega_2 = = 911$ rad/s), but, at the same time (see Figure 4), out of pass band $\Delta f_2 \approx 14.5$ Hz ($\Delta\omega_1 = 91$ rad/s).

The results of experiment are presented in Figure 5 in form of reaction of welding current $i(t)$ on effect of v_e = const and series of rectangular pulses $u_s(t)$.

Comparison of this results shows that the pulses of welding current at $L'_* = 0.05$ mH (Figure 5, *a*) have sufficiently large amplitude. It can be explained by the fact that $f < f_2$ and welding circuit as a band-pass filter do not have in this case significant effect on pulse amplitude. At $L''_* = 0.5$ mH the welding current pulses (Figure 5, *b*), as it was predicted, are significantly suppressed by welding circuit since $f > f_2$ in this case.

Conclusions

Carried investigation shows that the parameters of welding circuit, in particular, inductance L_*, have significant effect on characteristics of the welding current pulses. Effect of inductance L_* on rate of increase and rate of reduction of welding current in the pulse is well known to the specialists dealing with PAW problems. However, up to the moment the level of its effect on amplitude of these pulses was not clear. It is shown as a result that the welding circuit as a dynamic system is characterized by specific pass band of the welding current pulses. If pulse passing frequency is out of the limits of this band, the amplitude of pulses is dramatically reduced, that can have negative effect on PAW efficiency.

Relationship (9), obtained in this work, sets in algebraic form a connection between the frequency of passing welding current pulses f and parameters of welding circuit R_w and L_*. This relationship using known parameters R_w and L_* allows sufficiently easy evaluating the upper boundary of pass band of specific welding circuit, inside which a necessary amplitude of welding current pulses is provided. Obviously, that relationship (9) provides a possibility to solve an inverse problem, i.e. to determine the boundary of allowed values of inductance of welding circuit L_* on preliminary selected frequency of pulse passing f and R_w known value.

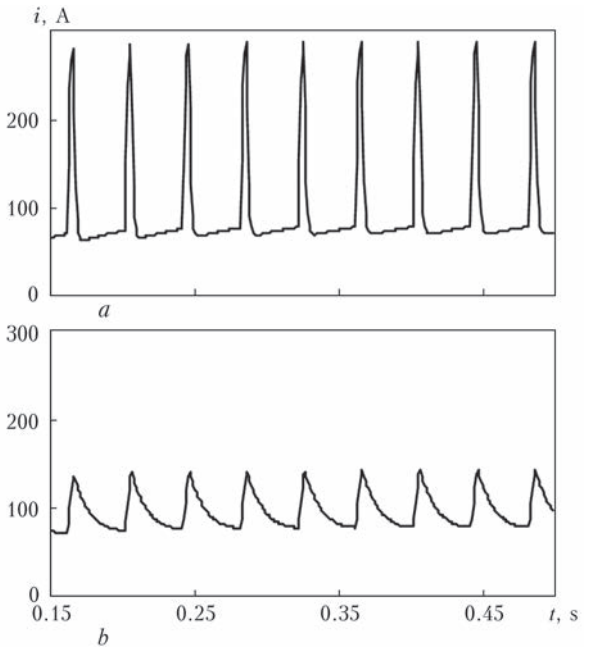

Figure 5. Pulses of welding current at L'_* = 0.05 (*a*) and 0.5 (*b*) mH

1. Paton, B.E., Potapievsky, A.G., Podola, N.V. (1964) Consumable electrode pulsed arc welding with programmable control of process. *Avtomatich. Svarka*, **1**, 1–6.
2. Amin, M. (1983) Pulse current parameters for arc stability and controlled metal transfer in arc welding. *Welding J.*, **5**, 272–278.
3. Matsunawa, A., Yamamoto, G., Hiramoto, S. (1984) Pulsed arc welding. *J. of JWS*, 53(**6**), 20–28.
4. Shejko, P.P., Pavshuk, V.M. (1992) Power source for consumable electrode pulsed-arc welding with smooth control of parameters. *Avtomatich. Svarka*, **6**, 44–46.
5. Saraev, Yu.N. (1994) *Pulsed technological processes of welding and surfacing*. Novosibirsk: Nauka.
6. Voropaj, N.M., Ilyushenko, V.M., Lankin, Yu.N. (1999) Specifics of pulsed arc welding with synergic control of parameters (Review). *Avtomatich. Svarka*, **6**, 26–32.
7. Sudnik, V.A., Ivanov, A.V., Diltey, U. (2000) Mathematical model of heat source in shielded metal-arc welding. Pt 2: Pulsed process. *Svarochn. Proizvodstvo*, **9**, 9–15.
8. Saraev, Yu.N. (2002) Adaptive pulsed arc mechanized welding in construction of main pipelines. *Ibid.*, **1**, 4–11.
9. Paton, B.E., Shejko, P.P., Zhernosekov, A.M. et al. (2003) Stabilization of the process of consumable electrode pulse-arc welding. *The Paton Welding J.*, **8**, 2–5.
10. Dyurgerov, N.G., Sagirov, D.Kh. (2004) Determination of properties in pulsed welding processes. *Svarochn. Proizvodstvo*, **4**, 14–18.
11. Nong, H., Ueyama, T. (2004) Solutions to problems of tiny spatter and arc pulsed MIG welding. *Q. J. of JWS*, 22(**2**), 249–247.
12. Tsybulkin, G.A. (2005) Influence of frequency properties of the welding circuit on current parameters in pulsed-arc welding processes. *The Paton Welding J.*, **10**, 9–13.
13. Knyazkov, A.F., Krampit, N.Yu., Krampit, A.G. et al. (2005) Study of the process of electrode metal transfer in pulsed supply of welding arc. *Tekhnologiya Metallov*, **7**, 18–21.
14. Krampit, N.Yu., Krampit, A.G. (2014) Study of process of consumable electrode pulsed-arc CO_2-shielded welding. *Vestnik MGTU im. N.E. Baumana. Series Mashinostroenie*, **5**, 106–111.
15. Dyurgerov, N.G., Lenivkin, V.A. (2015) Technological stability of consumable electrode pulsed-arc welding. *Svarochn. Proizvodstvo*, **2**, 3–7.
16. Tsybulkin, G.A. (2014) *Adaptive control in arc welding*. Kiev: Stal.
17. Gutnikov, V.S. (1990) *Filtration of measuring signals*. Leningrad: Energoatomizdat.
18. Makarov, I.M., Mensky, B.M. (1977) *Linear automatic systems (elements of theory, methods of calculation and reference material)*. Moscow: Mashinostroenie.
19. Leskov, G.I. (1970) *Electric welding arc*. Moscow: Mashinostroenie.

Received 15.03.2016

doi.org/10.15407/tpwj2016.09.04

SUPERSONIC ELECTRIC ARC SPRAYING OF CRITICAL PARTS OF ROLLING STOCK OF RAILWAY TRANSPORT*

V.N. KORZHIK[1, 2], **N.P. LYUTIK**[2], **A.A. CHAJKA**[2], **V.I. TKACHUK**[2, 3], **I.D. GOS**[2] and **Yu.A. NIKITYUK**[4]

[1]Guangdong Welding Institute (Chinese-Ukrainian E.O. Paton Welding Institute)
510650, Guangzhou, PRC. E-mail:vnkorzhyk@qq.com
[2]E.O. Paton Electric Welding Institute, NASU
11 Kazimir Malevich Str., 03680, Kiev, Ukraine. E-mail: office@paton.kiev.ua
Scientific and Production Center «PLAZER»
10-A Filatova Str., 01042, Kiev, Ukraine. E-mail: plazer2010@metal.ua
[4]Scientific-Production Company «VISP»
23 Moskovsky Ave., 04655, Kiev, Ukraine. E-mail: vizp@i.ua

Rise of efficiency of application of railway transport requires new technologies and materials for increase of their life, first of all of the critical parts of rolling stock. In this aspect one of the most perspective technologies is a supersonic electric arc spraying or supersonic air-gas electric arc metallizing. It allows eliminating the main disadvantages of a traditional electric arc spraying related with low quality of coating, namely, increased burning out of the alloying elements of wire metal being sprayed due to air jet effect, low adhesion strength of the coating with the base material. 12 Ref., 2 Tables, 8 Figures.

Keywords: *supersonic electric arc spraying, railway transport, critical assembly units, coating properties, coating cohesion strength*

An improved supersonic electric arc metallizing (EAM) torch PLAZER15-SA-EM of PLAZER15-SA unit [1–10], containing a torch with combustion chamber operating under positive pressure (Figure 1), was developed for realizing a technology of supersonic electric arc spraying. Such a supersonic metallizing torch is based on a process, in which stabilized electric arc blowing is carried out by hot natural gas combustion products with supersonic velocity.

This is a hybrid technology combining an electric arc spraying with a supersonic flame spraying with formation of a single flow of supersonic high-temperature gas

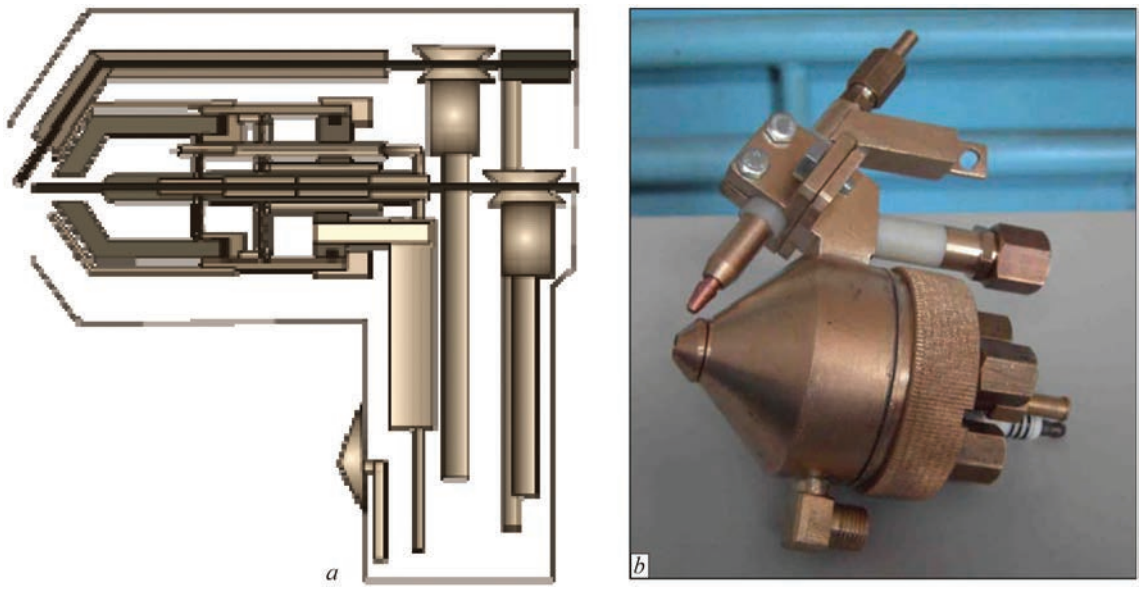

Figure 1. Scheme (*a*) and view (*b*) of supersonic electric arc metallizing torch

*Based on materials of work made in scope of complex program of the NAS of Ukraine «Problems of service life and safety of structures, constructions and machines» (2013–2015).

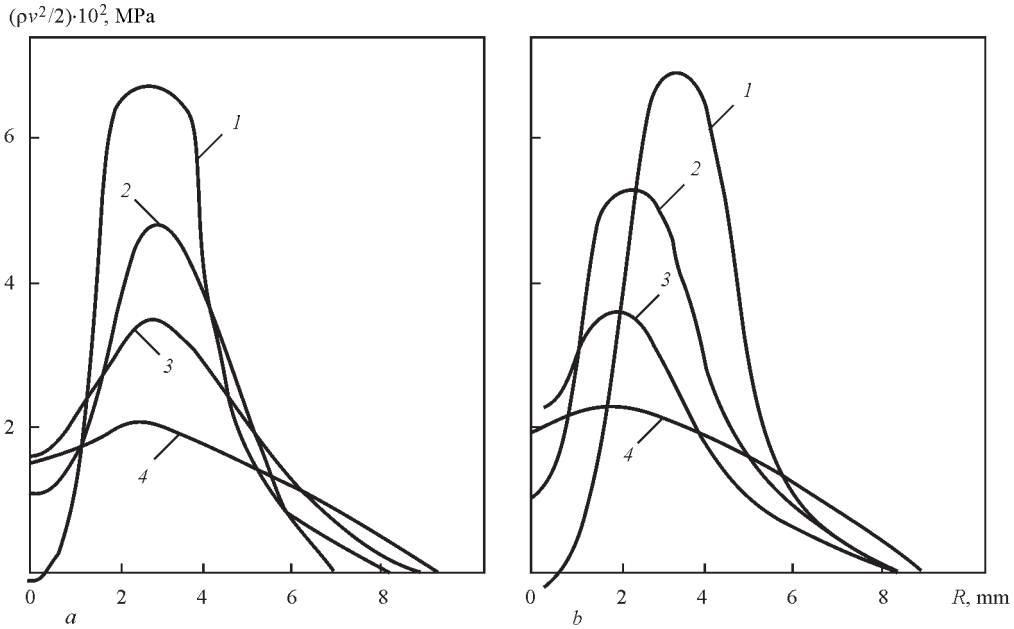

Figure 2. Profiles of dynamic pressing of supersonic metallizing torch at α = 1.2 (*a*) and 0.9 (*b*) and distance from nozzle end: *1* — 2; *2* — 7; *3* — 12; *4* — 22 mm

and molten particles of wire material being sprayed. An electric arc is oriented along the high-temperature gas flow, velocity of which makes 1.5 Mach and burns between two consumable electrodes. Such a system provides for high level of arcing due to its orienting along the gas flow and, thus, a process of heat transfer into electrodes, i.e. intensive acceleration and refinement of molten metal particles, their resistance to in-flight oxidation, reduction of amount of evaporated material (due to formation of double-phase flow by supersonic jet of combustion product).

Indicated supersonic EAM torch for spraying the electric arc melted wires applies a weakly underexpanded supersonic jet of hot products of hydrocarbon gas combustion with air coming from sonic nozzle. The main disturbances in the flow are made by side wire. An area of air shadow is formed behind it down the jet. Figure 2 shows the radial changes of the velocity heads in jet cross section at 2.7, 12, 22 mm distance below the meeting point of side and central wires. Comparison of Figures 2, *a* and 2, *b* shows that a flow pattern is changed depending on mode of operation of the EAM torch in the supersonic flow with an obstacle in form of wire. The flow is focused behind the side wire if operated using enriched mixture, when excess air factor α = 0.9 (Figure 2, *b*) in contrast to diluted mixture with α ~ 1.2 (Figure 2, *a*). Scattering of the dispersed particles in the supersonic flow is determined by a direction of vector of average velocity along a particle trajectory and turbulence parameters. Direction of the vector of average velocity (see Figure 2, *b*) promotes constriction of metal flow, and at near-sonic velocity the level of turbulent fluctuations is reduced, the flow is laminated.

These two circumstances are decisive for reduction of scattering of dispersed phase, decreasing an expansion angle of metal flow and spread of particle velocities. Besides, a gas-dynamic situation (see Figure 2) formed behind the side electrode of the metallizing torch (see Figure 1) determines a nature of carrying, breaking of wire melt and dissipation of the dispersed phase. The metal jet stream takes place in the shadow zone of the side electrode equal 2.5–3.0 of calibers from nozzle edge. Further, aerodynamic breaking of the melt and acceleration of the dispersed particles take place downstream. It is particularly important using the flux-cored wires, when obtaining of the alloyed particles takes place at interaction of shell from low-carbon steel with flux core components. In this case alloying takes place during wire melting and melt jet stream.

Presence of a velocity component of blowing flow behind the side electrode, directed to jet axis (see Figure 2, *b*), provides for constriction of metal flow, promoting reduction of dispersed phase dissipation. The expansion angle makes 7–10°.

It is known fact that one of the significant disadvantages of the coatings, produced using EAM, is a high level of their oxidation. This fact is usually considered as negative. The coatings being formed by oxidized particles are also characterized by high porosity and low coating to base cohesion strength. The main reason of material oxidation is its interaction with oxygen in zone of electric arc burning between the electrode wires.

The method for reduction of oxygen effect on molten metal is using the hydrocarbon gases (mostly methane) for oxygen «binding» . For this the combustible

Table 1. Modes of spraying the coating from flux-cored wires using different types of electric arc metallizing torches

Type of electric arc equipment	Voltage, V	Current, A	Air consumption, m^3/h	Propane consumption, m^3/h	Air pressure, MPa	Spraying distance, mm
Serial metallizing torch EM-14 (Barnaul Hardware and Mechanical Plant, RF) (Figure 3, *a*)	32–34	200–250	120–130	–	0.6–0.7	150–180
Modernized torch EM-14M with two profiled nozzles (Figure 3, *b*)	32–34	200–250	120–130	–	0.6–0.7	150–180
Supersonic torch PLAZER15-SA-EM for unit PLAZER15-SA (Figure 1)	34–36	160–180	90	4.0	0.6	70–130
Notes. 1. Diameter of flux-cored wires is 1.8 mm. 2. Flux-cored wires of the systems based on Fe–B (with powder filling based on ferroboron) and Fe–Cr–C (based on carbon ferrochromium) were used for spraying.						

Table 2. Effect of types of electric arc metallizing torches on characteristics of process of spraying of coatings from flux-cored wire of Fe–B and Fe–Cr–C system

Type of electric arc equipment	Velocity of particles being sprayed *v*, m/s, at 50 mm distance	Average size of particle being sprayed *d*, μm	Size of spraying spot B_1, mm, at 65 mm distance	Content of oxygen in the coating, wt.%
Serial metallizing torch EM-14	30–80	150–180	45–55	1.8–2.5
Modernized torch EM-14M with two profiled nozzles	100–160	80–120	30–40	0.73–1
Supersonic torch PLAZER15-SA-EM for unit PLAZER15-SA	370–400	40–90	20–30	0.50–0.65

gases are added to air being sprayed. The perspectives of application of such air-gas mixtures as a spraying gas can be estimated by analysis of material oxidation in a zone of its dispersion. This is the zone where the most active interaction of metal with gases takes place due to high temperatures (6000–10000 K). A quality analysis of particles' oxidation can be obtained based on the results of thermodynamic equilibrium calculation of material–gas medium system.

The experiments show that there is no oxidation of the particles in spraying by air-gas mixture at natural gas/air ratio of 1/8. Further increase of methane fraction in the sprayed flow is unreasonable from economy point of view. Complete protection of the metal from oxidation under real conditions is virtually impossible since the coating material oxidizes already in particle cooling from melting temperature to environment temperature. The mentioned above is experimentally proved for metallizing torch by data on content of iron oxides in the investigated system depending on natural gas concentration in the air-gas mixture.

The second condition, which promotes for reduction of oxidation of the sprayed material in supersonic flow, is reduction of time of contact of the molten particles with atmosphere due to their higher velocity.

The central and side electrodes in the metallizing torch (see Figure 1) operate under different conditions. The central electrode is melted under effect of heat from arc near-cathode (anode) area with wire heating by hot combustion products at extension length behind the guided nozzle. The side electrode is melted under the effect of heat from arc plasma and anode (cathode) potential fall. Obviously, that the side wire gets more heat and velocity of its melting is always higher than that of the central one. A current level (at supply from constant-voltage power source) is set using a central wire feed rate. The rate of side wire feed is selected in such a way that its end melting takes place on a line continuing central wire surface. This is the case for providing the minimum level of arc current and voltage pulsation, uniform and stable melting of the wires, the narrowest range of melt dispersion and the smallest metal flow expansion angle. Such a mode of operation of supersonic metallizing torch on combustible products is an optimum one.

The comparative investigations of the process of supersonic spraying with the processes of electric arc spraying at subsonic regime of high-temperature jet flow (Tables 1 and 2) proved significant increase of velocity and reduction of size of particles of flux-cored wire (FCW) material being sprayed, decrease of size of spraying spot as well as significant reduction of oxidation of the material being sprayed. Serial metallizing torch EM-14 (Figure 3, *a*) as well as the same redesigned metallizing torch (Figure 3, *b*) equipped with special nozzles for formation of air flow, which provides for contraction of the jet being sprayed, increase of its velocity and reduction of material oxidation, were used.

Such an improvement of virtually all technological parameters of the supersonic electric arc spraying is explained by reduction (in the case of application of such a technology) of mass of liquid metal formed at the end of FCW and, respectively, cutting of size of the sprayed material particle. Increase of dispersion

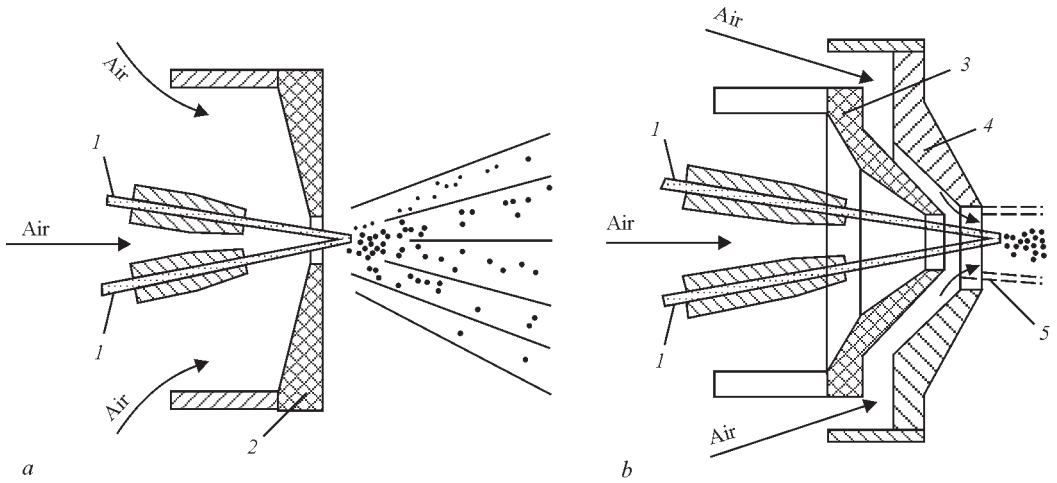

Figure 3. Basic diagram of serial EM-14 (*a*) and modernized EM-14M (*b*) EAM torches, used for comparative investigations of spraying process and coating characteristics: *1* — flux-cored wire; *2* — standard nozzle; *3* — shaped ceramic nozzle; *4* — additional nozzle for formation of concurrent air nozzle; *5* — concurrent air flow

of the sprayed material particles results in rise of their velocity and intensifying the dynamic interaction with the base, reduction of coating porosity, decrease of size of sprayed lamellae, and respectively, rise of velocity of cooling of sprayed particles on the base and increase of amount of fast-quenched metastable structures in the coating.

Analysis of expression (1) [11] shows that the higher rate of electrode melting, frequency of release of liquid metal and reduction of mass of molten metal at the wire end is provided at the same value of welding current , density of material and geometry of FCW being sprayed due to presence of two heat sources at supersonic electric arc spraying (electric arc and high-temperature flow of hydrocarbon gas combustion products) as well as more efficient structure of the metallizing torch, from point of view of melting of FCWs:

$$m_{\text{l.m}}^{nn} = \frac{AI_{\text{a}}^2\gamma v_{\text{e}}^2\left(1+2.3\lg\dfrac{r_{\text{e}}}{4\delta\sin\dfrac{\omega}{2}}\right)\left(\dfrac{M}{\gamma}\right)^{2/3}}{12.6f^2(1.5T_{\text{b}}-T_{\text{l.m}})\sin^2\left(\text{arctg}\dfrac{2v_{\text{e}}\sin\omega}{fd_{\text{e}}}\right)}, \quad (1)$$

where I_{a} is the arc current; γ is the density of electrode metal; v_{e} is the rate of electrode melting (feed); ω is the angle between the electrodes; M is the molecular weight of electrode material; f is the frequency of liquid metal release; T_{b} is the temperature of electrode metal boiling; $T_{\text{l.m}}$ is the temperature of liquid electrode metal; d_{e}, r_{e} are the diameter and radius of electrodes being sprayed; δ is the thickness of shell of FCW; $A = 0.005$ N/A^2 is the coefficient.

The experimental data (see Table 2) verify the results of theoretical analysis.

Sparcely alloyed FCW based on Fe–Cr–C system was used as a material for spraying. Carbon ferrochrome is the main component of powder core. Selection of composition of this FCW is based on further development of approaches to alloying of the FCWs for metallizing [6, 11]. These approaches provide for such a choice of the components of powder filler promoting formation of the sprayed coating on composition close to chromium steels, containing 1–2 % C and 4–10 % Cr and having tendency to quenching from liquid state and, as a results, increased wear resistance. Since the coatings of friction assemblies of railway rolling stock parts operate at increased dynamic loads, they have increased requirements to cohesion strength. Therefore, the following methods were used for increase the cohesion strength of such coatings with the base in development of composition of FCWs for deposition of coatings on the indicated types of parts, taking into account the peculiarities of technology of supersonic electric arc spraying:

- increase of temperature of the particles being sprayed due to aluminothermic reactions, which are provided by means of addition of hematite and aluminum (Fe_2O_3 + Al = Al_2O_3 + Fe + Q) mixture. The result of such reaction is a rise of temperature of the particles being sprayed, and formation of aluminum oxide strengthening phase in the coating;
- reduction of iron oxides, forming during melting and dispergation of FCW shell and charge, by means of introduction of alumo-containing additives and foundry alloys including mish metals, with exothermal reactions;
- increase of arc temperature and reduction of size of arc column due to entering of optimum amounts of additives of alkali metal halogenides.

Rise of temperature of the particles being sprayed and increase of their dispersion is very important, particularly, when applying spraying at supersonic velocities of jet flow, since in this case the time of

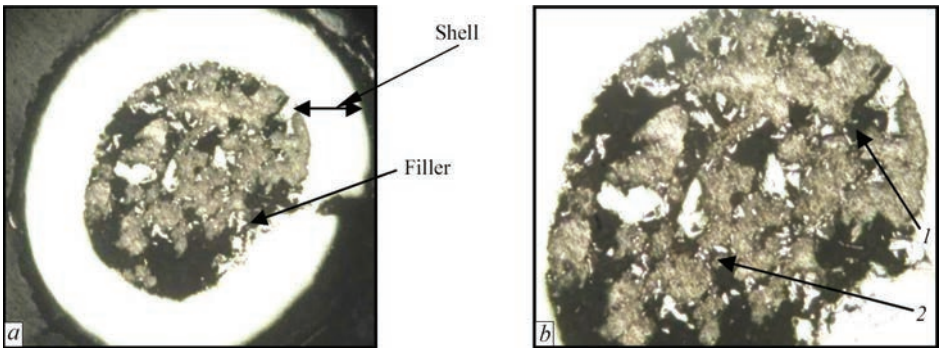

Figure 4. Microstructure of cross section of PP-AN202-S FCW (*a* — ×50; *b* — ×100): *1* — composition of particles 16.6 Fe, 82.8 Cr, 0.36 Al, 0.2 Mn; *2* — 0.36 Fe, 0.2 Cr, 99.67 Al, 0.07 Mn

holding of molten droplet at the wire end in high-temperature zone of electric arc is significantly reduced in comparison with the traditional technologies of spraying using low-velocity (subsonic) jets. Also, at that strong metallurgical bonds between the particles being sprayed and metallic base are developed due to activation of chemical interaction between them and base and receiving solid and strong oxides.

Due to the fact that different hardness indices are necessary depending on types of parts of rolling stock, a range of compositions of PP-AN202-S FCWs were developed for providing different hardness and tribotechnical characteristics. The mandatory requirement as a result of supersonic electric arc spraying of such FCW was to receive an alloy having a tendency to quenching from liquid state, and obtaining the coating on composition close to chromium steels with 1–2 % C and 4–10 % Cr containing metastable quenching structures based on oversaturated solution.

Calculation of relationship of elements' concentration in the sprayed layer and concentration of components of powder charge was carried out based on solving the system of equations [11]

$$A_a = \frac{\eta_a}{100}(x_1 k_1^{(a)} + x_2 k_2^{(a)} + \dots x_n k_n^{(a)})k_f,$$

$$A_i = \frac{\eta_i}{100}(x_1 k_1^{(i)} + x_2 k_2^{(i)} + \dots x_n k_n^{(i)})k_f,$$

where a, … i are the alloying elements; η_a, η_i are the coefficients of transfer of these elements; x, … x_n is the fraction of materials (ferromanganese, ferrochromium, metallic aluminum etc.); $k_1^{(a)} \dots k_n^{(a)}$, $k_1^{(i)} \dots k_n^{(i)}$ is the concentration of elements in corresponding materials, being introduced into the charge of flux-cored rod; k_f is the filling coefficient (k_f = 0.15–0.45).

Composition and microstructure of initial FCW of Fe–Cr–C system and coatings, produced by electric arc spraying method using subsonic and supersonic jets, were investigated. 08kp steel strip was used for manufacture of shell of this FCW. The main components of the flux-cored charge were high-carbon ferrochromium FKh900 and iron powder with ferromanganese additives. PZhR5.315.28 hematite MRTU 14-14r-84 and aluminum powder PA-3s of up to 150 μm particle size were used as exothermal additives. The microstructure and composition of this FCW and powder filler are shown in Figure 4.

Analysis of the results of metallographic examinations of the coatings showed that the microstructure at subsonic velocities of air flow is inhomogeneous, coarse grained, with large amount of pores and oxide inclusions. Material of the coating is overheated, oxidized, oxide interlayers contain 29–32 % of oxygen, and weight fraction of oxygen in the lamellae reaches 2.5 %. Spherical shape particles are also observed. They due to slow flight velocity had time to cool down before collision with the surface being sprayed (Figure 5, *a*). The coating, made using modernized standard unit applying additional air flow and regulated expansion angle of particles' flow, is less oxidized. Weight fraction of oxygen in the lamellae and oxide interlayers makes 1.6–1.8 and 29–30 %, respectively. The thickness of lamellae for these coatings is the same as in similar subsonic modes and makes δ = 10–30 μm (Figure 5, *b*), coating porosity is 2–3 %.

At transfer to the supersonic air-gas method of metallizing, rise of air jet velocity promotes for increase of particle flow and microstructure of the received coating undergoes significant changes. Combination of small size of the particles being sprayed and their high velocities during collision with the base surface results in high velocities of cooling of their material. The particles are mainly of lamellar shape and undergo significant deformation. No inclusions of the globular particles are observed. Thin oxide interlayers are noted. The coatings on the whole thickness have uniform thin lamellar structure that indicates process stability. Thickness of the coatings, deposited at supersonic air-gas spraying, lie in δ = 5–10 μm range (Figure 5, *c*). Porosity of the structure reduces and makes 0.4 %.

The analysis of the results of X-ray spectrum microanalysis and diffractograms of the coatings

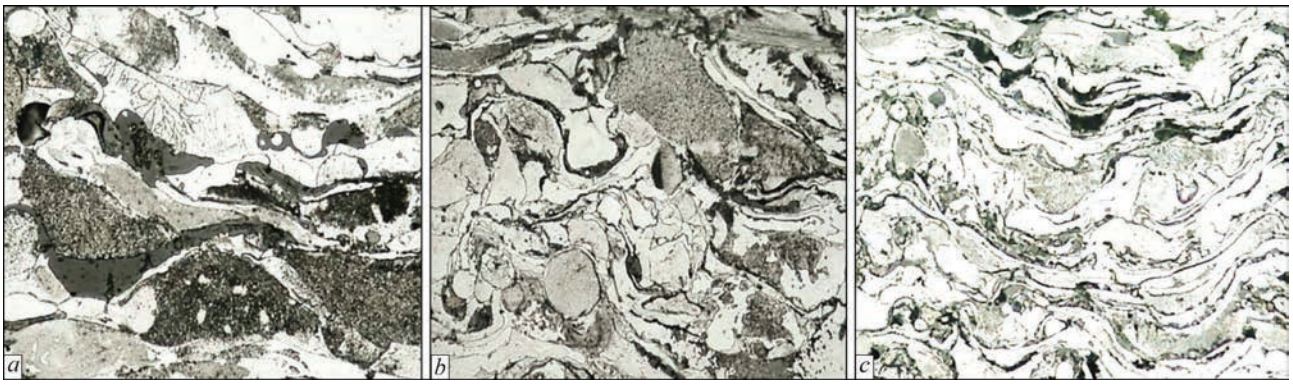

Figure 5. Microstructure (×400) of coatings from flux-cored wire of Fe–Cr–Al system produced by spraying using serial EAM torch EM-14 (*a*), modernized torch EM-14M (*b*) and supersonic torch PLAZER15-SA-EM (*c*)

showed that all examined coatings, produced by methods of usual subsonic EAM, modernized and supersonic EAM contain a solid solution of aluminum and chromium in α-iron (body-centered cubic lattice with a = 0.287 nm), and solid solutions of aluminum and chromium in γ-iron with face-centered cubic lattice and different content of these elements. Based on data of X-ray spectrum microanalysis, the prevailing structure in the coating at simple arc and modernized metallizing is a solid solution of chromium with aluminum in α-iron, and in the case of supersonic EAM the main phase of the coating is γ-phase. At supersonic EAM and modernized EAM the phase constituent of γ-iron with changed parameters exists in two modifications, namely γ_1 = Fe (Cr, Al) with a = 0.3677 nm and γ_2 = Fe (Cr, Al) with a = 0.3633 nm [12].

The difference in values of parameters of γ_1-Fe and γ_2-Fe lattice indicate the different content of alloying elements. It is determined that the maximum concentration of chromium in the solid solution based on iron in the lamellae of the coatings, produced at simple and modernized spraying, makes 16.8–17.1 and 15.0–15.4 wt.%, respectively, under the same conditions the aluminum content is approximately from 4.0 to 6.2 %. Besides, in process of spraying aluminum reacts with oxygen forming Al_2O_3 inclusions, containing 35–39 wt.% Al and 29–32 wt.% O [12]. In use of supersonic jets a turbulent mode of jet flow is turned into lamellar one, that reduces air admixing and, simultaneously, increases particles' velocity due to rise of gas jet velocity. At supersonic spraying amount of chromium and aluminum, dissolved in iron, rises and the maximum concentration of chromium in the lamellae reaches 20.0–20.5 wt.%. Solid solution of such concentration is characterized by high oxidation resistance of air oxygen. The level of oxidation of the sprayed coating is significantly reduced. The lamellae include around 1 % O. Work [12] gives more detailed results of investigations of structure of these types of coatings.

The comparison of microhardness values of the coatings from FCWs, sprayed by different methods, shows that the microhardness of coating, produced at simple EAM, varied in 1930–4200 MPa ranges, the microhardness of coating, made on modernized unit, changes in the range from 2540 to 5100 MPa. The maximum microhardness is typical for the supersonic coatings, where the range of values lies in 3900–6100 MPa limits that can be related with increase of chromium content in iron-based solid solution.

The value of failure stress in coating–steel 45 base combination at normal tear, determined on «tapered pin» technology, was used in a comparative estimation of coating cohesion strength σ_{coh} with the base. The results of testing prove the efficiency of application of the supersonic electric arc spraying technology and almost 2 times increase of the values of cohesion strength of coating to base in comparison with the traditional technology (Figure 6).

Tribotechnical tests of considered coatings were carried out under conditions with limited lubrication using disc with coating–block schemes (rider — cast iron SCh-20 and steel 40Kh, P = 10 MPa, ν = 1 m/s, oil NS20, 30 drop/min). It is determined that the technology of electric arc spraying has significant effect on intensity of wear-out of the coatings from FCW based on Fe–Cr–C of PP-AN202-S grade. A value of wear-out intensity of the coatings, deposited using supersonic electric arc spraying with the help of EAM torch PLAZER15-SA-EM, makes 3.1 μm/km, when this index for the coatings, deposited using modernized EAM torch EM-14M, makes 4.3 μm/km, and for serial metallizing torch EM-14 it is 7.8 μm/km. Application of technology of the supersonic electric arc spraying allows more than 2.5 times increase of coating wear resistance. At the same time, all investigated coatings exceed EAM of steel 20, the wear values of which makes around 10 μm/km.

Based on the technological investigations and experience of the supersonic wear resistance, the developed

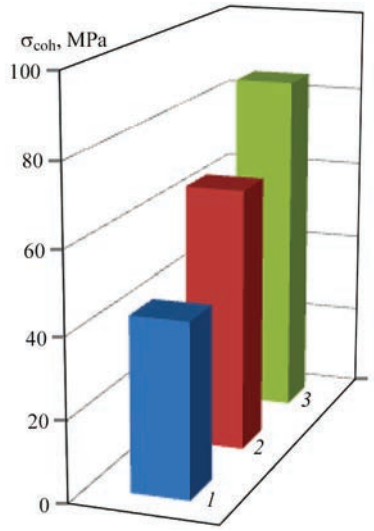

Figure 6. Cohesion strength of steel 45 base to coatings from PP-AN202-S FCW produced with serial EAM torch EM-14 (*1*), modernized torch EM-14M (*2*) and supersonic torch PLAZER15-SA-EM (*3*)

technology and FCW based on Fe–Cr–C of PP-AN202-S grade were used for reconstruction of the heavy-duty crankshafts of locomotive diesels 12VFE 17/24 of D1 trains of Hungarian production. Improved supersonic EAM torch PLAZER15-SA-EM (Figure 7, *a*) was used in 2012–2013 to modernize the process area for electric arc spraying of crankshafts of locomotive diesels 12VFE 17/24 at locomotive facility in Illovaysk (Ukraine).

It is determined as a result of operation of the reconstructed locomotive crankshafts of these grades that no technical defects of the coating and shafts were registered, and service period of the reconstructed crankshaft journals is 2 times more than in new ones. It is important that the coating has a high survivability in comparison with the base metal of the crankshaft under extreme and emergency situations (stop of oil supply, presence of abrasive particles).

Also this technology became a basis for organizing a process area of supersonic electric arc spraying of axles of wheel sets of railway transport (Figure 8) at Korosten locomotive facility in 2013. It is shown that application of the developed technology and equipment for supersonic electric arc spraying of coatings on journals and seats of wheel sets of freight cars, simultaneously with application in spraying of sparcely-alloyed FCW based on Fe–Cr–C of PP-AN202-S grade allow acquiring higher surface hardness and larger depth of strengthened layer in comparison with the requirements of reference documents.

In the conclusion it should be noted:

1. Improvement of quality of wear-resistant coatings for critical parts of rolling stock by means of application of the developed technology of supersonic electric arc spraying was received due to the following new engineering solutions:

● application of improved design supersonic EAM torch PLASER15-SA-EM realizing hybrid process combining electric arc spraying with supersonic gas spraying at formation of single supersonic high-temperature gas flow and blowing of the stabilized electric arc with natural gas hot combustion products;

● application of special FCW based on Fe–Cr–C of PP-AN202-S grade developed for the supersonic electric arc spraying having alloying system providing formation of the sprayed coating close on composition to chromium steels containing 1–2 % C and 4–10 % Cr, which are characterized by a tendency to quenching from liquid state. At that given FCWs include the additives realizing a series of effects and providing rise of cohesion strength of sprayed coatings to the base, namely:

♦ increase of temperature of the particles being sprayed due to alumothermal reactions, which are provided by means of addition of hematite and aluminum mixture ($Fe_2O_3 + Al = Al_2O_3 + Fe + Q$). A result of such a reaction is increase of temperature of sprayed particles, and formation of oxide aluminum strengthening phase in the coating;

♦ reduction of iron oxides, forming in process of melting and dispersion of shell and charge of the FCW

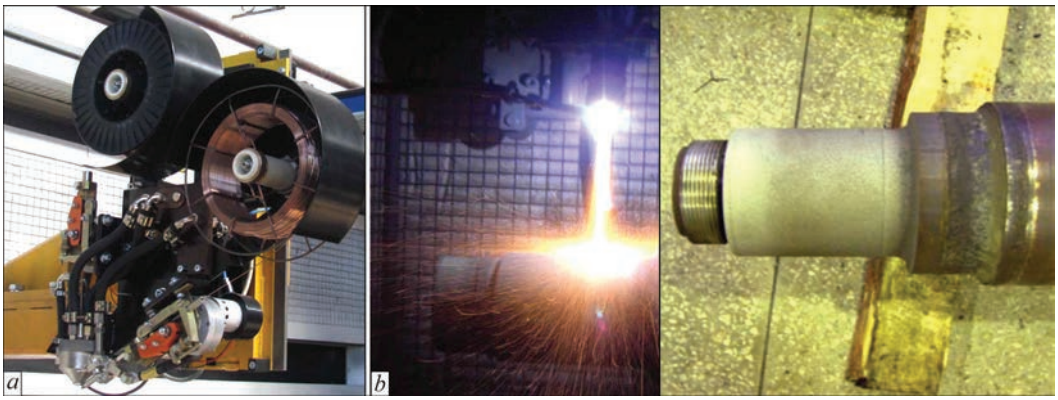

Figure 7. Appearance of block of machine supersonic metallizing torch PLAZER15-SA-EM of PLAZER15-SA unit (*a*), and process of spraying of wear-resistant coating from Fe–Cr–C-based FCW on on axle journals of railway transport wheel set (*b*)

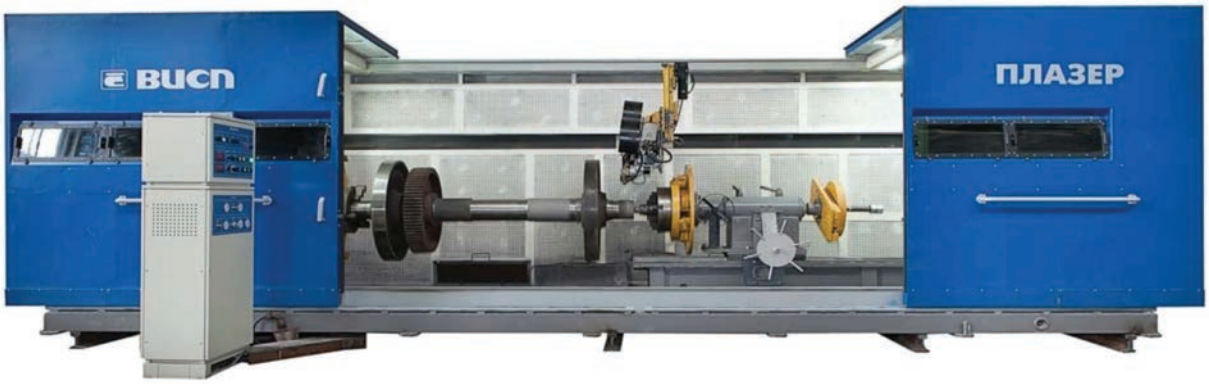

Figure 8. Appearance of engineering complex for supersonic spraying of wear-resistant coatings on axle journals of wheel sets at Korosten locomotive facility (Ukraine)

by means of entering aluminum-containing additives and foundry alloys with mishmetals and exothermal reactions;

♦ increase of arc temperature and reduction of size of arc column due to introduction of optimum amount of additives of alkali metals halogenides.

2. The coatings produced using developed technology of supersonic electric arc spraying applying FCW based on Fe–Cr–C system of PP-AN202-S grade have a structure with austenite content up to 80 wt.%. Coating strengthening is provided by formation of the oversaturated solid solution of iron with increased content of chromium to 20.5 wt.% and aluminum to 6.2 wt.%.

Microhardness of the coating is approximately 30–50 % higher than the microhardness of the electric arc coatings from the same wire, produced using traditional subsonic technology, oxidation of the material being sprayed is 2–3 times reduced, and porosity decreases 3–5 times. Cohesion strength of steel coating with steel base rises from 25–30 to 80 MPa in comparison with application of serial metallizing torch, coating porosity reduces from 15–20 to 0.5–3.0 %, material oxidation drops 2 times. Also, the technology of supersonic electric arc spraying, in comparison with traditional EAM methods, allows increasing wear resistance of the coatings more than 2.5 times.

3. Developed technology, equipment and consumables were used in order to increase the quality of the coatings for reconstruction of the critical parts of railway stock at modernizing the process area for electric arc spraying of crank shafts of locomotive diesels 12VFE 17/24 at Illovaysk locomotive facility in 2012–2013 as well as during organizing of the process area for supersonic electric arc spraying of wheel set axles of railway transport at Korosten locomotive facility in 2013.

The work was carried out under support of Chinese Program of Foreign Experts No. WQ20124400119, Guangdong Innovative Research Team Program No. 201101C014901263, Project of Guangdong Provincial Key Laboratory No. 2012A061400011, China.

1. Kuzmin, V.P., Berdin, M.M., Kuleshov, E.S. et al. (2002) Reconditioning of axle necks of wheel pairs by surfacing. *Zheleznodoroznhy Transport*, **1**, 46–49.
2. Kuzmin, V.P. (2001) Reconditioning of axle necks of car wheel pairs by arc spraying. *Vestnik VNIIZhT*, **1**, 46.
3. Korzhik, V.N., Krivtsun, I.V., Petrov, S.V. et al. (2009) New technology PLAZER for reconditioning of railway parts. *Remont, Vosstanovlenie, Modernizatsiya*, **1**, 20–22.
4. Korzhik, V.N., Kharlamov, M.Yu., Petrov, S.V. et al. (2001) Technology and equipment for reconditioning of railway transport critical parts by plasma-arc spraying. *Vestnik VostochnoukrNU*, **14**, 76–84.
5. Zelenin, V.I., Kavunenko, P.V., Tisenkov, V.V. et al. (2009) Application of plasma-arc metallization for restoration of wheel pairs. *The Paton Welding J.*, **12**, 28–31.
6. Pokhmursky, V.I., Student, M.M., Dovgunyk, V.M. et al. (2003) Structure and tribotechnical characteristics of coatings produced by electric arc metallizing using flux-cored wires. *Ibid.*, **8**, 12–16.
7. Borisov, Yu.S., Petrov, S.V. (1995) Application of supersonic jets in thermal spraying technology. *Avtomatich. Svarka*, **1**, 41–44.
8. Frolov, V.A., Poklad, V.A., Ryabenko, B.V. et al. (2006) Technological specifics of methods of supersonic thermal spraying (Review). *Svarochn. Proizvodstvo*, **11**, 38–47.
9. Petrov, S.V., Karp, I.N. (1993) *Plasma air spraying*. Kiev: Naukova Dumka.
10. Petrov, S.V., Karp, I.N. (2011) Unit of supersonic arc spraying PLAZER15-SA. *Svarshchik*, **1**, 17–21.
11. Royanov, V.A. *Theoretical principles of development and commercialization of sparcely-alloyed flux-cored wires for arc spraying of wear-resistant coatings with improved operational properties*: Syn. of Thesis for Dr. of Techn. Sci. Degree. Minsk: BPI.
12. Korzhik, V.N., Borisova, A.L., Gordan, G.N. et al. (2014) Peculiarities of structure of coatings of Fe–Cr–Al system flux-cored wire produced under conditions of supersonic electric arc metallization. *The Paton Welding J.*, **2**, 31–36.

Received 22.12.2016

doi.org/10.15407/tpwj2016.09.05

INVESTIGATION OF WEAR RESISTANCE OF PROTECTIVE COATINGS UNDER CONDITIONS OF HYDROABRASIVE WEAR

B.V. STEFANIV
E.O. Paton Electric Welding Institute, NASU
11 Kazimir Malevich Str., 03680, Kiev, Ukraine. E-mail: office@paton.kiev.ua

Increase of service life of the drill bits with protective coatings, operating under conditions of abrasive, erosion and corrosion wear, is the most relevant problem in Ukraine. Aim of present work is to study wear resistance of the protective coatings under conditions of hydroabrasive wear. The investigation of wear resistance was made on the protective coatings, containing tungsten carbides, TeroCote 7888T, Diamax M and relite LZ-11-7, being arc deposited on steel 45, under conditions of abrasive wear. It is determined that wear resistance of relite LZ-11-7 and Diamax M composite alloys, consisting of Fe-based reinforcing particles (fused spherical and crushed tungsten carbide), has selective character and insignificant dependence on properties and hardness of a matrix. Application of Ni-based composite alloy TeroCote 7888T (split tungsten carbide) provides for efficient protection under conditions of hydroabrasive wear. At room temperature the wear resistance of the protective TeroCote 7888T coating 1.5 and 2 times exceeds the wear resistance of relite LZ-11-7 and Diamax M, respectively. This alloy allows increasing service life of the protective coatings of reconditioned defect areas of drill bits' bodies, which operate under heavy conditions of corrosion-abrasive wear. 10 Ref., 3 Tables, 5 Figures.

Keywords: *surfacing, surfacing consumables, tungsten carbides, structure, strength, wear resistance, composite alloys, hardness, relite*

In recent decades, the steel drill bits with protective coatings of work tools have acquired wide application in drilling of gas and oil wells. Carried analysis of the waste drill bits having protective coatings showed that drilling mostly provokes wear of blades, seats and less often fluid-discharge ports of the drill bits' bodies [1–4]. The specific attention was paid on wear of the blade seats, since the blades take the major load in drilling. Mechanic interaction with mine rock provides for breaking of the blades as well as the seats. The wear-resistant coatings preserve the seats of cutting blades and the assemblies of fluid-discharge ports of drill bits' bodies from hydroabrasive and corrosion wear.

Increase of service life of the drill tool operating under conditions of hydroabrasive wear and impact loading is a relevant problem in Ukraine. Currently, there are only methods for reconstruction of worn blades of the drill bits. Reconstruction of the protective coatings of the seats of work tools requires reconstruction of geometry of the base metal opening, i.e. deposition of intermediate layer of base metal and after this a layer of protective hard-alloy coating using different methods. The leading foreign companies have been using the wear-resistant coatings of different functional designation in their products for a long time [5–9].

The main task of this work is an investigation of wear resistance of the protective coatings under conditions of hydroabrasive wear.

Surfacing composite alloys consisting of reinforcing WC particles and matrix differ by high wear resistance under conditions of abrasive, erosion and corrosion wear. A typical peculiarity of the wear-out process of such alloys is a step-by-step wear of the separate components of the composition. At that, such a called shadowing effect, when the prominent more wear-resistant reinforcing particles bear the major load of the destructive forces, thus preserving alloy matrix from wear, can be observed.

The protective coating is a surface layer of the drill bit work tool, which is intentionally developed by environment effect on drill material surface and characterized by final thickness as well as chemical composition and structure-phase state different from the similar characteristics of base metal. The existing methods of coating deposition over the base metal can be classified as mechanical, physical, chemical and electro-physical on production method; galvanic, vacuum and deposits on methods of technological process; wear-, corrosion-, heat-resistant and others on their functional designation.

The results of investigation of technology of drill bits repair [2–4] were used for carrying out the works on selection of a method of protective coating deposition on the worn parts of bodies' work tool. The properties

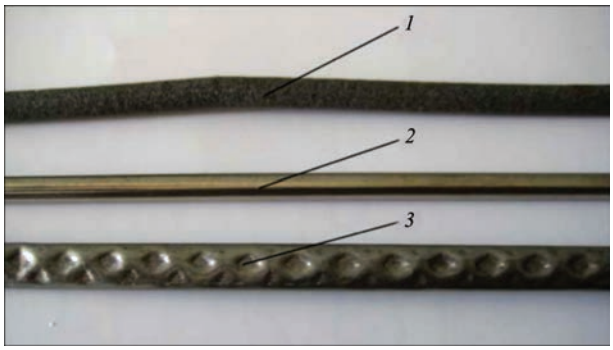

Figure 1. Appearance of surfacing consumables: *1* — TeroCote 7888T (Castolin) based on nickel; *2* — Diamax M (Castolin) based on iron; *3* — relite LZ-11-7 (Ukraine) based on iron

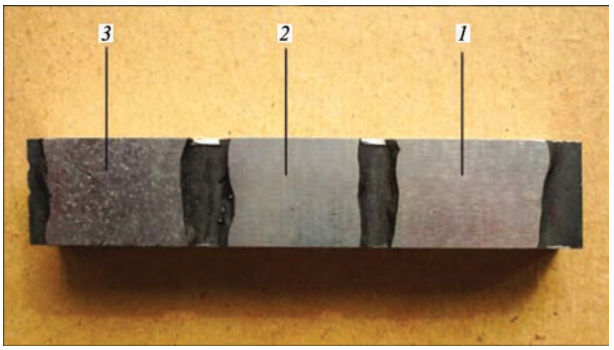

Figure 2. Macrostructure of specimen with protective coatings deposited using surfacing consumables: *1* — TeroCote 7888T; *2* — Diamax M; *3* — relite LZ-11-7

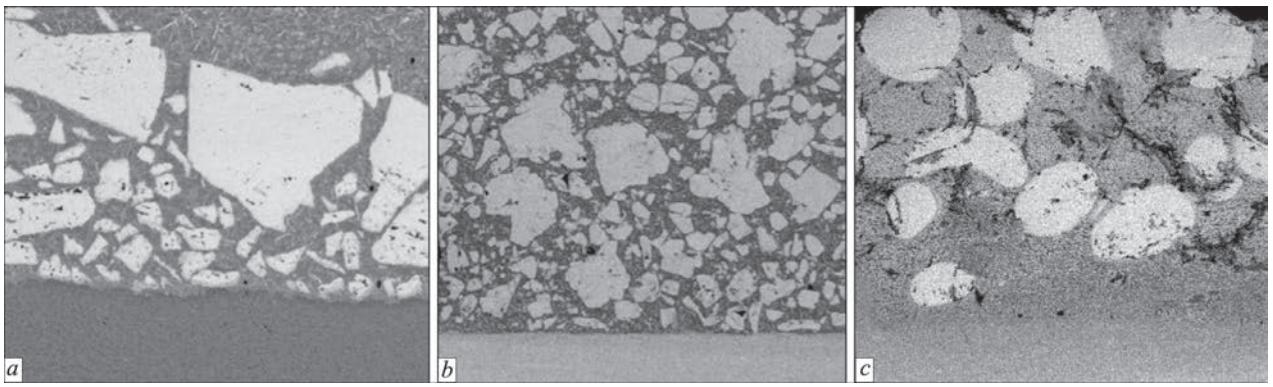

Figure 3. Microstructure (x100) of metal of coatings produced using filler materials: *a* — TeroCote 7888T; *b* — Diamax M; *c* — relite LZ-11-7

of existing wear-resistant materials and reconstruction technology, which could provide all physical-chemical properties of the base metal of steel drill body, were investigated for fulfilment of this task.

Composite materials, containing different-based tungsten carbides (Figure 1), were taken for investigation of wear resistance of the protective coatings under conditions of hydroabrasive wear.

Table 1. Composition and hardness of layers deposited on steel 45

Surfacing consumables	Type of tungsten carbide granules	Composition, wt.%							Hardness *HRC* (average)
		C	Ni	Cr	Fe	Si	W	Mn	
TeroCote 7888T	Split	9.31	33.49	3.62	1.15	–	50.38	–	48.3
Diamax M	Crushed	13.19	–	–	27.60	–	58.32	0.89	57
Relite LZ-11-7	Spherical	11.98	–	0.14	21.23	–	65.33	1.32	58.8
Reference specimen	Steel 45	0.42–0.50	0.25	0.25	97	0.17–0.37	–	0.5–0.8	30

Table 2. Composition, hardness and wear of deposited layers (L = 250 m)

Number of specimen	Surfacing consumables	Surfacing method	Matrix hardness *HRC*	Mass of specimens, g		
				Before	After	Difference
Reference specimen 1	Steel 45	–	30	12.82	12.51	0.31
1.1	TeroCote 7888T	Arc	45	14.26	14.23	0.03
1.2		Arc	50	13.95	13.91	0.04
1.3		Arc	50	14.32	14.28	0.04
Reference specimen 2	Steel 45	–	30	12.90	12.59	0.31
2.1	Diamax M	Arc	56	14.36	14.26	0.10
2.2		Arc	59.5	14.28	14.20	0.08
2.3		Arc	55.5	14.22	14.08	0.14
Reference specimen 3	Steel 45	–	30	12.86	12.56	0.30
3.1	Relite LZ-11-7	Arc	55	14.25	14.20	0.05
3.2		Arc	60	14.23	14.16	0.07
3.3		Arc	61.5	14.05	13.98	0.07

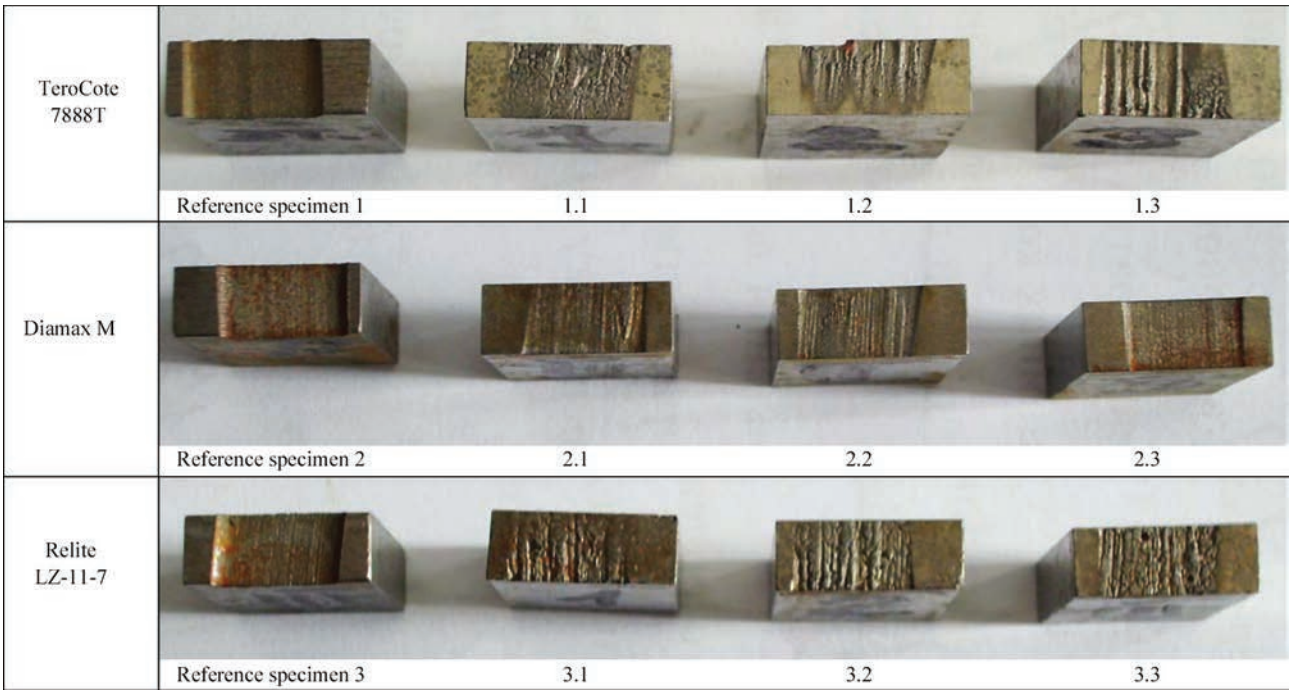

Figure 4. Appearance of specimens, deposited with different composite materials, after hydroabrasive wear testing (L = 250 m)

Pilot specimens produced from steel 45 of 20 mm thickness (Figure 2) were used to investigate the deposits using selected wear-resistant materials. Manual shielded gas (technical argon) TIG welding was taken as a method of surfacing.

Measurements of hardness *HRC* on the deposit surface were carried out using versatile device TP5006. As a result it was determined that hardness of the deposited layers in surfacing on steel 45 (reference) using filler materials Diamax M and relite LZ-11-7 is on average 15–20 % higher than using TeroCote 7888T (Table 1). Metallographic examinations of the deposited specimens were carried out using optical microscope Neophot-32 (Figure 3). WC particles can be observed in the coatings based on nickel (TeroCote 7888T) and iron (Diamax M and relite LZ-11-7). At that, the reinforcing particles are chaotically located along the deposited bead section. Such an inhomogeneity of tungsten carbide particle distribution along the deposited bead section is caused by variation of hardness depth and can effect coating resistance to hydroabrasive wear. Works [2–4] show that composite wear-resistant material TeroCore 7888T is more perspective. It contains ultra-hard tungsten carbides in a solid matrix of nickel-chromium alloy, which absorbs impact loads and improves resistance to abrasive wear and corrosion, while uniform split profile particles of tungsten carbides make difficult their breakaway from the matrix.

Resistance of the deposited coating to hydroabrasive wear was determined on NK-M machine [10]. Test validity for each composite material was evaluated on three specimens. Quartz glass of 0.05–0.50 mm was used as an abrasive. The plates of 20×16×6 mm were applied as specimens. They were produced in the following way. Wear-resistant materials based on nickel

Table 3. Composition, hardness and wear of deposited layer (L =1250 m)

Number of specimen	Surfacing consumables	Surfacing method	Matrix hardness *HRC*	Mass of specimens, g		
				Before	After	Difference
Reference specimen 1	Steel 45	–	30	12.20	10.70	1.50
1.1	TeroCote 7888T	Arc	45	12.07	11.85	0.22
1.2		Arc	50	13.57	13.39	0.18
1.3		Arc	50	13.95	13.70	0.25
Reference specimen 2	Steel 45	–	30	12.18	11.30	1.50
2.1	Diamax M	Arc	56	13.93	13.53	0.40
2.2		Arc	59.5	13.84	13.29	0.55
2.3		Arc	55.5	13.87	13.56	0.31
Reference specimen 3	Steel 45	–	30	12.15	10.66	1.49
3.1	Relite LZ-11-7	Arc	55	13.64	13.35	0.29
3.2		Arc	60	13.85	13.64	0.21
3.3		Arc	61.5	13.69	13.20	0.49

and iron with tungsten carbide were deposited on plate of 22×20×100 mm size (see Figure 2) by arc surfacing. Thickness of the deposited layers made 5–7 mm. After surfacing the specimens of 21×17×7 mm were cut out by erosion. Each specimen was polished to bring to necessary size of 20×16×6 mm. Thickness of the deposited layer made 3 mm. Wear of the specimen was evaluated on loss of its weight (Figure 4, Table 2). Weighing was carried out on electronic scales OHAUS with measurement accuracy 0.01 g. At that specific loading on the specimen made 0.5 MPa, friction velocity 0.58 m/s, friction distance 250 m.

Wear resistance of the composite alloys in hydroabrasive wear was evaluated by loss of weight of the deposited layer on friction distance. Firstly, wearing out of the matrix takes place, baring the tungsten carbides, which in turn provokes significant delay of wear of the protective coating. And further, after tungsten carbide wear out the cycle is repeated (Figure 4, Table 2). Nature of wear of the deposited layer for all composite materials approaches to linear dependence (Table 3) at increase of wear distance (L = 1250 m).

Figure 5 shows the average values of wear of the deposited layer of composite alloys in hydroabrasive wear depending on friction distance.

Conclusions

1. The results of investigations show that resistance to hydroabrasive wear of the protective coating TeroCote 7888T with split particles of tungsten carbide is 1.5 and 2 times more than wear resistance of relite LZ-11-7 (spherical granules of tungsten carbide) and Diamax M (crushed particles of tungsten carbide), respectively.

2. Composite material Castolin TeroCote 7888T is the most perspective for deposition of the protective coatings on the work tools of drill bits. The protective coatings based on this alloy allow increasing service life of the drill tool at drilling of gas and oil wells.

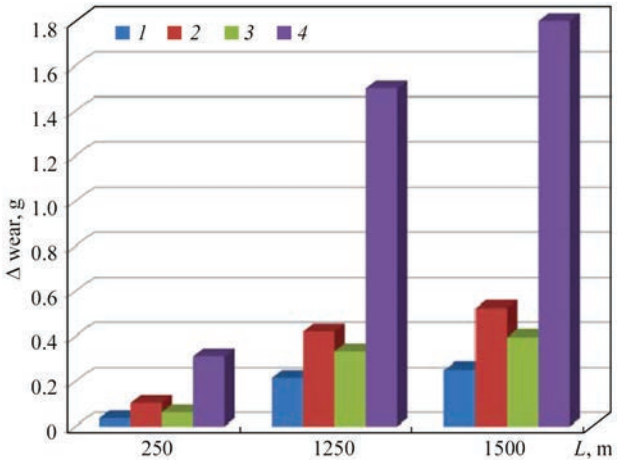

Figure 5. Wear of deposited layer from composite materials and steel 45: *1* — TeroCote 7888T; *2* — Diamax M; *3* — relite LZ-11-7; *4* — steel 45

1. Khorunov, V.F., Stefaniv, B.V., Sabadash, O.M. et al. (2012) Peculiarities of technologies for repair of drill bits with diamond-carbide cutters. In: *Problems of service life and safety of structures, constructions and machines*: Transact., 488–493. Kiev: PWI.
2. Stefaniv, B.V., Khorunov, V.F., Sabadash, O.M. (2014) Features of reconditioning steel drill bit watercourse. *The Paton Welding J.*, **11**, 50–54.
3. Stefaniv, B.V., Khorunov, V.F., Sabadash, O.M. et al. (2015) Peculiarities of restoration of working parts of drilling bit matrix bodies. *Ibid.*, **8**, 47–50.
4. Stefaniv, B.V., Khorunov, V.F., Sabadash, O.M. et al. (2012) Features of technology for repair of wear working parts of steel and drilling bit matrix bodies. In: *Problems of service life and safety of structures, constructions and machines*: Transact., 688-696. Kiev: PWI.
5. Information of company Postalloy (USA) for surfacing of protective coatings. *http*://www.postle.com
6. Information for soldering and surfacing TeroCote®. *http*://www.castolin.com.ua
7. Surfacing materials BAT-Service. *http*://www.b-trans.com.ua/qw/id/79
8. Materials for surfacing and spraying. *http*://www.kennametal.com/stellite
9. Surfacing alloy relite of LZ type. *http*://www.resource@aranei.com
10. Yuzvenko, Y.A., Zhudra, A.P., Frumin, E.I. (1973) Abrasive wear of composite alloys. *Avtomatich. Svarka*, **7**, 62–63.

Received 12.04.2016

doi.org/10.15407/tpwj2016.09.06

EFFECT OF CURRENT PULSES ON ACTIVATION OF WELDED SURFACES OF PLATES FROM DISSIMILAR METALS (STEEL 20 + COPPER M1)

L.I. MARKASHOVA[1], **N.A. ONATSKAYA**[2] and **L.Yu. DEMIDENKO**[2]
[1]E.O. Paton Electric Welding Institute, NASU
11 Kazimir Malevich Str., 03680, Kiev, Ukraine. E-mail: office@paton.kiev.ua
[2]Institute of Pulse Processes and Technologies, NASU
43-A Oktyabrsky Ave., 54018, Nikolaev, Ukraine. E-mail: iipt@iipt.com.ua

Presented are the results of engineering process of welding of plates from dissimilar metals (steel 20 + copper M1) under conditions of passing of high-density current pulses. Pulse current generator GIT-50, developed in the Institute of Pulse Processes and Technologies of the NAS of Ukraine, was used for welding processes activation. Application of complex investigation method allowed determining that different stages of the process of welded joint formation take place on a contact interaction surface of macroscopic size. It is caused by inhomogeneity of the real surfaces of solid bodies even at high class of their treatment. The results of examination of steel surface fine structure indicate that treatment of the preliminary compressed plates with the high-density pulses results in significant activation of the dislocation transformations, having significant effect on development of the third stage of solid state welding process, i.e. stage of volumetric interaction. 7 Ref., 2 Figures.

Keywords: *welded joints, dissimilar materials, high-density current pulses, contact zone, electron microscopy, dislocation structure, activation of contact surface*

Bimetallic joints, i.e. joints consisting of dissimilar on their properties metals and alloys [1, 2], are widely used in recent time in different products of current engineering. This allows using in full scope the specific properties of each of them as well as reducing the consumption of expansive and scarce metals and obtaining the parts with high service properties. Since the majority of combinations of dissimilar metals and alloys are characterized by different physical-chemical properties, it is clear that such type of differences will result in significant difficulties in receiving their quality welded joints, in particular, under fusion welding conditions. Therefore, different methods of pressure welding are used for performance of such types of dissimilar joints.

The necessary condition of welded joint formation for any method of pressure welding is a plastic deformation of the materials being welded [3, 4]. However, in some cases the processes of plastic deformation appear to be frozen due to high resistance of corresponding material to deformation. Then the special methods are used intensifying further deformation development. One of the methods, which has found application in industry, is a high-density pulse current (~ 10^9 A/m) impact of the deformed metal [5]. Earlier we have proved an activating effect of current pulses on plastic deformation of the preliminary compressed plates of similar materials (such as steel 20 + steel 20) under effect of high-density current pulses in pressure welding [6]. However, now scientific-and–technical literature contains no information on processes, taking place in the near-contact zones of metal of joined plates from dissimilar materials under such effect.

An aim of this work is to study an effect of high-density current pulses on the processes promoting activation of the contact surfaces of steel 20 + copper M1 dissimilar metals in their joining in solid state.

Materials and procedures used for investigations. Plates of 170×12×2.5 mm size were taken as reference specimens, where a welding zone $l \approx 22$ m was taken in the middle of the specimen.

Contact surface of the copper plate were polished to comb (roughness peaks) height from ~ 8 to ~ 10 μm. Combs' height of the surface of more rigid steel plate after polishing made from ~ 2 to ~ 3 μm. A difference on height of geometry of welded surfaces is caused by the fact that formation of physical contact in welding of dissimilar materials takes place, as a rule, as a result of microplastic deformation of softer material [4]. After cleaning the surfaces of both plates (acetone degreasing) the plastic deformation of microprojections of contact surfaces was carried out in special device at 50 MPa pressure, and then pulse current of up to 10^9–10^{10} A/m^2 density was passed at pulse duration $\tau \geq 2 \cdot 10^{-4}$ s [7].

Investigation of processes of activation of joined surfaced in welding of the compressed plates from dissimilar metals using high-density current pulses were

carried out using a complex of methods for analysis of physical processes, taking place in a contact zone of surfaces being welded. A method of scanning microdiffraction electron microscopy with JEOL JEM-200 CX unit (Japan) was used for examination of the peculiarities of dislocation structure change in sub-surface layers of metal in the contact zone. At that, the specimens for examination were prepared using the methods of special thinning by ionized beams of argon. It allows obtaining a real picture of distribution nature of dislocation density, dislocation geometry and peculiarities of formation of different types of substructures in local zones of welded metals. At that, as an object for investigation the templates of steel plate were used. They were cut out from a central part of the contact zone, where the maximum area of surface geometry crushing was registered. A reference specimen was a plate from steel 20 in as-received state. In pressure welding of dissimilar metals, having different deformation resistance, the process of joining is limited by activation of the contact surface of harder metal [4]. Therefore, the peculiarities of dislocation structure change in the sub-surface layers of deformed metal after indicated above technological effect were examined in the contact zone from the side of indicated type of metal, namely, steel 20.

Experiment results. Examinations of a fine structure of sub-surface layers of the plate from steel 20 in as-received state showed that the analyzed structure is characterized by general minimum volumetric dislocation density making from $\rho \sim 10^8$ to $\sim 2 \cdot 10^9$ cm^{-2}, comparably uniform structure of intergranular boundaries, stable dimensions of around 0.65–1 μm (Figure 1, *a*) of substructure elements (subgrains and cells) as well as clearly directed cementite plates without deformation signs (Figure 1, *b*).

After treatment of the compressed plates by current pulses the structure of sub-surface layers of plates from steel 20 takes abundant signs of deformation, namely:

- sufficiently high dislocation density from $\rho \sim 10^{10}$ to $\sim 10^{11}$ cm^{-2} was registered along the examined surface. It is almost 2 times higher the dislocation density of metal surface in as-received state;
- structure of separate grains is significantly fragmented with formation of pronounced boundaries of fragments (in Figure 2, *a* intragranular fragments of ~ (1.2–1.5) μm size are registered);
- crushing (breaking) of cementite plates takes place. Such an effect, as a rule, occurs after cold treatment of metal (Figure 2, *b*);
- structural details of the zones of geometry combs crushing are clearly developed. They represent itself a laminar pattern, including a system of shear (deformation) bands (Figure 2, *c*) forming as a result of upsetting of roughness peaks in deformation. Appearance of the shear bands (distortion of slip bands) of different width from 2 to 4 μm is caused by the peculiarities of dislocation configuration, i.e. their accumulation in the boundary slip bands. Shear band length of >> 8 μm was registered;
- fragmentation of structure, related with actively passing (in parallel with plastic deformation processes) relaxation processes are observed inside the separate shear bands. In Figure 2, *d* the relaxation is developed as formation of blocks (almost perfect areas with discrete mutual misorientation) of 0.6–1.2 μm size in the shear band from 3.3 to 3.5 μm. Figure 2, *e* shows structure fragmentation in the shear band of h = 1–3.7 μm size, accompanied by formation of ball-cellular structure with dislocation density $\rho \approx 8.6 \cdot 10^9$ cm^{-2}.

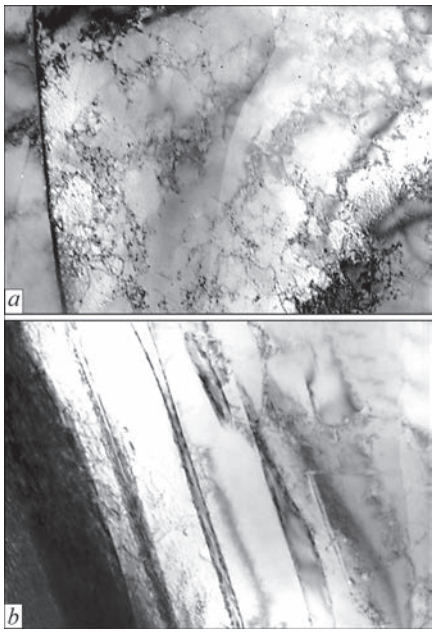

Figure 1. Dislocation structure of sub-surface layers of plates from steel 20 in as-received state: *a* — stressless grain boundary and cell structure (×20000); *b* — undeformed cementite plates (×30000)

It should be noted that in the structure of crushed roughness combs, in addition to shear band system, there are also cavities of different depth. They are characterized by lower dislocation density, corresponding on value to dislocation density in undeformed metal. These zones are the areas, where physical contact has not been yet formed, as a result of what the corresponding areas of the joint contain the pores, further healing of which is possible in a diffusion way by means of subsequent heating. Figure 2, *f* shows the structure of shear bands in roughness combs crushing, where structure of the roughness cavity (light area – potential pores) is subgrains of ~ 0.75 μm size and cells from 0.13 to 0.2 μm size with minimum density dislocation. Sufficiently high dislocation density, approximately 10^{11} cm^{-2}, is registered in the zone of roughness comb deformation (dark area — zone of deformation).

Analysis of obtained research results of the fine structure of the sub-surface layers of steel plate after treatment of preliminary compressed plates by current

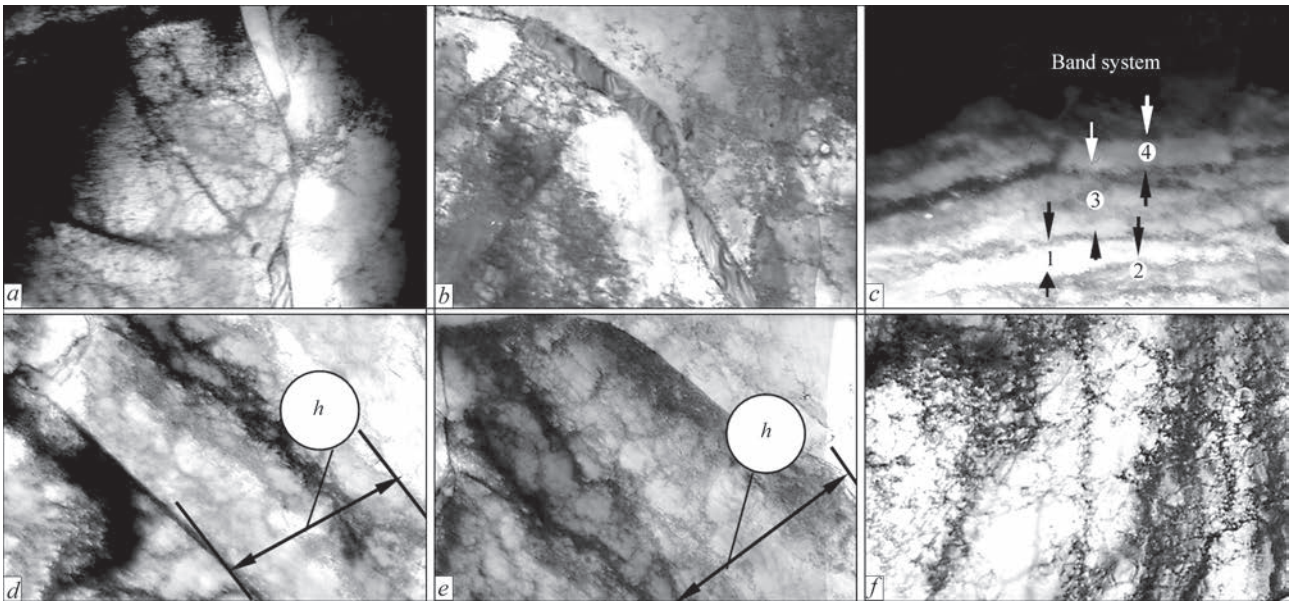

Figure 2. Dislocation structure of sub-surface layers of steel 20 plates after engineering effect: *a* — grain fragmentation (×15000); *b* — broken cementite plate (×15000); *c* — system of shear band 1–4 (×10000); *d* — formation of blocks in shear band (×10000); *e* — fragmentation of structure with formation of ball-cellular structure in shear band; *f* — structure of shear layers in crushing of roughness comb (×20000)

pulses indicate that the separate microareas (roughness combs) as a results of technological influence become the zones with high level of deformation, having typical dislocation transformations of the following types:

- more than order increase of values of dislocation density in this area, that indicates significant rise of level of internal stresses in deformation local zone;
- nonuniformity of distribution of dislocation density in the zone of localizing of steel 20 surface deformation;
- formation of shear (deformation) bands as a result of upsetting of roughness combs in the process of deformation of steel surface layers caused by build-up of dislocation accumulations in the adjacent slip planes;
- significant structure fragmentation inside the deformation bands, accompanied by formation of ball-cellular structures, indicate a rapid activation of dislocation interaction and active transformation of the fine structure, that, as a result, promotes formation of ends of dislocation jogs so called active centers [4] on steel deformed surface, resulting in activation of the contact surface.

Thus, there are two simultaneous process taking place in areas of the deformed steel surface, namely formation of the physical contact and formation of the active centers, i.e. joining zones in the layers of surface deformation, that promotes for formation of interatomic bonding. Together with mentioned above, there are also the areas (roughness cavities — pores), at which formation of physical contact is not observed.

Conclusions

1. Different stages of the process of welded joint formation take place on the contact interaction surface, having macroscopic size. It is caused by inhomogeneity of real surfaces of solid bodies even at high class of their treatment. Therefore, division of the welding process on separate stages is only true for microscopic areas of the contact surface.

2. The results of examination of the fine structure of steel surface indicate that treatment with the high-density pulses results in significant dislocation transformations, which can significantly effect the development of the third stage of solid-state welding process, i.e. stage of volumetric interaction.

1. Middeldorf, K., von Hofe, D. (2008) Trends in joining technology. *The Paton Welding J.*, **11**, 33–39.
2. Reisgen, U., Stein, L., Steiners, M. (2010) Stahl-Aluminium-Mischverbindungen: Schweissen oder Loeten? Die Kombination zweier etablierter Fuegetechnologien macht Unmoegliches moeglich. *Schweissen und Schneiden*, 62(**5**), 278–284.
3. Karakozov, E.S. (1976) *Joining of metals in solid phase*. Moscow: Metallurgiya.
4. Karakozov, E.S. (1986) *Pressure welding of metals*. Moscow: Mashinostroenie.
5. Troitsky, O.A., Baranov, Yu.V., Avraamov, Yu.S. et al. (2004) *Physical principles and technology of treatment of modern materials*. Vol.1: Theory, technology, structure and properties. Moscow; Izhevsk: IKI.
6. Onatskaya, N.A., Demidenko, L.Yu. (2010) Influence of circuit processing by current pulses on formation of physical contact in pressure welding. *Elektronn. Obrab. Materialov*, **3**, 19–21.
7. Vovchenko, A.I., Demidenko, L.Yu., Onatskaya, N.A. (2011) Intensification of plastic deformation of metal surfaces under action of current pulses in pressure welding. *Naukovi Notatky*, **32**, 63–68.

Received 23.12.2015

doi.org/10.15407/tpwj2016.09.07

EXPERIENCE IN APPLICATION OF ELECTRIC ARC SURFACING WITH FLUX-CORED WIRE AT THE ENTERPRISES OF UKRAINE

A.A. GOLYAKEVICH[1], **L.N. ORLOV**[1], **L.S. MALINOV**[2] and **V.I. TITARENKO**[3]
[1]Company «TM.VELTEK»
15 Kazimir Malevich Str., 03680, Kiev, Ukraine. E-mail: office@veldtec.ua
[2]Priazovsky State Technical University
7 Universitetskaya Str., 87500, Mariupol, Ukraine
[3]Company «REMMASH»
29 Gazeta Pravda Ave., Dnepropetrovsk, Ukraine

The surfacing using flux-cored wire finds a wide application in many branches of industry and, first of all, in the repair works. At the present time the largest manufacturer of flux-cored wires for surfacing in Ukraine is the enterprise «TM. VELTEK». In the present work the developments of this enterprise and the experience of their use in repair surfacing of rolls of rolling stands, CCM rollers, wheel cranes and also the rollers of straightening machines and critical parts of hydraulic supports of mining equipment are described. 20 Ref., 3 Tables, 7 Figures.

Keywords: *arc surfacing, flux-cored wires, repair works, wear resistance, hardness, microstructure, increase in service llife*

The first flux-cored wires for electric arc surfacing were developed in the 1950s at the E.O. Paton Electric Welding Institute [1]. In the following years due to versatility, simplicity and efficiency of manufacturing technology this type of electrode materials for arc surfacing found a wide spreading in different branches of industry [2–4]. The majority of grades of flux-cored wires of different purpose were developed at the PWI and manufactured by the PWI Experimental Production and the PWI Pilot Plant of Welding Materials [5–7]. In the 1990s and the following years the production of flux-cored wires for welding and surfacing in Ukraine was mastered by a number of new companies. Also the flux-cored wires of foreign companies appeared at the market of Ukraine.

In this article the experience of application of flux-cored wires in different branches of industry is described, which are developed and manufactured by Company «TM.VELTEK».

Surfacing of rolls of rolling stands. For surfacing of steel rolls of rolling stands of different purpose the repair services of metallurgical plants of Ukraine apply the electric arc surfacing using flux-cored wires PP-Np-35V9Kh3SF, PP-Np-25Kh5FMS, PP-AN132, PP-AN147 etc. [1, 2, 6]. The main causes of failure of steel rolls of hot rolling is the oxidation, abrasive wear and thermal fatigue. To a large extent such wear of the working surface of the roll is connected with the structural state of the metal and the morphology of its structural components [8, 9].

For surfacing of rolls of blooming stands «TM. VELTEK» proposed flux-cored wire Veltek-N505 (alloying system Fe–C–Si–Mn–W–Cr–Mo–Ni–V). The existing methods of tests on thermal resistance, heat resistance and wear at high temperatures can not provide a reliable determination of resistance of deposited metal of a particular type directly under the conditions of rolling. The field tests of rolls of rolling mill NZS-730 of the workshop «Blooming-1» at the Krivoy Rog Mining and Metallurgy Plant «Krivorozhstal» were performed deposited with flux-cored wires PP-Np-35V9Kh3SF and Veltek-N505.

The averaged values of the relative wear resistance and relative resistance to fire crack formation in deposited rolls of rolling mill NZS-730 are given in Table 1. As compared to wire PP-Np-35V9Kh3SF the formation and development of fire cracks in the depth of their penetration is 2–4 times reduced [10], which significantly reduces the depth of the groove during repair of rolls.

Table 1. Wear resistance and crack resistance of deposited rolls of rolling mill NZS-730 of the workshop «Blooming-1» at the «Krivorozhstal»

Grade of flux-cored wire	Hardness of deposited metal *HRC*	Relative wear resistance	Relative crack resistance
PP-Np-35V9Kh3SF	46–48	1.0	1.0
Veltek-N505	50–54	1.3	2.0

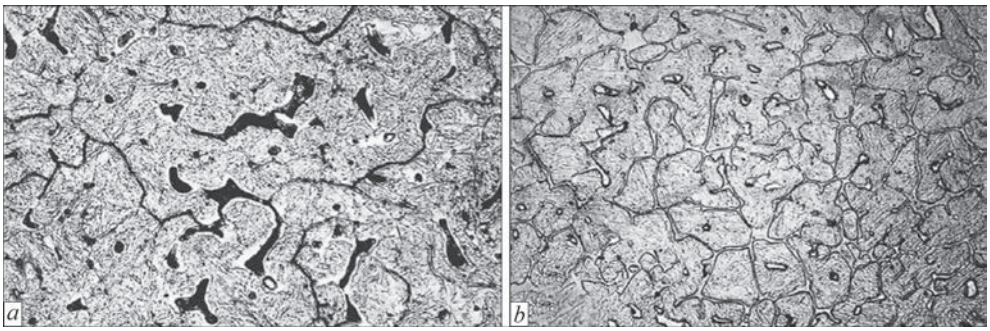

Figure 1. Microstructure (×500) of metal deposited using flux-cored wire: *a* — PP-Np-35V9Kh3SF; *b* — Veltek-N505

The microstructure of deposited metal of both types was investigated. The structure of metal deposited using wire PP-Np-35V9Kh3SF represents a coarse acicular martensite with the islands of residual austenite and elongated layers of carbide eutectics along the boundaries of primary austenite grains (Figure 1, *a*). In the body of grains and at their boundaries the carbides of chromium, tungsten and dispersed vanadium carbides are observed.

The metal deposited using wire Veltek-N505 has predominantly the structure of a fine-acicular martensite with the fringes of residual austenite along the boundaries of the primary grains. Inside the grains the uniformly distributed carbides of chromium, tungsten, molybdenum and vanadium are also observed (Figure 1, *b*).

For surfacing of rolls of the first and the second stands of pipe rolling mill TPA 30-102 of the Nikopol Seamless Pipe Plant «Niko Tube» flux-cored wire Veltek-N480NT (alloying system Fe–C–Si–Mn–Cr–V–Mo–W) was proposed. The structure of metal deposited using that wire consists of a fine-acicular martensite, residual austenite at the grain boundaries and small formations in the body of grains (Figure 2). Carbide precipitates along the grain boundaries are negligible. The dispersed carbides are uniformly distributed in the grain body along their boundaries. The hardness of deposited metal is *HRC* 50–56.

The rolls of the first stand, deposited using flux-cored wire Veltek-N480NT, were removed from the mill after 5000 t rolling of pipes. The wear on the bottom of the caliber was 0.3–0.5 mm. The condition of a surface of roll calibers is satisfactory, the surface is smooth and the cracks were absent. The wear of rolls of the second stand was 1.5–2.0 mm after rolling the 8790 t of pipes. The life of rolls of the second stand was increased from 1,200 to 8,000 t of pipe rolling.

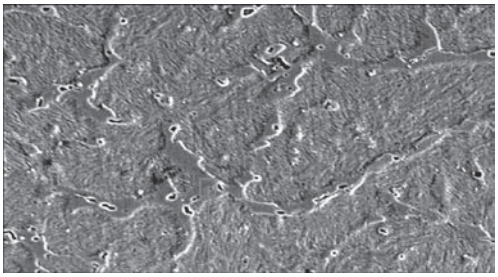

Figure 2. Microstructure (×1000) of metal deposited using flux-cored wire Veltek-N480NT

Surfacing of MCCB rollers. The domestic [11–14] and international experience shows that for surfacing of working layer of MCCB rollers the following alloying systems are mainly used: Fe–C–Cr (predominantly for straight areas of MCCB), Fe–Cr–Ni–Mo–N and Fe–C–Cr–Ni–Mo–V–Nb (predominantly for curvilinear areas of MCCB).

For surfacing of rollers of MCCB the «TM. VELTEK» proposed flux-cored wires Veltek-N470 (for submerged surfacing) and Veltek-N470G (for surfacing in the mixture of shielding gases) of alloying system Fe–C–Cr–Ni–Mo–V–Nb–N.

In the manufacture and repair of the rollers at the «Azovstal», Iliich Metallurgical Plant (Mariupol) and Novo-Kramatorsk Metallurgical Works the technology of surfacing was applied using wire Veltek-N470 of 3.0–3.6 mm diameter under fluxes AN-20 or AN-26 on a screw line using a single arc, without oscillation and with transverse oscillations. The Starokramatorsk Machine Building Plant (Kramatorsk) performed surfacing of rollers of MCCB using wire Veltek-N470G of 2.0 mm diameter in the mixture of Ar + 18 % CO_2.

The hardness of the deposited metal after smoothing amounts to *HRC* 44–48 and corresponded to the technical task of the customer. The structure of the deposited metal represents a low-carbon fine-acicular martensite hardenedd with dispersed carbides and nitrides (Figure 3). At the «Azovstal» the manufacture and repair surfacing with the mentioned flux-cored wires provided the treatment of the radial area with 3000 melts and the straight area with 7500 melts at the volume of one melt being 175 t.

Surfacing of crane wheels. For surfacing of crane wheels, as a rule, the surfacing materials are applied which provide producing the deposited metal of the type of low-alloyed steels 18Kh1G1M or 30KhGSA. However, during surfacing of heavily-loaded wheels of cranes, which operate at the metallurgical enterprises, these materials do not provide the required service life.

The increase in wear resistance of parts of the similar type can be achieved using the surfacing materials providing producing the deposited metal with the structure of metastable austenite undergoing transfor-

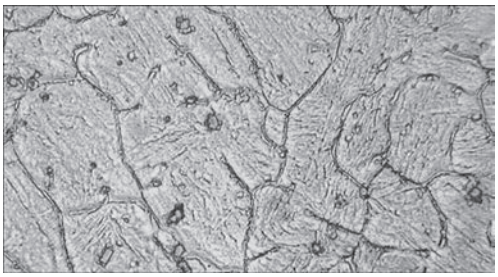

Figure 3. Microstructure (×1000) of metal deposited using flux-cored wire Veltek-N470 with volume fraction of δ-ferrite of 5.2 % and hardness after surfacing *HRC* 42–46

mation into martensite under the influence of deformations occurring at loading of a part in the process of service [15–18].

At the Iliich Metallurgical Plant for surfacing of the heavily loaded crane wheels it was proposed to apply flux-cored wire Veltek-N285.01 (alloying system Fe–C–Cr–Mn–Mo–V). In the deposited metal of this type the structure of metastable austenite is formed, which is considerably hardened during cold work hardening (Figure 4). After tempering at 600 °C, applied for inner stresses relieving the precipitations of dispersed carbides of chromium, vanadium and molybdenum are observed. As a result of depletion of matrix grains wtih carbon and alloying elements, the deformational martensite transformation is intensified, which leads to a significant increase in wear resistance of metal of the deposited rolling surface of the wheel. According to the data of X-ray structural analysis, on the deposited surface of the wheel after annealing the fraction of martensite is 1.5–2 times increased and amounts to about 30–35 vol.%. The hardness of metal after surfacing is *HB* 217–220 and after cold work hardening it amounts to *HB* 380–410.

According to the data of laboratory tests, in sliding friction according to the shoe–roller scheme and at the abrasive effect, the highest wear resistance was obtained in surfacing using wire Veltek-N285.01 (PP-Np-14Kh12G12MF) (Table 2). Two variants of technology for surfacing of crane wheels were realized: 1 — surfacing of ledges and rolling surface using wire Veltek-N285.01, and 2 — surfacing the rolling surface with wires Np-30KhGSA or PP-Np-18Kh-1G1M and rims — with Veltek-N285.01 wire. A 3 times increase in service life of the crane wheels was achieved, which allows enterprises to reduce significantly the operating costs on the cranes.

Surfacing of rollers of straightening machines. The rollers of straightening machines are traditionally manufactured of steel 90Kh1 with a surface heat treatment. In the process of surfacing on steel 90Kh1 the high preheating temperature of 400–450 °C and its stable maintaining along the whole length of the part are required due to a high tendency of steel 90Kh1 to hot and cold crack formation. However, the severe conditions of operation of these rollers, especially during straightening of sheet products and rolled

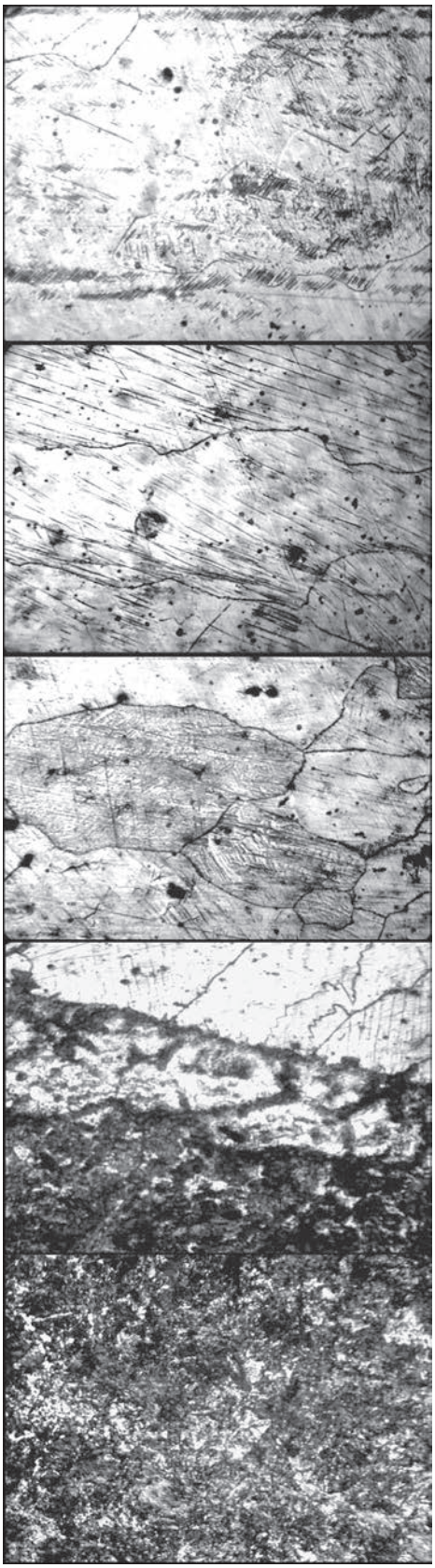

Figure 4. Microstructure (×550) of metal layers from the base metal surface (from top to bottom) deposited using flux-cored wire Veltek-N285.01

sections of alloyed grades of steel with a scale cause their premature failure. An insufficient resistance of straightening machine rollers of steel 90Kh1 with a

Table 2. Relative wear resistance of metal deposited using different flux-cored wires

Surfacing material	Heat treatment mode	Relative abrasive wear resistance*	Relative wear resistance under the conditions of dry friction*
PP-Np-18Kh1G1M (reference)	Surfacing + annealing at 550 °C (1 h)	1.0	1.0
Np-30Kh10G10	Surfacing + annealing at 550 °C (1 h)	2.0	3.0
Veltek-N285.01	Surfacing + annealing at 600 °C (1 h)	2.3	3.2
*Determined by ratio of mass loss of the deposited metal of the reference to mass loss of the corresponding deposited metal.			

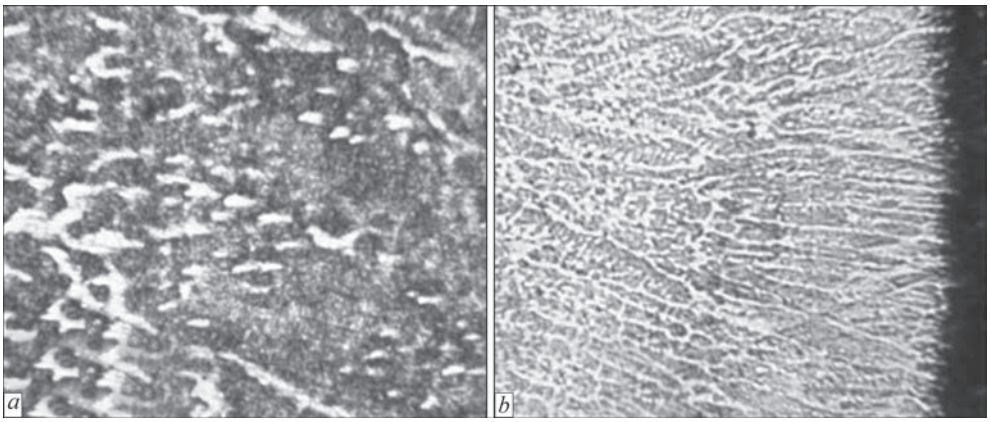

Figure 5. Microstructure (*a* — ×1000; *b* — ×100) of working layer metal of the roller deposited using flux-cored wire Veltek-N545

surface hardening even when a sufficiently high hardness (*HRC* 61–63) is provided, is explained by insufficient number of hardening phases (carbides, carbonitrides) in the structure of metal of these rollers and insufficient thickness of the hardened layer (from 1.5 to 5 mm). Moreover, so far nobody has repaired the straightening machine rollers of steel 90Kh1 because of a poor weldability of this steel grade.

The efficient technological solution to this problem was proposed by the Company «Vosstanovlenie» (Lipetsk) and Company «TM.VELTEK». It is proposed to manufacture rollers of heat-treated steel 40Kh and to perform their surfacing using wires Veltek-WT550.01-F (Fe–C–W–Mo–Cr–V) and Veltek-WT545-F (Fe–C–Mo–Cr–V–Ni). The hardness of deposited layer in this case is *HRC* 57–60.

The high wear resistance and hardness of the working surface of rollers is achieved by formation of martensite structure hardened by dispersed carbides and also by decrease in the structure of primary grain size by performing a process of surfacing using the wire of 2.0 mm diameter at the modes with an optimum combination of efficiency and heat input (Figure 5). The surfacing process was carried out at direct current of reverse polarity under flux AN-26p at I_a = 260–280 A, U_a = 30 V, v_w = 28–30 m/h.

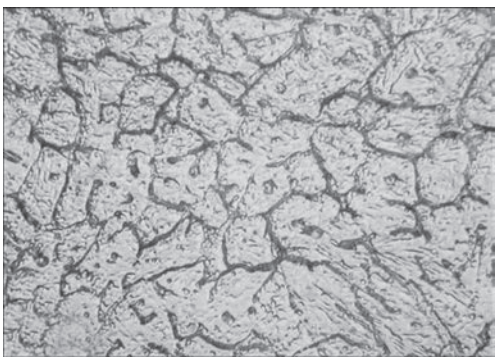

Figure 6. Microstructure (×1000) of metal of hardening layer deposited using flux-cored wire Veltek-N425

The rollers of straightening sheet metal machines with diameter of the barrel of 190, 230, 250 and 360 mm, restored applying the new technology provided the «Vyksa Metallurgical Plant» with 3–4 times increase in service life as compared to the new rollers of steel 90Kh1 with surface hardening. Moreover, the cost of repair of these rollers applying the new technology was less than a half of the cost of the new ones, manufactured of steel 90Kh1.

Surfacing of rods and plungers of hydraulic power supports of mining equipment. The rods and plungers of hydraulic power supports are subjected to chrome plating during manufacturing process. During operation process they are subjected to corrosion and abrasive wear. Together with the Department of Corrosion of the G.V. Karpenko Physical-Mechanical Institute of the NAS of Ukraine (Lvov) the investigations on influence of the chemical composition of the deposited metal on the development of the corrosion process were carried out [19, 20]. The cause of the corrosion is the formation of chromium carbides $Cr_{23}C_6$ along the grain boundaries of metal in the HAZ. The additional alloying of deposited metal provided producing metal with the structure of martensite-aging steel, where during welding and heat treatment the intermetallics are formed resulting in the further hardening of metal and a significant reduction in the probability of formation of chromium carbides $Cr_{23}C_6$ along the grain boundaries (Figure 6).

According to the results of investigations the alloying system Fe–C–Mn–Si–Cr–Ni–Mo–V was

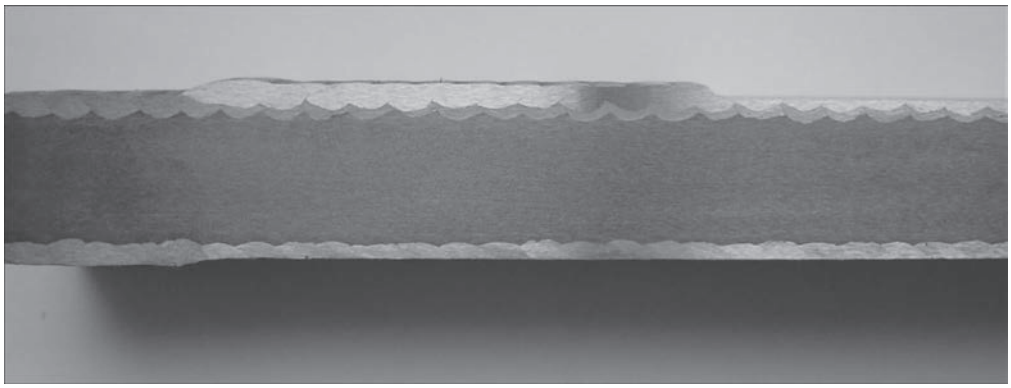

Figure 7. Macrosection of plunger fragment after surfacing

optimized using flux-cored wires Veltek-N425, Veltek-N425.01 and Veltek-N425.02 differing by corrosion resistance of deposited metal in the underground waters of different aggressiveness.

Together with the specialists of the plant «NPP Spetsuglemash» (Gorlovka) the technology of two-layer surfacing was developed using wire Veltek-N425 of 2.0 mm diameter under flux AN-26p (Figure 7). The thickness of the deposited layer is 3.0–3.5 mm considering the allowance for machining of 1.5 mm. In the period of 2005–2010 together with the specialists of «Spetsuglemash» performed the works on surfacing of rods and plungers of the stands of domestic and foreign production like M88, MT, 1KD80, 3KD90, 3KD90T, 1M103, DM «Glinnik», «Fazos», the assemblies of sections of the power support MVPO as well as the works on manufacture of new power supports KGUM, 1M103, KTS, sections OPK, supports SPG4000, SSh2.00.000 were successfully carried out. Depending on the volume of orders the consumption of surfacing flux-cored wire was in the ranges of 7–12 t per month.

In the shop conditions the repair surfacing of parts of critical equipment was successfully applied using flux-cored wire. Due to increase in wear resistance of working surfaces the increase in service life of equipment and the cost savings on repair and maintenance were achieved.

1. Frumin, I.I. (1961) *Automatic electric arc surfacing*. Kharkov: Metallurgizdat.
2. Ryabtsev, I.A., Kondratiev, I.A. (1999) *Mechanized arc surfacing of metallurgical equipment parts*. Kiev: Ekotekhnologiya.
3. Ryabtsev, I.A., Senchenkov, I.K. (2013) *Theory and practice of surfacing operations*. Kiev: Ekotekhnologiya.
4. (1979) *Surfacing materials of countries-members of CMEA*: Catalogue. Kiev; Moscow: MTsNiTI.
5. Ryabtsev, I.A., Kondratiev, I.A., Zhudra, A.P. et al. (2002) Flux-cored wires for surfacing developed in PWI. *Svarshchik*, **2**, 34–35.
6. Kondratiev, I.A., Ryabtsev, I.A. (2014) Flux-cored wires for surfacing of steel rollers for hot rolling. *The Paton Welding J.*, **6/7**, 95–96.
7. *TUU 28.7.05416923.066–2002:* Flux-cored wires for surfacing. Kiev: PWI.
8. Kondratiev, I.A., Vasiliev, V.G., Dzykovich, I.Ya. (1996) Examination of structural heterogeneity of deposited metal of 35V9Kh3SF type and its influence of serviceability of surfaced mill rolls. *Avtomatich. Svarka*, **6**, 17–20.
9. Kalianov, V.N. (1997) Structure and characteristics of wear-resistant sparsely-alloyed deposited metal. *Svarochn. Proizvodstvo*, **4**, 13–17.
10. Lyasov, V.G., Panishchenko, S.A., Kuzmenko, D.Yu. et al. (2010) Experience of application of high-tech flux-cored wires for strengthening-repair surfacing of mill rolls. In: *Proc. of 10th Sci.-Techn. Conf. on Current Problems of Production and Repair in Industry and Transport* (Ukraine, Svalyava, 22–26 Febr., 2010).
11. Oparin, L.I., Malikin, V.L., Gladky, P.V. et al. (1991) Surfacing of rolls of slab continuous-casting machines. *Avtomatich. Svarka*, **4**, 63–66.
12. Dombrovsky, F.S., Leshchinsky, L.K. (1995) *Serviceability of surfaced rolls of continuous-casting machines*. Kiev: PWI.
13. Korotkov, V.A., Mikhajlov, I.D., Veselov, A.S. et al. (2003) Surfacing of rolls of continuous-casting machines. *Stal*, **8**, 60–63.
14. Yakushin, B.F., Tsirko, P.A (2009) Specifics of arc surfacing technology for rolls of continuous-casting machines. *Svarka i Diagnostika*, **5**, 35–40.
15. Razikov, M.I., Iliin, V.P. (1964) *Welding and surfacing of cavitation steel of 30Kh10G10 grade*. Moscow: NIIMASh.
16. Malinov, L.S., Chejlyakh, A.P., Kharlanova, E.Ya. et al. (1994) Selection of composition of chrome-manganese steel with metastable austenite as a base of surfacing material. *Izvestiya Vuzov. Chyorn. Metallurgiya*, **8**, 45–46.
17. Malinov, L.S., Malinov, V.L. (2001) Manganese-containing surfacing materials. *Svarochn. Proizvodstvo*, **8**, 34–36.
18. Kuskov, Yu.M., Chernyak, Ya.P., Ostrik, I.G. et al. (2004) Reconditioning of rotary support rings of MKT-250 crane. *Svarshchik*, **4**, 35–38.
19. Golyakevich, A.A., Orlov, L.M., Pokhmurska, G.V. et al. (2014) Corrosion characteristics of the layers deposited on hydraulic cylinders rods of mineral resource equipment. *Khimichna Mekhanika Materialiv. Problemy Korozii ta Protykoroz. Zakhystu Materialiv*, **10**, 651–656.
20. Holyakevich, A.A., Orlov, L.M., Pokhmurs'ka, H.V. et al. (2015) Influence of the phase composition of the layers deposited on the rods of hydraulic cylinders on their local corrosion. *Materials Sci.*, **50**(Issue 5), 740–747.

Received 28.07.2016

doi.org/10.15407/tpwj2016.09.08

TECHNOLOGICAL PROPERTIES OF COVERING MASSES OF ELECTRODE COATINGS

M.F. GNATENKO
Company «Velma»
3 Kaunasskaya Str., 02160, Kiev, Ukraine. E-mail: mavel@ukrpost.ua

In domestic and foreign publications the problems of quality of manufacture of coated electrodes are considered quite insufficiently. In the present work an attempt was made to consider the causes for insufficient stability of the process of molding the electrodes and to share a practical experience in their elimination. The recommendations on optimizing the coating process in the manufacture of electrodes were given. 4 Ref.

Keywords: *manufacture of welding electrodes, covering masses, technological properties, optimization, granulometric composition, composition and properties of charge*

The quality of manufacture of coated welding electrodes is determined mainly by technological properties of covering masses. The most significant indicator of the quality is the difference in thickness of coating. This indicator manifests itself at the stage of deposition of covering mass (coating) on rods in the process of their molding under the pressures on mass of up to 800 kg/cm^2 and at speeds of up to 400 m/min.

For 90 % the stability of molding process, including the polythickness of coating, is determined by molding (plastic) properties of covering masses.

It is characteristic that in the publications on this problem there are no clear regularities about the influence of different parameters and characteristics of technological components on molding properties and, moreover, there are no clear practical recommendations for technologists and manufactures.

The aim of the work is to consider the causes of instability of the process of molding the electrodes and the possible ways of their elimination.

Technological properties of masses. They include:

● molding (plastic) properties of covering masses: pressure of molding (the lower the better at a sufficient resistance to dents), degree of stability of flows formation at the lead-in molding area and, accordingly, the stability of polythickness of coating deposition on rods at molding; the degree of mass (coating) adhesion to the rod at their contact in the molding chamber;

● properties of raw masses (coating), which characterize their tendency to processing (to rupture of coating in plane of mating the rods of electrodes after coming out from the molding head), to cleaning the coating for the electrode holder and the contact end, to sticking of electrodes, sticking to the frames, etc.;

● drying properties of covering masses: resistance of structure of covering masses to the passage of humidity (removal from inner layers); degree of softening the masses during heating at the initial stages of drying; tendency of masses to shrinkage and to micro/macrocracks; to delamination from the rod surface (cracks and delamination reduce the strength of electrodes coating);

● strength properties of coating of ready electrodes.

Causes of low technological properties and ways of their optimization. The results of experiments, manufacturing experience and their analysis on the basis of the available scientific publications [1–4] allow stating that molding properties of covering masses are determined by:

● composition of the charge (properties and the amount of any components); degree of wetting and chemical interaction of charge powders with a liquid glass; strength characteristics of particles components, etc.;

● properties of liquid glass;

● volumetric granulometric composition of the charge;

● properties of plasticizer (including different additives, salts, surface-active agents, etc.);

● type of mixer for preparation of covering masses (considered in the work).

First of all, let us consider the most obvious factor of influence on molding properties of masses — granulometric composition of the charge (volumetric):

● maximum size of particles of the components should not exceed the thickness of the electrode coating. To be more precise, it should be 2–3 times smaller, because during interaction 2–3 particles in the

thickness of the coating can lock the channel when there are many such particles in the charge;

● there should be a maximum density of packing the charge particles to prevent dilatency and pulsation;

● it is necessary to minimize the friction coefficient between the layers of flow during formation of the electrodes coating flow at the inlet to a die (forming bushing). This is achieved by reducing the middle fraction (+0.063 – 0.16) in the charge to a minimum, i.e. the coarse fraction (–0.16 + 0.355: 30–35 %) amounts to the thickness of one layer (frame layer), and the fine fraction (–0.063) in the layer thickness provides a maximum packing density and a minimum roughness of the layer;

● volume of fine fraction (–0.063) of more than 65–70 % should not be admitted in the charge, as a number of flow layers at the stage of formation of coating thickness increases sharply (by tens of times), and accordingly, a number of degrees of the layers shear also increases sharply. This results in unstable formation of flows in place and time (polythickness pulsation).

All the other problems associated with polythickness (causes and consequences) will be considered at the following condition:

● granulometric composition of the charge of covering masses is optimum and the same;

● purely chemical interaction of components with liquid glass is absent (including that with evolution of gaseous products).

Composition of charge and physicochemical properties of individual components are the following:

● presence of components with anisodiametrical shape of particles (mica, talc, vollostanit, kaolin, cellulose etc.) in a sufficient amount (not lower than 4–6 %) in the charge reduces the inner friction in the covering mass during formation of flows from the diameter of sleeve to the diameter of coating. It is also important that such particles reinforce the covering mass and, respectively, the coating, i.e. the resistance to dents, etc. increases. As a rule, such components are used in coatings of rutile, rutile-cellulose, ilmenite type, etc. The covering masses of such electrodes are characterized by good molding properties (ANO-4, OZS-4, MP3, ANO-13, ANO-36, etc.);

● presence of components in the charge which have the fracture strength on compression and shear being at the level of pressures to the mass during molding of electrodes of 300–800 kg/cm^2. It is known that this field covers strength characteristics of marble, magnesite, dolomite, etc. The most outstanding representatives of such charges (covering masses) are the electrodes of grades UONI 13/45, UONI 13/55, ANO-9, etc. In the composition of such charges there is approximately 50 % of marble with the fracture strength of about 500 kg/cm^2. The covering masses of such electrodes are characterized by low molding properties (and, in general, by technological ones). At their molding at the pressures higher than 400–500 kg/cm^2 (on mass) in the inlet area and in the molding chamber a partial destruction (spalling) of marble particles occurs with formation of new surfaces, which withdraw a part of moisture from the film of liquid glass gel. In those areas the mass thickens, the «crackers» are formed, the stability of mass flow formation is violated, the polythickness begins to pulsate in the direction and time. Also, frequently an increase in pressure up to locking the channels occurs.

The production experience gained earlier shows that, for example, the electrodes of grade ANO-4 are usually molded at pressures of 600–700 kg/cm^2 (on mass), and UONI 13/55 — at pressures of 350–450 kg/cm^2. In the first case, the mass contains much mica in its composition (24 %) and little relatively soft particles of magnesite (only 15 %). Electrodes ANO-4 can be molded at high pressures without violation of integrity of magnesite particles, especially in the presence of mica. In case of UONI 13/55 the effect is the opposite and it must be considered during molding, providing an increased stability of this process due to improvement of molding properties of masses using the appropriate methods of plasticizing; reducing the pressure of molding by using the effective molding of inlet areas and heads; application of intensive mixers for preparation of masses, as well as using the grade of marble with the strength in the range of 1000 kg/cm^2.

The application of flotation fluorite may influence on deterioration of molding properties of covering masses of electrode UONI 13/55 (etc.) of fluoride calcium type, which often contains particles of a relatively large amount of flotation reagents on the surface. This greatly reduces the wetting of fluorite with liquid glass. The degree of adhesion of liquid glass (gel) to fluorite particles decreases and the friction between the particles increases. The flow becomes more unstable, i.e. the degree of wetting of the charge particles determines the quality of coating of liquid glass and the level of friction between the particles during the flow increases. The molding process becomes less stable.

Role of liquid glass in the properties of covering masses. The technological, including molding, properties of covering masses depend by 70–80 % on the type, characteristics and properties of liquid glass (its influence on welding and technological characteristics is not considered).

The main purpose of liquid glass in covering masses (from the viewpoint of molding) is to mini-

mize friction between the particles of charge during formation of flow from the diameter of press cylinder to the diameter of electrodes coating at their molding and after molding the coating should have sufficient resistance against dents and mechanical damages. And now let us look how covering and reinforcing properties of liquid glass in a covering mass manifest themselves.

To establish the mechanisms and processes occurring during preparation of covering masses, it is necessary to divide this stage into two stages.

The first stage: distribution of liquid glass in charge, i.e. the coating of charge of particles with liquid glass. This stage should be carried out as quickly as possible. Moreover, it is necessary to provide a good wettability of surfaces of almost all the particles with liquid glass (by applying the corresponding special surfactants, if necessary). For preparation of masses the most effective are intensive mixers.

The second stage: formation of certain physical and mechanical properties of covering masses, as a consequence of reaction of liquid glass on the contact interaction with surface of particles of different components, such as:

- withdrawal of moisture from the film of liquid glass;
- adsorption processes (including interaction of electric potentials on the boundary surface);
- ion exchange between liquid glass and individual components;
- different influence of different types of plasticizers and special additives on liquid glass.

From work [2] it is known that as a result of such similar processes a gelling occurs in liquid glass (sharp increase in viscosity, polymerization, formation of organosilicon structures: gelling, coagulation). At the same time, depending on the characteristics of liquid glass, its parameters and influencing factors, the structure of liquid glass gel is produced different: soft, medium and hard.

To soft structure of the produced gel the liquid glasses are prone having a low modulus (< 2.9). To hard structure those are prone having a high modulus (> 3.1) and, of course, to medium one — those with modulus of > 2.9 and < 3.1. Let us see how it is manifested. If one takes a low modulus liquid glass on an index finger and rub it with a thumb, then its condition will not change for a long time. It will remain sticky (soft structure). If the same procedure will be done with a liquid glass of a high modulus, then very quickly a dry «sand» will form between the fingers (hard structure of the gel). And with a medium modulus, a layer of jelly type — the gel structure of medium hardness — will be formed between the fingers. In covering masses it is manifested during their preparation, i.e. if the mass is sticky, it «does not twist» for a long time, it is not stirred, then a gel structure is soft. If the mass becomes dry very quickly and requires an additional amount of liquid glass, if it moves hard between the fingers, crumbles, then a gel structure of liquid glass becomes hard. In a medium variant the mass becomes not sticky, but under an index finger and a thumb it moves well (even at repeated punching).

What is the cause of formation of different structures of liquid glass gel in the film of covering masses and their properties? In the process of liquid glass gelling, as is known, the processes of polymerization, gelling and coagulation of colloid particles of organosilicon compounds occur. As a result, both planar weak structures (soft), as well as volume structure (hard) may be formed depending on the modulus of liquid glass. At the medium modulus in the structure of a gel, both planar as well as three-dimensional structures in combination are present. At the moment of gelling (coagulation) the microformations (particles) have high adhesive and cohesive properties. As far as at the first stage the liquid glass has already covered the particles, at the second stage the gelling (coagulation) of film of liquid glass occurs, which is accompanied by a high adhesion, resulting in a quality coating of gel particles. It does provide the flow of covering masses at molding. So:

- at a low modulus the gelling is very weak (planar), adhesion to the particles is weak, the friction between the particles is high, the flow is unstable;
- at a high modulus the gelling is very intensive (coagulation), volumetric, the cohesion in the film of liquid glass is higher than the adhesion to the particles, so they are coated unevenly, the flow is not stable, and the coating «is loosened» as far as the mass in the structure is not restored (break of continuity). The flow in this case cannot be stable in the directions and time. The coating is poorly maintained on the rod. Apparently, the structure of such a gel has an elasticity associated with a porous structure, due to a large quantity of cohesive forces in microparticles of the gel. This is also in favor of the process of «loosening» the mass.

So, how do we control the gel structure? In case of a soft gel structure, it is necessary to harden it. In case of a hard structure, it should be soften bringing it to the medium level using the appropriate methods. In order to harden the gel structure from soft to medium it is necessary to apply an active plasticizer. This is potash, soda, technical CMC, etc. The electrolyte components cause activation of gelling process, as a result of which the medium gel structure is produced and the effect of increasing plastic (molding) proper-

ties is achieved. It should be noted that there are also other methods for increasing the degree of gelling: increase in viscosity of the applied liquid glass, use of finer component which activates the gelling process in liquid glass more intensively, or applying the liquid glass with a higher modulus.

If the gel structure of liquid glass in the covering mass becomes hard, it is necessary to:

- reduce the viscosity of a liquid glass, or to exclude active plasticizers from the charge;
- apply the inactive plasticizers (purified CMC, pure electrode cellulose, etc.). Thus, CMC, «being dissolved» in the film of a liquid glass (with reduced viscosity), prevents the formation of a hard gel;
- it is necessary that the components actively influencing the process of gelling were applied with a larger granulometric composition;
- use additives of alkali solutions (Na, K) to decrease the modulus of liquid glass.

Some of the mentioned methods (both such as the first ones for soft, as well as the second ones for hard) can be realized already at the stage of preparation of covering masses (if the mass becomes soft, then active plasticizers should be added, and if dry, then the water and some purified CMC (EC) should be added.

The covering mass, like the charge–liquid glass–plasticizer system considering the activity of individual components, should be prepared to produce a film of liquid glass gel of medium hardness structure.

In our opinion, the causes of poor plastic (molding) properties of covering masses and the ways of their improvement (optimization) were defined.

Conclusions

1. Granulometric composition of the charge (volumetric) should be the following: with the maximum density of packing, otherwise dilatency (pulsation and squeezing of liquid phase) will occur; with the minimum roughness of the layer flowing-sliding and the minimum pressure of molding (minimum content of medium fraction); with a minimum number of layers of up to three at the formation of mass flow reaching the thickness of coating (amount of soft fraction in the charge of more than 65–70 % should not be admitted, otherwise, a strong pulsation will occur).

2. A high content of carbonates in the charge (electrodes UONI, ANO-9, etc.) negatively influences the plastic properties of the masses, as far as their strength is low (about 500 kg/cm^2) and at the pressures of molding on the masses the fracture of particles of such components (erasing) occurs, which causes the formation of crackers, violation of the formation of flows and pulsation.

It is required to apply the effective methods of plasticizing in order that the pressure of molding does not exceed about 500 kg/cm^2 (on the mass); to minimize the pressure losses in the inlet and molding areas; to use the grades of high-strength carbonates (including marble of 1000 kg/cm^2 strength); to produce electrodes of the corresponding grades with a small amount of carbonates.

3. To use a liquid glass with modulus of 3±1 and the corresponding plasticizers, depending on the activity of a charge. It is also possible to use the high modulus liquid glasses, but of a very low viscosity and only in combination with a high-quality purified CMC. In all the cases it is necessary to try achieving the structure of medium hardness of the gel, which provides the highest plastic properties of masses.

1. Vornovitsky, I.N. (2001) *Quality control of welding electrodes during their manufacture*. Moscow: IKAR.
2. Ignatkina, O.I., Lukianova, O.I., Borsuk, P.A. et al. (1999) Rheological properties of gels formed in interaction of liquid glass and hardeners of complex ether type. *Lit. Proizvodstvo*, **10**, 39–41.
3. Marchenko, A.E., Gnatenko, M.F. (1980) Peculiarities of flow of electrode covering masses detected by capillary plastometer. In: *Information of CMEA on Development of scientific principles and new technological processes of welding, surfacing and thermal cutting of materials and alloys for manufacturing of welded structures and efficient welding consumables and equipment*, Issue 1, 106–117.
4. Marchenko, A.E. (2016) Rheological investigations of non-isothermal pressure flows of coating mixtures for welding electrodes. *The Paton Welding J.*, **1**, 17–29.

Received 28.07.2016

doi.org/10.15407/tpwj2016.09.09

INFLUENCE OF CORROSION DAMAGE ON CYCLIC FATIGUE LIFE OF TEE WELDED JOINTS TREATED BY HIGH-FREQUENCY MECHANICAL PEENING

V.V. KNYSH, S.A. SOLOVEJ, L.I. NYRKOVA, L.G. SHITOVA and A.A. KADYSHEV
E.O. Paton Electric Welding Institute, NASU
11 Kazimir Malevich Str., 03680, Kiev, Ukraine. E-mail: office@paton.kiev.ua

We studied the effectiveness of application of high-frequency mechanical peening to improve fatigue resistance characteristics of tee welded joints in metal structures which are operated in a sea climate. Corrosion damage characteristic for such structures after long-term service was produced by soaking the welded joints in KST-1 salt spray chamber for 1200 h. Metallographic studies were conducted of weld zone and HAZ of welded joints in the initial (unstrengthened) state and in the state of strengthening by the HFMP technology after the impact of corrosive environment. It was established that strengthening by this technology does not improve the joint resistance to the impact of neutral salt spray. Fatigue testing of welded joints were performed in the initial and strengthened state after the impact of neutral salt spay. It was found that strengthening tee welded joints by HFMP before the corrosive impact allows increasing their fatigue strength at $2 \cdot 10^6$ cycles by 48 % and increasing cyclic fatigue life by 2–5 times. 19 Ref., 1 Table, 6 Figures.

Keywords: *tee welded joint, neutral salt spray, fatigue, high-frequency mechanical peening, ultrasonic impact treatment, increase of corrosion fatigue resistance*

Various treatments of surface layer of metals and alloys are widely used to improve their corrosion resistance, promoting a change of their structure, hardness improvement, relieving tensile residual stresses and inducing compressive residual stresses, as well as reducing stress concentration. Papers of recent years on this subject are devoted both to studying the technological features of surface strengthening by traditional methods of plastic deformation of metal (for instance, shot blasting), and to investigation of new treatments [1–5]. Compared to such costly and unproductive treatments as surface melting by nanopulsed laser [3] or high-power pulsed electron beam [4], steel ball attrition treatment with vacuum chamber application [5], swaging in the hot or cold state [6–8], application of high-frequency mechanical peening [9, 10] has a number of advantages.

Compactness, mobility and low cost of equipment for high-frequency mechanical peening (HFMP) allows strengthening parts of machines and metal structures in any spatial position in the field, in particular under the water [11]. Works [12–15] give the results of experimental studies of the effectiveness of application of HFMP technology, known in foreign publications as «ultrasonic shock treatment», to improve corrosion resistance and characteristics of corrosion fatigue resistance of welded joints. In these studies assessment of corrosion resistance, corrosion rate and corrosion fatigue of welded joints was performed in NaCl solutions.

Analysis of polarization fatigue curves showed that strengthening by HFMP technology increases the corrosion potential and lowers the corrosion rate of peening zone (line of weld metal transition to HAZ). Here, cyclic fatigue life of butt welded joints of pipes rises 2 times, and that of tee joints — up to 6 times. It should be noted that the above data of accelerated corrosion testing do not give an idea about lowering of service properties of HFMP-treated welded joints as the strengthened metal layer is destroyed.

Influence of partial corrosion loss of HFMP-strengthened metal layer on residual stress fields and cyclic fatigue life of welded joints is considered in [16, 17]. In [16] it is shown that corrosion damage of welded joints of low-alloyed shipbuilding steel equivalent to 7.5 years of operation leads to reduction of the thickness of surface layer of metal with induced residual compressive stresses approximately from 1.5 to 1.0 mm, and lowering of their maximum level. The authors came to the conclusion about the rationality of welded joint treatment by HFMP, as compressive residual stresses are induced in the peening zone instead of tensile residual stresses, and they are preserved even at partial loss of the strengthened layer. In [17] metallographic studies showed that soaking of welded joints of weather-resistant steel in moisture chamber G4 at elevated temperature and moisture for 1200 h leads to partial damage of the strengthened metal layer as a result of formation of corrosion cavi-

ties. Experimental data, obtained on tee welded joints after corrosion impact, show that pre-strengthening by HFMP improves the fatigue strength at $2 \cdot 10^6$ cycles of such joints by approximately 48 %, and their cyclic fatigue life rises 6 to 8 times. Unlike low-alloyed steels, soaking of stainless steel samples in aggressive media for 1000 h does not lead to a significant damage of strengthened metal layer [18, 19].

Thus, results of studies [16–19] show that establishing the characteristics of fatigue resistance of welded joints at considerable damage (corrosion loss) of HFMP-strengthened layer of metal is an urgent task. Significant corrosion damage can be produced by prior soaking of welded joints in salt spray chamber, which allows simulation of metal structure operation in sea climate.

The objective of this work is assessment of fatigue resistance characteristics of tee welded joints strengthened by HFMP after soaking in neutral salt spray environment.

Material and investigation procedure. Experimental studies for corrosion fatigue were conducted on samples of tee welded joints of low-alloyed steel 15KhSND (σ_y = 400 MPa, σ_t = 565 MPa), which is extensively applied for fabrication of elements of metal structures for long-term operation (for instance, in superstructures of railway and road bridges), has higher strength, good weldability, is resistant to atmospheric conditions and operative in the temperature range from –70 up to 45 ºC.

Blanks for welded joint samples were cut out of hot-rolled sheet of 12 mm thickness, category 12. Dimensions of blanks for tee joints were 350×70 mm. Tee joints were produced by welding on transverse stiffeners (also from 15KhSND steel) by manual arc process with electrodes of UONI 13/55 grade by fillet welds from two sides of the plate. Root weld (first layer) was made with 3 mm diameter electrodes, and face weld (second layer) — with 4 mm electrodes. Shape and geometrical dimensions of samples of tee welded joints are given in Figure 1. Sample thickness is due to wide applicability of 12 mm rolled stock in engineering welded metal structures, and working part width of 50 mm was selected, proceeding from test equipment capacity.

Experimental studies were conducted in servo-hydraulic machine URS-20 at alternating tension with cycle asymmetry R_σ = 0 and frequency of 5 Hz at regular loading. Criterion of test completion was complete failure of samples or exceeding test base of $2 \cdot 10^6$ cycles of stress reversal. Samples were tested in the initial state and in HFMP-strengthened state after soaking in corrosive medium.

Welded joint strengthening by HFMP technology was performed with USTREAT-1.0 equipment,

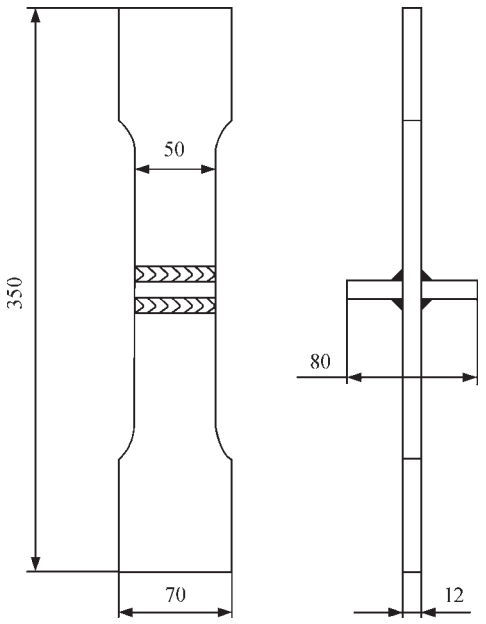

Figure 1. Shape and dimensions of tee welded joint samples

in which manual compact impact tool with piezoceramic converter is connected to ultrasonic generator of 500 W power. At strengthening of welded joints by HFMP, surface plastic deformation was applied to a narrow zone of weld metal transition to HAZ (along the fusion line). Single-row four-striker attachment with striker diameter of 3 mm was used as the strengthening tool. Speed of HFMP performance in treatment of tee welded joints was equal to 1 mm/s, and amplitude of oscillations of the end of waveguide of manual impact tool was 25 μm.

To produce preliminary corrosion damage welded samples were placed into KST-1 salt spray chamber. Investigations were conducted to GOST 9.401–91 «USCAP. Paint coatings. General requirements and methods of accelerated tests on resistance to the action of climatic factors (method 1, B)» in KST-1 at temperature of (35 ± 2) ºC with spraying of sodium chloride solution for 15 min every 45 min of studies. Sodium chloride concentration in the solution was (50 ± 5) g/dm^3, pH was from 6.5 to 7.2, and density was 1.03 g/cm^3. Conductivity of distilled water for preparation of sodium chloride solution is not more than 20 μOhm/cm at temperature of (25 ± 2) ºC. Duration of welded sample staying under the impact of salt spray was 1200 h.

Metallographic studies of surface layer of weld metal and HAZ of tee welded joints after soaking in KST-1 salt spray chamber were conducted on samples in the initial (unstrengthened) state and in HFMP-strengthened state. Results of metallographic studies of the surface layer of the metal of weld and HAZ of similar welded joints in the initial and HFMP-strengthened states prior to corrosion impact are given in [17].

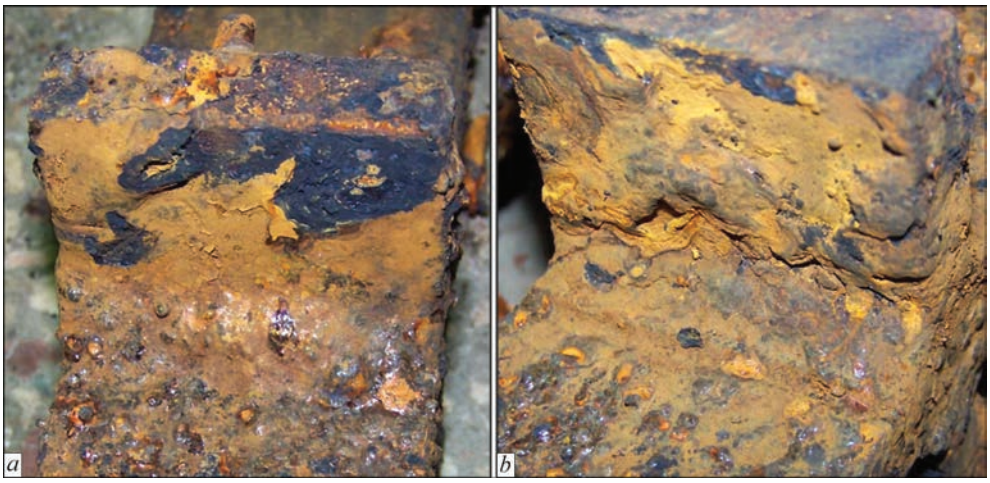

Figure 2. Appearance of weld zone of tee welded joint in the initial (*a*) and HFMP-strengthened (*b*) states after exposure to neutral salt spray for 1200 h

Investigation results. After soaking in salt spray chamber for 1200 h the samples were coated by the layer of corrosion products of up to 1–2 mm (Figure 2). In surface layers of weld metal of tee welded joint in unstrengthened state after soaking in chamber quite extended corrosion damage is observed in the form of spots and cavities of 1.95×0.65, 4.16×0.26, 2.73×0.195 mm size. In HAZ metal corrosion damage is less extended, but deeper, of up to 0.56×0.52 and 1.30×0.65 mm size. Corrosion damage in the HAZ surface layers is located predominantly along the fusion boundary of coarse grain zone, and in some cases they cavities are filled with corrosion products (Figure 3).

After HFMP strengthening plastically deformed layers of weld metal 1.70–1.82 mm wide and of HAZ metal 1.3–1.7 mm wide formed under the groove. Here their depth, due to visible changes of metal structure under the groove, was equal to 390–650 μm, before placing into chamber. After soaking tee welded joint samples in chamber, the width of strengthened metal layer decreased to 0.52–1.30 mm, and its depth — to 65–455 μm. Individual regions showed just traces of HFMP-strengthened metal layer 0.52 mm wide and 65–91 μm deep, located either in weld metal or in HAZ metal, that is indicative of practically complete damage (loss) of the strengthened layer.

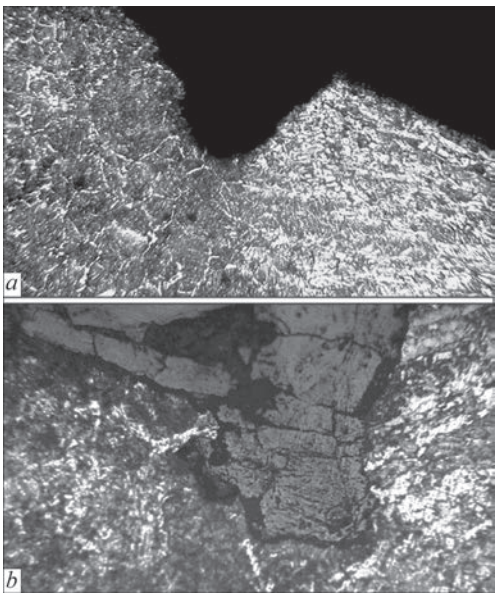

Figure 3. Corrosion cavities in surface layer of metal of coarse grain zone in tee welded joint after exposure to neutral salt spray for 1200 h: *a* — ×100; *b* — ×250

In strengthened surface layers of metal of fillet welds and HAZ of welded joints after soaking in chamber, cavities of 2.60×0.26, 2.08×0.65 mm in the weld metal and of 1.69×0.65 and 0.36×0.78 mm size in the HAZ metal were found along the fusion boundary. Characteristic corrosion damage of strengthened surface layer of metal is as follows: spot corrosion with different penetration depth (Figure 4, *a*); surface corrosion to the depth from 0.02 to 0.13 mm (Figure 4, *b*); complex corrosion damage, which are cavities, developing into pitting, and corrosion cracks, developing into cavities, filled with corrosion products (Figure 4, *c*).

Results of metallographic investigations with computed values of the extent of damage and total projected damage surface area, depth of corrosion spot and cavity penetration into the surface layers of metal of fillet welds and HAZ in tee welded joints are given in the Table. Depth of penetration of corrosion spots in the surface layer of metal of the weld and HAZ for welded joints in the initial and HFMP-strengthened states is practically the same and is equal to 0.65 and 0.78 mm, respectively. Thus, strengthening by HFMP technology does not improve the corrosion resistance of samples of tee welded joints under the conditions of exposure to neutral salt spray.

Results of fatigue testing of samples of tee welded joint of 15KhSND steel after soaking in salt spray chamber are shown in Figure 5. Experimental data

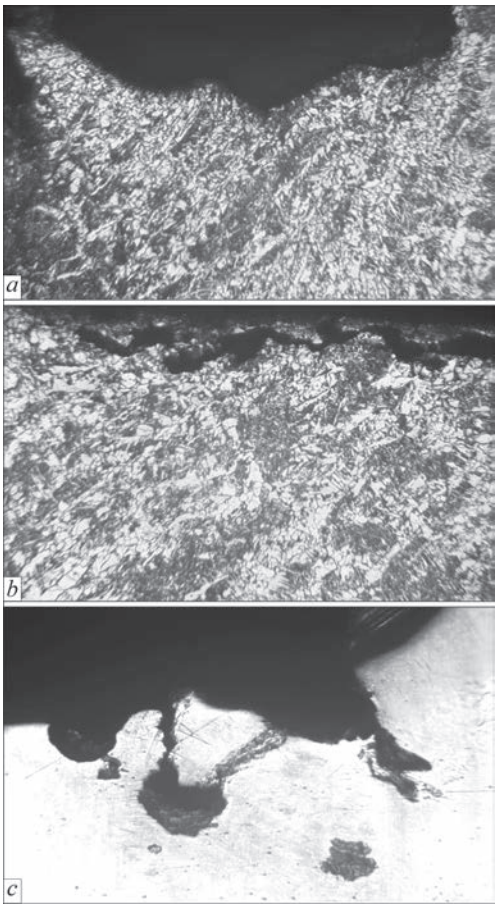

Figure 4. Corrosion damage of HFMP-strengthened surface layer of metal of tee welded joint after exposure to neutral salt spray for 1200 h (*a*, *b* — ×110; *c* — ×250)

obtained in [17] on identical welded joints without corrosion damage are also given there.

Soaking of samples of tee welded joints in salt spray chamber for 1200 h leads to lowering of fatigue strength at $2 \cdot 10^6$ cycles in unstrengthened welded joints by 25 % (from 180 to 135 MPa), and in HFMP-strengthened joints — by approximately 24.5 % (from 265 to 200 MPa).

Application of HFMP as a method of surface plastic deformation of the joint metal near the points of fatigue damage localizing improves fatigue resistance characteristics of tee welded joints, both in air and at exposure to corrosive environment. Results obtained in welded joints after corrosive impact (see curves *2* and *4* in Figure 5) show that pre-strengthening by

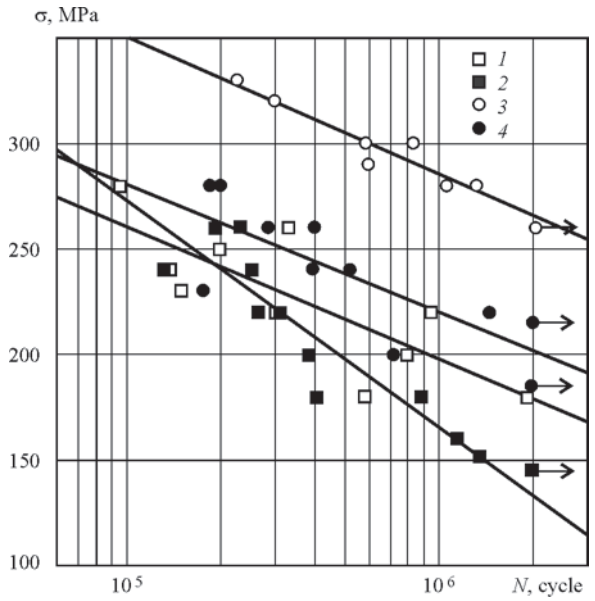

Figure 5. Fatigue curves of tee welded joints of 15KhSND steel: *1*, *3* — in initial and HFMP-strengthened states in air [17]; *2*, *4* — the same after exposure to neutral salt spray for 1200 h, respectively

HFMP technology increases the fatigue strength at $2 \cdot 10^6$ cycles of such joints by approximately 48 % (from 135 up to 200 MPa), and improves cyclic fatigue life 2–5 times. It should be also noted that fracture of unstrengthened welded joints after soaking in chamber occurred along the line of weld metal transition to HAZ metal (Figure 6, *a*), and that of strengthened ones took place at a distance from the weld and HAZ, predominantly near the grip part (Figure 6, *b*). Such fracture is indicative of comparability of fatigue resistance characteristics of HFMP-strengthened welded joint and base metal with corrosion damage.

Thus, experimental results are indicative of the rationality of application of HFMP technology to improve fatigue resistance characteristics of tee welded joints of metal structures, exposed to alternating loading and sea climate in operation (see curves *2* and *4* in Figure 5). Despite corrosion loss of the main part of strengthened layer, fracture of welded joints runs through the base metal from surface corrosion damage. Here, it should be noted that protection of HFMP-strengthened surface layer of metal from direct impact of aggressive media, and from corrosion

Dimensions of corrosion damage in surface layers of metal of welds and HAZ in tee welded joints of 15KhSND steel after soaking for 1200 h in salt spray chamber

Sample state	Spot corrosion of surface layers of weld metal			Spot corrosion of surface layers of HAZ metal		
	Damage extent, %	Damage depth, mm	Total projected damage area, mm	Damage extent, %	Damage depth, mm	Total projected damage area, mm
Unstrengthened	50.4	0.039–0.65	26.52	64	0.065–0.65	9.78
HFMP-strengthened	72	0.075–0.65	40.10	62.5	0.065–0.78	10

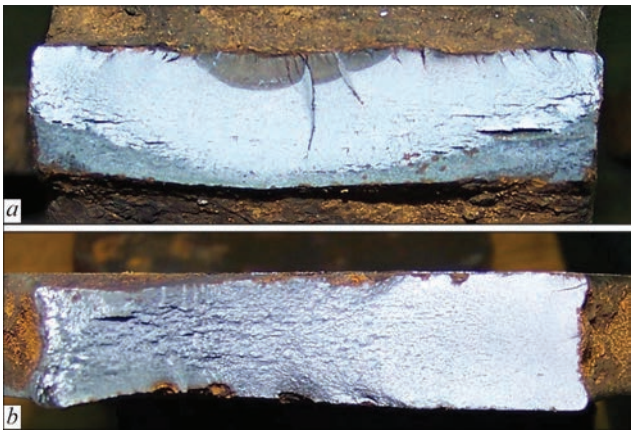

Figure 6. General view of fracture surface of tee welded joints in the initial (*a*) and HFMP-strengthened (*b*) states after corrosive impact and fatigue testing

damage, accordingly (for instance, by application of lacquer-paint coatings), allows achieving maximum characteristics of joint fatigue resistance (curve *1*, Figure 5).

Conclusions

1. The paper gives the results of metallographic assessment of surface layers of metal of the weld and HAZ of welded joints in the initial (unstrengthened) and HFMP-strengthened state after exposure to neutral salt spray. It is found that strengthening by HFMP does not lead to improvement of joint resistance to the impact of neutral salt spray.

2. The high effectiveness of HFMP technology application to improve the fatigue resistance characteristics of welded joints in metal structures, operating in sea climate, was established. HFMP strengthening of tee welded joints of 15KhSND steel before soaking in neutral salt spray chamber for 1200 h leads to improvement of cyclic fatigue life 2–5 times, depending on the levels of applied stresses, and to 48 % increase of fatigue strength at $2 \cdot 10^6$ cycles.

3. It is shown that fracture of unstrengthened welded joints after soaking in salt spray chamber proceeds along the line of transition of weld metal to HAZ metal, and in HFMP-strengthened joints it occurs at a distance from the weld and HAZ, predominantly near the grip part (in base metal). Such a fracture is indicative of comparability of fatigue resistance characteristics of HFMP-strengthened welded joint and base metal with corrosion damage.

1. Ahmed, A.A., Mhaede, M., Basta, M. et al. (2015) Effect of shot peening parameters and hydroxyapatite coating on surface properties and corrosion behavior of medical grade AISI 316L stainless steel. *Surface & Coating Techn.*, **280**, 347–358.
2. Zhiming, L., Laimin, S., Shenjin, Z. et al. (2015) Effect of high energy shot peening pressure on the stress corrosion cracking of the weld joint of 304 austenitic stainless steel. *Materials Sci. and Eng. A*, **637**, 170–174.
3. Pacquentin, W., Caron, N., Oltra, R. (2015) Effect of microstructure and chemical composition on localized corrosion resistance of a AISI 304L stainless steel after nanopulsed-laser surface melting. *Appl. Surface Sci.*, **356**, 561–573.
4. Hao, S., Zhao, L., Zhang, Y. et al. (2015) Improving corrosion and wear resistance of FV520B steel by high current pulsed electron beam surface treatment. Nuclear *Instruments and Methods in Physics Research B: Beam Interactions with Materials and Atoms*, **356–357**, 12–16.
5. Balusamy, T., Sankara Narayanan, T.S.N., Ravichandran, K. et al. (2013) Influence of surface mechanical attrition treatment (SMAT) on the corrosion behavior of AISI 304 stainless steel. *Corrosion Sci.*, **74**, 332–344.
6. Arifvianto, B., Widodo, T.D. (2015) Effect of cold working and sandblasting on the microhardness, tensile strength and corrosion resistance of AISI 316L stainless steel. *Int. J. Minerals, Metallurgy and Materials*, **19**, 1093–1099.
7. Ahmed, A.A., Mhaede, M., Wollmann, M. et al. (2014) Effect of surface and bulk plastic deformations on the corrosion resistance and corrosion fatigue performance of AISI 316L. *Surface & Coating Techn.*, **259**, 448–455.
8. Pokhmursky, V.I., Khoma, M.S. (2008) *Corrosion fatigue of metals and alloys*. Lviv: Spolom.
9. Lobanov, L.M., Kirian, V.I., Knysh, V.V. et al. (2006) Improvement of fatigue resistance of welded joints in metal structures by high-frequency mechanical peening (Review). *The Paton Welding J.*, **9**, 2–8.
10. Malaki, M., Ding, H. (2015) A review of ultrasonic peening treatment. *Materials and Design*, **87**, 1072–1086.
11. Gao, W., Wang, D., Cheng, F. et al. (2015) Enhancement of the fatigue strength of underwater wet welds by grinding and ultrasonic impact treatment. *J. Materials Proc. Techn.*, **223**, 305–312.
12. Abdulah, A., Malaki, M., Eskandari, A. (2012) Strength enhancement of the welded structures by ultrasonic peening. *Materials & Design*, **38**, 7–18.
13. Prokopenko, G.I., Mordyuk, B.N., Knysh, V.V. et al. (2014) Improvement of fatigue strength and corrosion resistance of welded joints by ultrasonic impact peening and electrical-discharge alloying. *Tekhn. Diagnostika i Nerazrush. Kontrol*, **3**, 34–40.
14. Daavary, M., Sadough Vanini, S.A. (2015) Corrosion fatigue enhancement of welded steel pipes by ultrasonic impact treatment. *Materials Let.*, **139**, 462–466.
15. Daavary, M., Sadough Vanini, S.A. (2015) The effect of ultrasonic peening on service life of the butt-welded high-temperature steel pipes. *J. Materials Eng. and Performance*, **24**, 3658–3665.
16. Ahmad, D., Fitzpatrick, M.E. (2015) Effect of ultrasonic peening and accelerated corrosion exposure on residual stress distribution in welded marine steel. *Metallurg. and Materials Transact. A*, **46**, 1214–1226.
17. Knysh, V.V., Solovej, S.A., Nyrkova, L.I. et al. (2016) Improvement of cyclic fatigue life of tee welded joints by high-frequency mechanical peening under the conditions of higher humidity and temperature. *The Paton Welding J.*, **3**, 12–17.
18. Dong, Z., Liu, Z., Li, M. et al. (2015) Effect of ultrasonic impact peening on the corrosion of ferritic-martensitic steels in supercritical water. *J. Nuclear Materials*, **457**, 266–272.
19. Nasilowska, B., Bogdanowicz, Z., Wojucki, M. (2015) Shot peening effect on 904L welds corrosion resistance *J. Construct. Steel Res.*, **115**, 276–282.

Received 22.02.2016

doi.org/10.15407/tpwj2016.09.10

SELECTION OF MODES OF HIGH-TEMPERATURE TEMPERING OF HEAT-RESISTANT STEEL WELDED JOINTS MADE BY ELECTRODES THERMANIT MTS616

V.Yu. SKULSKY, A.K. TSARYUK, A.R. GAVRIK, M.A. NIMKO and **G.N. STRIZHIUS**
E.O. Paton Electric Welding Institute, NASU
11 Kazimir Malevich Str., 03680, Kiev, Ukraine. E-mail: office@paton.kiev.ua

One of the problems in producing the welded joints of complexly-alloyed heat-resistant steels is the providing of the required level of weld metal impact toughness. The improvement of its ductility and toughness is attained by a postweld high-temperature tempering using the modes regulated by the developer of welding electrodes. In case of welding of an experimental high-chromium martensite steel by electrodes Thermanit MTS616 (10Kh9V2MFB type) with account for conditions of its fulfillment, the heat treatment was required by 30–40 °C lower than that usually applied for welds of the mentioned type. The effect of modes of the manual arc welding and duration of tempering at 730–720 °C on hardness and impact toughness of weld metals was determined. Intervals of holdings were found in tempering, during which the secondary hardening was observed. The modes were selected, providing the required level of impact toughness of welds (impact energy $KV \geq 41$ J). It is shown that alongside with the selected duration of temperature the important factor, providing the increase in toughness of the deposited metal, is the application of multi-pass welding at the reduced energy input. 11 Ref., 4 Figures.

Keywords: *heat-resistant martensite steel, manual arc welding with covered electrodes, weld metal, high-temperature heat treatment, tempering mode, hardness, impact toughness*

The producing of welded joints of hardening heat-resistant steels is connected with the need in postweld high-temperature heat treatment. The purpose of this operation is the providing of equilibrium state (tempering) to hardening structures, imparting the required mechanical properties to welded joints and relieving of residual stresses. Moreover, one of the problems, to which a special attention is paid during tempering of martensite steels with an increased chromium content, is the providing of the required level of impact toughness of weld metal, for example, for welds with 9 % Cr at impact energy of $KV \geq 41$ J at 20 °C (at Charpy test of specimens that corresponds to the specific energy of fracture $KCV \approx 51$ J/cm^2) [1, 2].

To guarantee the obtaining of high values of impact toughness the positive factor is the increase in temperature and holding duration at tempering. By this reason, if there is no special conditions as to the possible change in steel properties, the tempering is made at temperature of the base metal tempering at the stage of its producing. To avoid the additional reduction of strength properties of base metal the postweld tempering is specified by 20–40 °C below the temperature used in base metal producing [3].

The similar situation occurred in welding of one of the experimental martensite steels with increased content of chromium in the scopes of investigations, carried out by the project Z-Ultra of the 7th European program [4]. The electrodes Thermanit MTS616 (Bohler Thyssen Schweisstechnik) with a martensite deposited metal of 10Kh9V2MFB type were selected for welding. The recommended tempering for such metal of welds consisted in holding at 760 °C for 2 h [5]. The developer of the experimental steel specified the tempering of welded joints of not higher than 730–720 °C with account for its heat treatment condition. The need occurred in checking the feasibility of providing the required level of the impact toughness of welds at the above-mentioned tempering conditions.

The aim of the work was in selection of the mode of heat treatment of welded joints of heat-resistant steel with a martensite weld of MTS616 (10Kh9V2MFB) type at the temperature, being lower than that recommended by the developer of welding electrodes.

During experiments the properties of weld metals were studied, produced in manual arc welding of butt joints of 20 mm thick plates by electrodes Thermanit MTS616 of 3.2 mm diameter. Chemical composition of metal deposited by electrodes Thermanit MTS616 is following, wt%: 0.11 C, 0.19 Si, 0.63 Mn, 0.016 P, 0.006 S, 8.5 Cr, 0.56 Mo, 0.57 Ni, 0.18 V, 1.58 W, <0.1 Cu, 0.055 Nb, 0.044 N. As a base metal, the steel was used, somewhat differing from the system of alloying the metal, deposited by the selected electrodes. To avoid the stirring of steel and electrode metal the plate edges were lined with metal of MTS616 type.

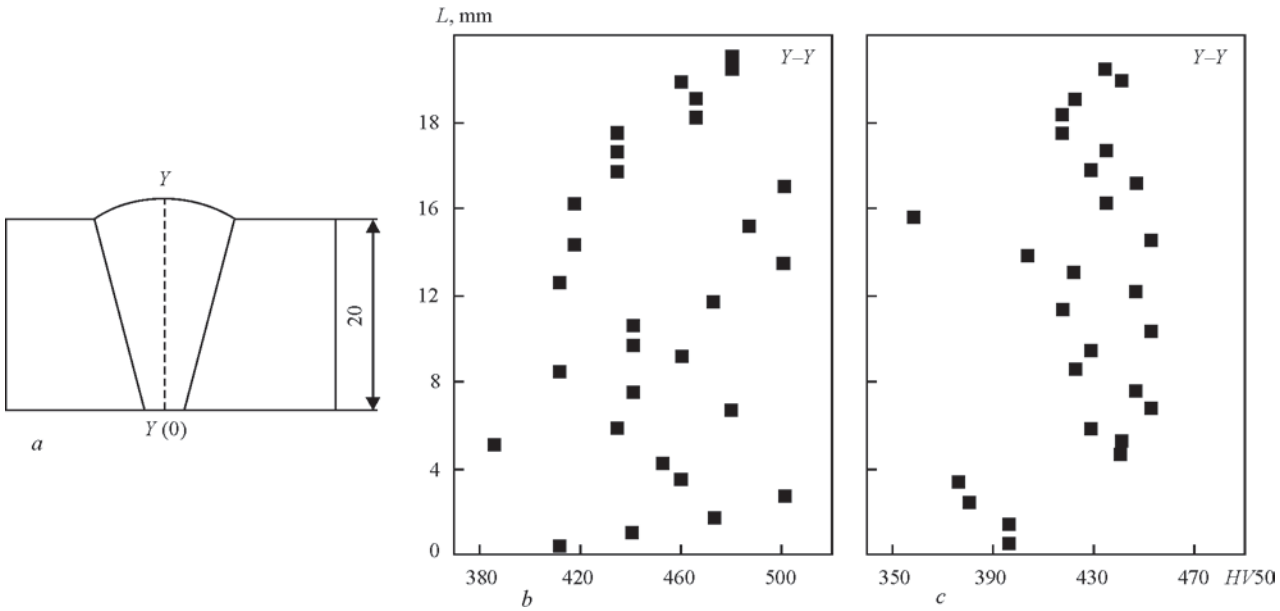

Figure 1. Change in hardness in the center of welds: *a* — zone of measurement; *b*, *c* — results for I_w = 100 and 120 A, respectively (point *Y*(0) in root pass corresponds to zero mark)

Such approach allowed evaluating the properties of «purely» electrode metal. The effect of tempering duration (in the ranges from 4 up to 12 h) at 720 and 730 °C on hardness and impact toughness of weld metal at room temperature was determined. Hardness was measured by using Vickers method at 5 kg load to indenter. The impact bend tests were performed by using 10×10 mm section specimens with a sharp notch (type IX by GOST 6996–66).

In practice the producing of joints of hard-to-weld heat-resistant steels is recommended by welding of beads of small thickness at the lowered modes to attain the improved values of the weld metal impact toughness [6, 7]. This provides the producing of fine-crystalline primary structure, as well as a partial tempering of layers, made earlier, during laying out of next beads. The subsequent high tempering of welds with a disoriented crystalline microstructure and with a partially improved toughness allowed reaching the required level of the impact toughness values. The similar approach was used in the present work.

Preliminary the experiments were carried out for selection of welding modes providing a stable burning of electrodes, quality weld formation, good fusion of deposited and base metal, easy performance of welding process and beads of small thickness. The experiments showed that in welding at lowered current (80–90 A) minimum possible for the stable arcing it is more complicated to provide the fusion of metal being deposited and edges of steel being welded. Here, to have a good formation of the quality bead, welding should be performed at a low speed. Under such conditions the energy input *q/v* can have the more higher values than in case of welding at high current, because in the latter case the increase in rate of electrode melting allows increasing the welding speed without deterioration of the forming weld quality. It was found that the optimum is the welding current in the range of 100–120 A. For the conditions and welding procedure used in experiments the energy input for I_w = 100, A was *q/v* = 5.15 kJ/cm, for I_w = 120 A *q/v* = 3.29 kJ/cm. Current of more than 130–140 A leads to a great overheating of the electrode rod, damage of coating and strong spattering.

The evaluation of nature of change in hardness along the vertical axis *Y–Y* in cross section of welds in the as-welded state showed (Figure 1) that the weld metal made at 120 A current is more homogeneous, the values of hardness have a less scattering than in case of welding at 100 A current. As a whole, it can be noted that in the given type of welds the metal reaction to thermal tempering effect is weakly manifested in making the next passes. Under the effect of repeated heating the hardness is decreased negligibly and remained at the level close to the state of hardened martensite (*HV*50-420–500 in welding at I_w = 100 A and about *HV*50-400–450 at I_w = 120 A).

Figures 2 and 3 present the results of evaluation of effect of a long-term tempering at 720 and 730 °C on values of toughness (*KCV, KV*) and hardness of weld metals produced at currents 100 and 120 A. The measurements of hardness were made in four regions of the weld cross section, located from one another approximately by 1/4 of joint thickness (according to scheme in Figure 2, *a*). In all the cases after heat treatment the hardness of welds was in compliance with the requirements of DIN EN ISO 15614-1 [8]. It was less than *HV* 350 according to the standard for the

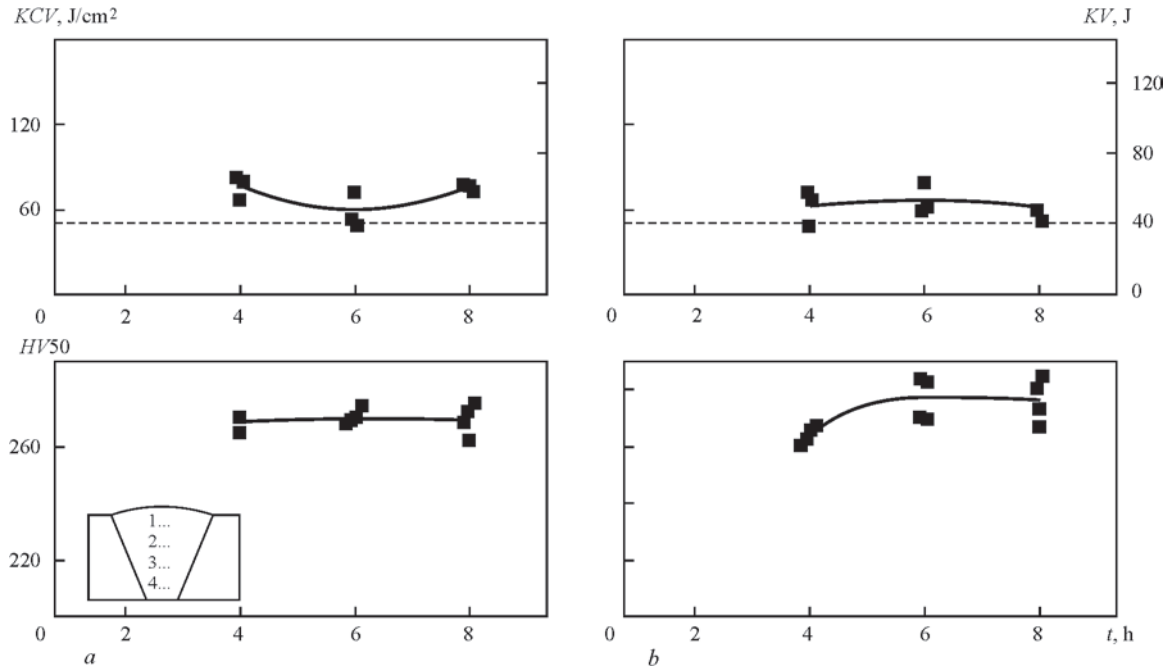

Figure 2. Effect of tempering mode on impact toughness and hardness of weld metal produced at I_w = 100 A: *a* — tempering at 720; *b* — 730 °C

joints of steels of group 6 (DIN CEN ISO/TR 15608 [9]), to which the metal of welds of the studied type is belonged. The values of impact toughness exceeded also the minimum allowable level (it is shown in diagrams by a horizontal intermittent line). However in weld made at 120 A the values of impact toughness were higher than in welds at 100 A current. This is, probably, connected with the higher homogeneity of deposited metal and more effective tempering of layers, made earlier, under the influence of the repeated welding heating. By this reason the condition of the multi-pass welding at 120 A current can be considered as more preferable.

As is seen from Figure 3, the hardness of welds, made at 120 A, after tempering at 720 °C for 4 h is at the higher level than that after the longer holding. Coming from the nature of change in hardness, the duration of tempering at this temperature, equal to about 5 h, can be taken as an acceptable one. Moreover, the sufficiently high impact toughness at the level of 100 J/cm^2 is provided.

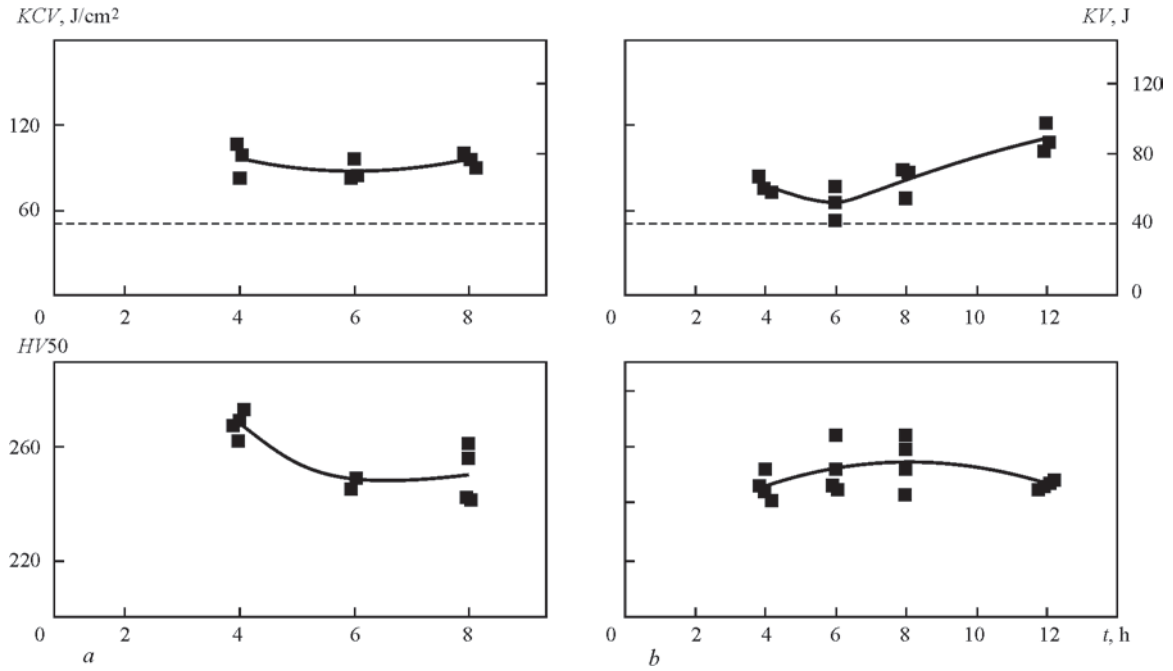

Figure 3. Effect of tempering mode on impact toughness and hardness of weld metal produced at I_w = 120 A: *a* — tempering at 720; *b* — 730 °C

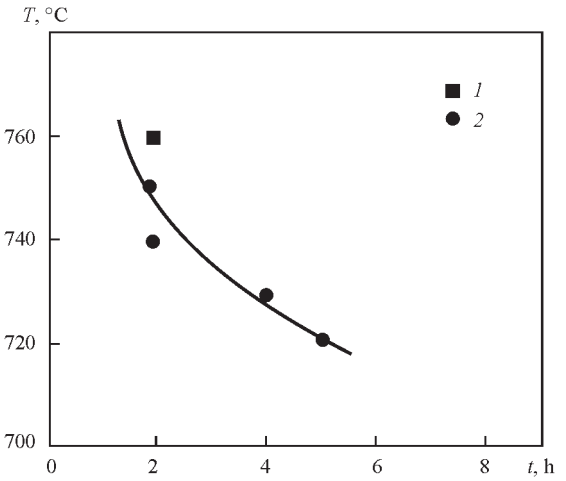

Figure 4. Temperature versus holding at high tempering to provide the required impact toughness of metal of welds in manual arc welding: *1* — recommendations of electrode manufacturer; *2* — results of experiments

During tempering at 730 °C and holding for more than 4 h the tendency to the secondary hardening was manifested in both types of studied welds (welded at 100 and 120 A modes). In this case, *KCV* values decreased noticeably in welds, made at 120 A current, which began to increase again after holding for 8 h and more. Taking into account that the high-temperature treatment is a power-consuming and an expensive operation, the tempering at possible lower holdings is economically more profitable. Therefore, in case of heat treatment at 730 °C it is rational to apply holding of about 4 h. After this tempering mode the *KCV* values reach the level of approximately 80 J/cm^2. The same tempering modes can be applied also for the welds made at 100 A current, however, as the obtained results showed, in this case the welds have the lower impact toughness (at the level of about 60 J/cm^2).

As a general conclusion, Figure 4 presents the dependence showing the relation between the temperature and holding duration in the process of high tempering, at which the impact energy of metal of welds is provided being of not lower than the minimum value 41 J.

It should be noted that in some cases in evaluation of weld metal properties the *KV* value of 27 J is used as a criterion of admissible value of the impact toughness [10]. This *KV* value was regulated for the cross section of seamless pipes of heat-resistant steels (see, for example, standard BS EN 1021602:2002 [11]). However, in our opinion, the application of this criterion for welds is seemed to be discussible. The lowered toughness in cross section of pipe wall in case of abrupt increase in acting loads (which are formed, for instance, in testing of pipe systems at hydraulic tests or putting the high-temperature components into operation) can cause more probably the fracture in the form of delamination without a through damage. The same lower toughness of weld metal with a cast structure can cause its transverse fracture, which is a rather hazardous defect. Therefore, the authors of the given work made all efforts to provide the higher values of impact toughness of weld metals, taking into account the requirement $KV \geq 41$ J.

Thus, the carried out investigations showed the feasibility of providing the requirement to the impact energy of $KV \geq 41$ J of metal of the martensite weld of 10Kh9V2MFB type, made by manual arc welding with electrodes Thermanit MTS616, using tempering at temperature by 30–40 °C lower than it is recommended by the developer of electrodes. The conditions of providing the required level of toughness are the following:

- multi-pass welding by small beads at modes with lowered energy input (for example 3.3–5.1 kJ/cm in welding with electrodes of 3.2 mm diameter);
- high-temperature postweld heat treatment at 730–720 °C for 4–5 h.

1. Bergquist, E.-L. (1999) Consumables and welding modified 9Cr-1Mo steel. *Svetsaren*, **1/2**, 22–25.
2. Hoiser, G. (1997) Filler materials for welding in power machine building. *Avtomatich. Svarka*, **9**, 40–44, 47.
3. Petrov, G.L., Zemzin, V.N., Gonserovsky, F.G. (1963) *Welding of heat-resistant stainless steels*. Moscow: Mashgiz.
4. Z phase strengthened steels for ultra-supercritical power plants. *http*://www.z-ultra.eu
5. (2005) *Welding filler metals. Welding guide*. Hamm: Boehler Thyssen Schweisstechnik.
6. Rosenbrock, L.A. (2001) A critical overview of the welding of P91 material. *Australian Welding J*., 46(2nd Quart.), 5–8.
7. Adam., W., Mischok, W., Wellnitz, G. et al. (1994) Welding of new types of steel for power plant construction. In: *Proc. of Conf. on Welding and Cutting* (Germany, Bremen, 28–30 Sept. 1994). Boehler Welding Special Add.
8. *DIN EN ISO 15614-1*: Anforderung und Qualifizierung von Schweissverfahren fuer metallische Werkstoffe – Schweissverfahrenspruefung. Teil 1: Lichtbogen- und Gasschweissen von Staehlen und Lichtbogenschweissen von Nickel und Nickellegierungen. Deutsche Fassung prEN ISO 15614-1:2013.
9. *DIN CEN ISO/TR 15608*: Schweissen – Richtlinien fuer eine Gruppeneinteilung von metallischen Werkstoffen. Deutsche Fassung CEN ISO/TR 15608:2013.
10. Mokhila, P., Foldynova, K. (2014) Influence of postweld heat treatment on mechanical properties of R92 steel welded joints made by submerged-arc welding. *Metallovedenie i Termich. Obrab. Metallov*, **4**, 36–39.
11. *BS EN 1021602:2002*: Seamless steel tubes for pressure purposes. Technical delivery conditions. Pt. 2: Non-alloy steel tubes with specified elevated temperature properties. CEN, 2007.

Received 29.02.2016

doi.org/10.15407/tpwj2016.09.11

FEATURES OF PORE FORMATION IN WELDED JOINTS OF STEAM LINES IN LONG-TERM OPERATION

V.V. DMITRIK[1], **A.V. GLUSHKO**[1] and **S.G. GRIGORENKO**[2]
[1]National Technical University «Kharkov Polytechnic Institute»
21 Frunze Str., 61002, Kharkov, Ukraine. E-mail: omsroot@kpi.kharkov.ua
[2]E.O. Paton Electric Welding Institute, NASU
11 Kazimir Malevich Str., 03680, Kiev, Ukraine. E-mail: office@paton.kiev.ua

The paper presents the results of investigation of pore formation in the metal of welded joints in steam lines operating for a long time under creep conditions. Features of pore formation in the regions of welded joint HAZ were revealed that allows improvement of diagnostic assessment of their residual life. Critical threshold of welded joint damage is local density of micropores of 0.8 μm and larger size on the level of 1500–1800 pores per mm^2. 7 Ref., 7 Figures.

Keywords: *steam line welded joints, pores, residual life, diagnostics, damageability, diffusion movement*

Diagnostics of residual life of welded joints of TPP steam circuit, which have exhausted their service life, currently is a most important task of thermal power generation in Ukraine.

During long-term operation of welded joints on Cr–Mo–V heat-resistant pearlitic steels under creep conditions, their damage is due predominantly to pore formation and development. Pore damage in the metal of HAZ, as well as weld and base metal is insufficiently studied, that does not allow diagnosing the residual life of steam line welded joints with sufficient accuracy.

Pore nucleation and development in steam line metal should be regarded as interconnected components of their damage process. The objective of the work was studying the features of the mechanism of pore formation in the metal of welded joints in steam lines from 15Kh1M1F and 12Kh1MF steels in long-term operation. Investigation results allowed lowering the intensity of pore formation and refining the diagnosis of residual life of steam line welded joints [1–7], which are damaged more intensively than the steam line proper.

Welded joint metal structure was studied using microstructural, microprobe and X-ray methods on experimental samples, as well as samples cut out of operating steam lines (Zmiev and Energodar TPPs). Processes of micropore and microcrack formation were examined by electron and optical microscopy.

Micropores nucleate as a result of conjugate effect of diffusion and deformation mechanisms. Diffusion mechanism provides directional displacement of alloying elements, that leads to formation of segregations, and also causes displacement of microdiscontinuities and their coalescence [1]. Deformation mechanism includes the process of dislocation displacement and their retardation, that provides local increase of dislocation density and formation of pore nuclei, the dimensions of which can be approximately 0.1 μm.

Diffusion-induced movement of alloying elements (chromium and molybdenum) from central zones of α-phase grains into their near-boundary zones, as well as movement of reduced elements along grain boundaries leads to formation of segregations, promoting running of carbide reactions of I gr [1]. Movement of alloying elements leads to decrease of strength characteristics of α-phase grains, that is confirmed by fragmentation (polygonization) of grains and higher level of their deformation, respectively [2]. It is found that the level of deformation of HAZ regions is much higher than mass deformation of the steam lines equal (at welded joint operating time of more than 250,000 h) to approximately 0.5–0.7 % (Figure 1). It can be shown that deformation of weld metal in welded joints is only slightly different from that of metal of steam lines proper.

In the initial metal of welded joints microdiscontinuities and micropores are chaotically arranged through the body of α-phase grains and along their boundaries. Such an arrangement is preserved approximately up to 150,000 h of steam line operation. During further operation, pore formation occurs with a certain orientation. Pore shape from spherical and ellipsoidal (regular) turns into branched (irregular) during their development. Then the merged pores develop into a crack (Figure 2). Creep cracks have a zigzag shape and develop after welded joints have operated for more than 270,000 h, predominantly in the brittle mode. Pore formation essentially depends on welded joint structure [7].

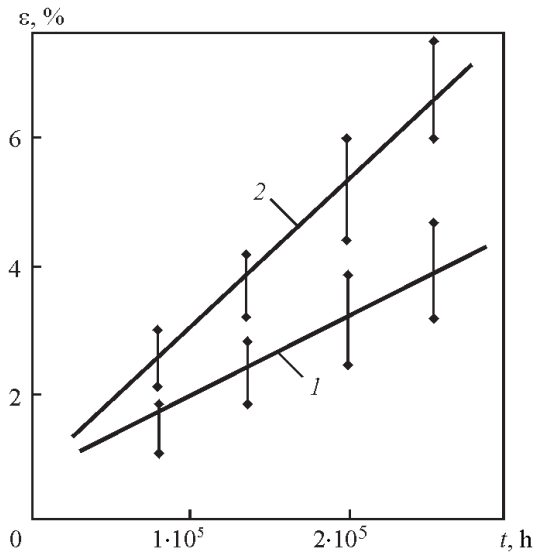

Figure 1. Dependence of relative deformation of metal of 12Kh1MF steel welded joints on its operating time: *1* — HAZ overheated region; *2* — incomplete recrystallization region

To refine the diagnosis of welded joint residual life, it is rational to determine pore density in those regions of welded joint HAZ, where the greatest structural inhomogeneity is noted, for instance, in incomplete recrystallization region, where new products of austenite decomposition are globular pearlite [6].

Pore formation occurs predominantly along the boundaries of α-phase grains and depends on the following: grain boundary location relative to working stresses; structure of grain boundaries (boundaries between two and three grains); and presence of second phase precipitates along the grain boundaries. Pore formation can be regarded as an effect of vacancy condensation due to the degree of plastic deformation, that leads to local oversaturation of grain boundaries with vacancies and formation of microdiscontinuities [4, 6]. Their formation under creep conditions is provided by development of inner slipping and sliding along the boundaries of α-phase grains. This is the most intensive in the locations of coagulating second phase precipitates [2].

Figure 2. Microsection (×500) of welded joint metal of 12Kh1MF steel line with creep damage after operating time of 280,000 h at 545–565 ºC

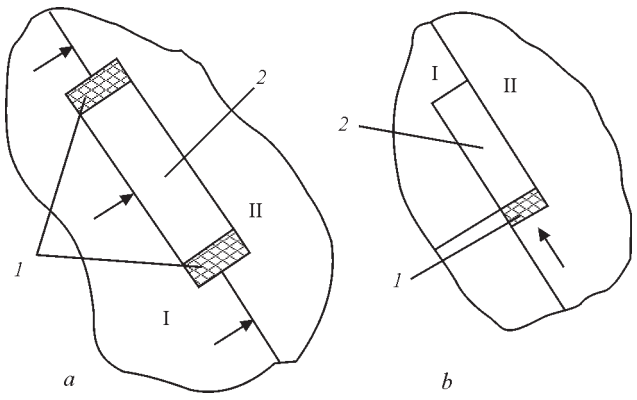

Figure 3. Schematic of micropore nucleus formation: *a* — formation of cavity *1* on edges of second phase precipitates *2*; *b* — sliding along the boundary at precipitate *2* leading to formation of micropore nucleus *1*; I, II — grains separated by boundary

Sliding along the boundaries of α-phase grains in locations of boundary interaction with a coagulating precipitate leads to opening up of the cavity, developing into a nucleating micropore (Figure 3). Further development of pore formation is characterized by certain stages and depends on the structure and conditions of steam line operation (Figure 4).

Under creep conditions (operating time of welded joints of more than 250,000–280,000 h) pore formation through α-phase grain body is of chaotic nature. However, pore arrangement along the grain boundaries has certain peculiarities. Micropores form:

- on boundaries normal to tensile stresses, in the points of location of coagulating precipitates of second phases (predominantly, $M_{23}C_6$) — about 70 %;
- at the junction of three grains without second phase precipitates — 20 % (Figure 5);
- at the junction of two grains — 10 %.

Micropore formation leads to lowering of metal ductility, and is associated with presence of residual deformation. For instance, at mass deformation of welded joint metal of 0.6 %, deformation of metal in HAZ incomplete recrystallization region can be equal to 4–6 % (operating time of 280,000 h) that is close to the data of Khromchenko (6–8 %, operating time of 250,000 h) [4].

Note that Khromchenko calls the region of HAZ incomplete recrystallization a «soft interlayer», although its hardness in welded joints of the considered steels 15Kh1M1F and 12Kh1MF can be not less than that of other HAZ regions. Incomplete recrystallization region is characterized by the highest oversaturation with vacancies, compared to other welded joint regions. Such oversaturation is due to self-diffusion of chromium and molybdenum from central zones of α-phase grains into near-boundary regions and formation of segregations, as well as diffusion of vacancies and generation of vacancy fluctuations [6]. Fluctua-

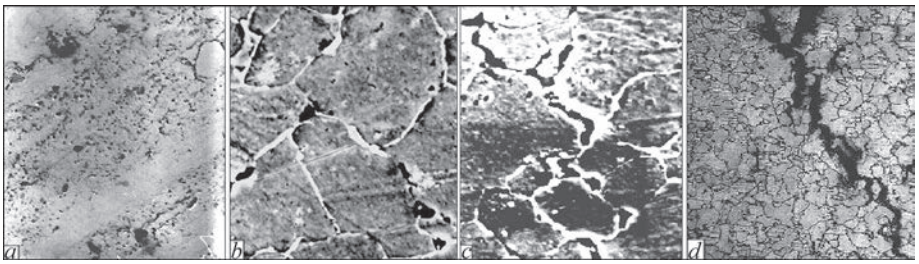

Figure 4. Sequence of pore development in welded joints of 12Kh1MF steel: *a* — pore nuclei of 0.1–0.3 μm diameter (×5000); *b* — separate pores of 1–4 μm diameter along grain boundaries (×2500); *c* — pores at the stage of coalescence into microcracks (×2500); *d* — creep crack (×500); reduction 2/3

tions tend to increase during welded joint operating time of more than 250,000 h. Greenwood's suggestion that pores on grain boundaries under creep conditions should be regarded as the effect of condensation of vacancies, the excess of which relative to the equilibrium concentration is due to plastic deformation, is confirmed [5]. It is found that the number of micropores is increased at increase of plastic deformation. Pore formation is promoted by reduction of the energy of grain boundaries at elimination of part of their surface, that can be regarded as the initial period of recrystallization. The connection between oversaturation with vacancies (Δ/c_0) and radius r of growing nucleus during diffusion-induced nucleation of a pore was established by Geguzin [5]:

$$r = 2\gamma V / kT(\Delta / c_0),$$

where γ is the surface energy; $V = b^2$ is the atomic volume; $\Delta = c_1 - c_0$ is the change of vacancy concentration; c_1 is the established concentration of vacancies; c_0 is the equilibrium concentration of vacancies; k is the Boltzmann constant; T is the temperature.

It can be assumed that vacancy concentration in welded joint metal (more than 250,000 h operating time) is 4 to 8 times higher than the equilibrium one.

Considering $b = 3.10^{-3}$ cm and $\gamma = 500$ erg/cm^2, we will obtain for temperature of 545 ºC the size of pore nucleus including approximately 10^7–10^9 vacancies. At further operation under the conditions of working stresses and temperatures, as well as the influence of additional factors (overheating, start/stop of the pipeline, local increase of stresses, etc.) the extent of oversaturation by vacancies can rise by approximately 30–40 %.

Respective tensile stresses are induced near the coagulating precipitates, where the dislocations accumulate. Dislocation accumulation is noted at electron microscopy studies of thin foils from samples of welded joints with operating time longer than 270,000 h. This is confirmed by formation of a polygonal structure of α-phase grains, i.e. their fragmentation (Figure 6). In the structure of α-phase crystals under creep conditions slipping occurs in the direction of the diagonals of cubic lattice <111> in the set of dodecahedral planes {110}. After welded joints operating for more than 250,000 h, slipping occurs first in planes {112}, and then also in planes {123}. Slipping along grain boundaries, depending on precipitate location, generates tensile and compressive stresses, respectively (see Figure 3). Long-acting tensile stresses lead to cavity opening. Micropore nucleation is also related to formation of sub-boundaries near coagulating precipitates.

Known models of pore formation did not allow for presence of coagulating precipitates along the grain boundaries. Note that the sliding speed, required for micropore formation in long-operated welded joints, can be different. Speed depends on arrangement of grain boundaries, their structure, presence of coagulating precipitates of second phases on them and their coagulation intensity. Length of precipitates located along the grain boundaries can be equal to 1–5 μm at welded joint operating time longer than 280,000 h. It is established that the quantity of pores forming on grain boundaries depends on their deformation.

For instance, in the metal of incomplete recrystallization region of welded joint HAZ in 15Kh1M1F steel at its deformation of 5–7 %, averaged density of pores of 2–8 μm size per 1 mm^2 was equal to 7.2 pcs. Deformation of HAZ regions essentially depends on their structure. In the presence of new products of austenite decomposition in the form of globularized pearlite in the structure of incomplete recrystallization region, its deformation can be equal to 5–7 %, if they have the form of sorbite it can be 1–2 %, in case of troostite it can be about 1% at mass deformation of

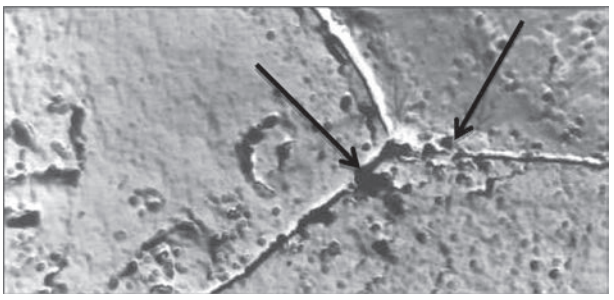

Figure 5. Microsection (×14000) of metal of incomplete recrystallization region in HAZ of 12Kh1MF steel welded joint showing pore nucleation along the junction of three grains (*arrows*) at operating time of 275,637 h

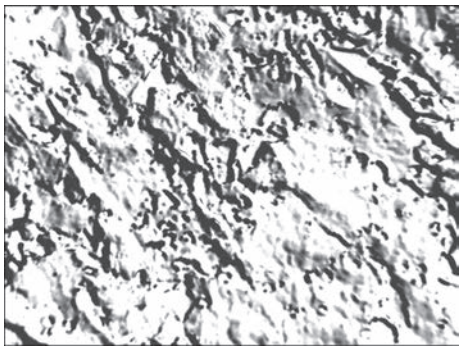

Figure 6. Fragmented structure (×6000) of incomplete recrystallization region in HAZ of 15Kh1M1F steel welded joint at operating time of 276,000 h

welded joints of about 0.7 %. Pore density, depending on operating time of welded joints with the respective structure of new products of austenite decomposition, was distributed as follows (Figure 7).

Obtained results show that the density of micropores of more than 0.8 μm size, equal to approximately 1500–1800 pcs per mm^2, can be regarded as critical. Further increase of pore density leads to their accelerated coalescence and formation of creep cracks. Such cracks develop, predominantly, in the brittle mode, that is promoted by presence of coagulating precipitates along the boundaries of α-phase grains and of grain-boundary segregations.

Quantity of pores at constantly applied tensile stresses depends on the interaction of inner slipping and sliding, that is initially provided by self-diffusion of chromium and molybdenum, as well as diffusion of vacancies. Their retardation, i.e. lowering of intensity, improves the structure stability under creep conditions.

Sliding can be regarded as the effect of relative displacement of local regions of grain boundaries. Nucleation of microdiscontinuities at the precipitates is related to violation of coherence of precipitates and α-phase grains, that is noted at precipitate coagulation. Increase of stability of metal structure in welded joints operating for a long time under creep conditions, essentially reduces the intensity of pore formation.

Conclusions

1. It is found that pore formation is the most intensive in the region of incomplete recrystallization of welded joint HAZ, where new products of austenite decomposition are globularized pearlite.

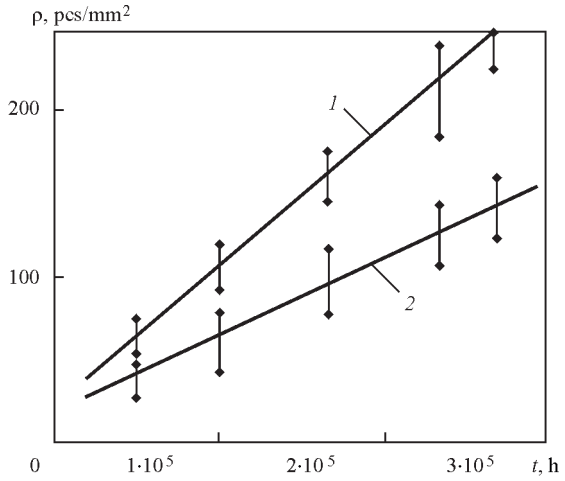

Figure 7. Dependence of density ρ of creep pore with longitudinal size of 0.5–1.1 μm formed in incomplete recrystallization region of HAZ of 12Kh1MF steel welded joint on its operating time *t* in the presence of new products of austenite decomposition in the form of globularized pearlite (*1*) and sorbite (*2*) at operating time of 276,000 h

2. It is established that at damage of welded joints in steam lines in long-term operation under creep conditions, density of micropores of 0.8 μm and greater size, equal to 1500–1800 pcs per mm^2, can be regarded as critical.

3. It is shown that the quantity of micropores in the regions of HAZ metal of steam line welded joints depends on the region deformations and is the largest in incomplete recrystallization region, where new products of austenite decomposition are globularized pearlite.

1. Dmitrik, V.V., Baumer, V.N. (2007) Carbide phases and damageability of welded joints in long-term service. *Metallofizika, Nov. Tekhnologii*, 2(**7**), 937–947.
2. Dmitrik, V.V., Sobol, O.V., Pogrebnoj, M.A. et al. (2015) Peculiarities of degradation of metal in welded joints of steam pipelines. *The Paton Welding J.*, **7**, 10–15.
3. Trubachev, V.M., Kamenskaya, N.I. (2012) Methods of evaluation of microdamageability of metal in long-term service steam pipelines of thermal power station. *Metallovedenie i Termich. Obrab. Metallov*, **8**, 49–54.
4. Khromchenko, F.A. (2002) *Service life of welded joints of steam pipelines*. Moscow: Mashinostroenie.
5. Rozenberg, V.M. (1967) *Creep of metals*. Moscow: Metallurgiya.
6. Dmitrik, V.V., Sirenko, T.A., Bartash, S.M. et al. (2015) Refinement of metal damageability mechanism of welded joints in long-term service steam pipelines. *Vost.-Evrop. Zhurnal Pered. Tekhnologij*, **6**, 13–18.
7. Berezina, T.G. (1986) Structural method for definition of residual life of parts in long-term service steam pipelines. *Teploenergetika*, **3**, 53–56.

Received 12.05.2016

doi.org/10.15407/tpwj2016.09.12

MODERN APPROACHES TO PERFORMANCE OF TOXICOLOGICAL AND HYGIENIC STUDIES OF WELDING FUMES (REVIEW)

A.O. LUKIANENKO[1] and **A.V. DEMETSKAYA**[2]
[1]E.O. Paton Electric Welding Institute, NASU
11 Kazimir Malevich Str., 03680, Kiev, Ukraine. E-mail: office@paton.kiev.ua
[2]Institute of Occupational Medicine, NAMSU
75 Saksagansky Str., 01033, Kiev, Ukraine

The paper provides an overview of the results of studying the nanoscale fractions in the working zone air during welding operations and in the welder's breathing zone, as well as data of toxicological studies of welding fumes (WF) in experiments on laboratory animals (in vivo) and in cell culture experiments (in vitro). It is suggested that the high disease rate in welders can be caused not only by toxicity of WF components having irritating and mutagenic effects, but also by the ability of nanoscale particles (nanoparticles) to penetrate deeply into the tissues. The data of hygienic studies of nanoparticle emission into the working zone air during welding operations, as well as of studying nanoscale fraction deposition in the respiratory tract of welders are presented. It is shown that decrease in the content of hexavalent chromium and manganese in the welding consumable involves increasing the concentrations of other metals, and thus does not guarantee safety for the welder. The role of prediction of WF harmful effects on the body by controlling the working conditions using modern hygienic approaches is substantiated. Simultaneous application of in vitro and in vivo methods to provide the most complete information about the potential hazards of WF, peculiarities of biological action of its components, as well as the need to develop not only informative, but also less time-consuming and costly express-methods of screening assessment of toxicity of WF, generated at different types of welding was substantiated. These methods will allow evaluation of the cumulative effect of the impact of totality of toxicants present in WF solid component, including unidentified components. 21 Ref.

Keywords: *welding fumes, solid component of welding fume, working zone air, cytotoxicity, in vitro, in vivo, nanoparticles*

Members of welding professions have a special place among the workers exposed to a set of harmful factors. This is due to broad application of welding technologies and operations in different industries, construction, transportation, etc. [1] with the number of welders is increasing steadily. While in 2008 their number was more than 1 mln persons, in 2010 already there were reports about 5 mln welders worldwide [2] that may be associated with increase in population and development of infrastructure.

Depending on the type of production operation, kind of metal, type of welding consumables and production technologies, the welder is exposed to harmful production factors of different nature. Investigations of presence of harmful substances in the air of working zone and breathing zone of workers, engaged in various types and processes of welding, showed that the most unfavourable factor is exactly the chemical one. Performance of welding operations is accompanied by formation of harmful factors of chemical nature, which are based on toxic components of welding fumes (WF), as weld as flux dust. In its turn, their quantitative and qualitative composition depends on welding process, metal composition, etc. [3].

Note that among the set of harmful industrial factors WF, in the opinion of many researchers, have the most negative influence on the human body. Biological activity of metal compounds, present in WF composition, depends on their ability to bind with blood and tissues proteins, increase the permeability of cell membranes or damage them, block intercellular and extracellular enzyme systems that, eventually, leads to pathological changes in the body. Results of analysis of electric welders' incidence rates revealed that the nervous, respiratory and osteomuscular systems are the most sensitive to the impact of the specific set of harmful factors [4]. Clinical and epidemiological studies confirm the association of pulmonological effects with higher rate of cardio-vascular disorders, and the results of recent in vivo toxicological studies on laboratory animals confirmed the hypothesis of direct damaging effect of WF on cardio-vascular system [5].

It is known that the level of risk of WF having a harmful effect on the body is, primarily, determined by welding process and type of welding equipment, technological parameters of welding modes (welding

current, arc voltage, electrode diameter), kind and composition of welding consumable. The nature and severity of welders' diseases caused by WF harmful substances depend on their concentration in the breathing zone. Concentration of WF solid component (WFSC) and other harmful substances in welders' breathing zone grows in proportion to their formation rate in the arc zone [1].

Despite the fact that WFs have been studied for quite a long time, many aspects of the dependence of their biological aggressiveness on the main physico-chemical properties are still unclear. The latter include dispersity of particles of WFSC, their structural parameters, and solubility of individual components. At present it has been suggested that the high incidence rate in electric welders is due not only to toxicity of WF components, characterized by irritating and mutagenous action, but also by ability of nanoscale particles (nanoparticles) to penetrate deeply into the tissues. It is known that sufficient experimental data has been accumulated in recent years, which indicate that the substances in the nanorange are characterized by higher bioactivity and damaging effect [6, 7].

In particular, results of conducted morphological and chemical studies are indicative of the same nature and similar mechanisms of WFSC formation in welding with electrodes with different types of coatings. Nanosized particles are the main components of all WFSC. They are mainly grouped into agglomerates, numbering from a few up to thousands of particles, which, according to X-ray microanalysis, consist predominantly of compounds of alkali metals, silicates and iron oxides. Integral chemical composition of WFSC nanosized particles essentially depends on the type of electrode coating. It is established that minimum dimensions of WFSC stable components are quite close (300–600 nm) in the studied welding electrodes (UONI 13/45 and 2TsM7) [8]. However, their characteristics of solubility in aqueous medium and stability to mechanical impact significantly differ.

This circumstance is extremely important in terms of potentially dangerous interaction of WF with the human body and necessitates investigations of WFSC nanosized fractions in the welder's breathing zone. In the European countries and the USA studies of nanosized particle deposition in the respiratory tract of members of welding professions are performed using personal samplers [9]. When studying the deposition of nanosized fractions of chromium, manganese and nickel in the respiratory tract in gas-shielded metal-arc welding of low-carbon and stainless steel and in flux-cored wire arc welding of low-carbon steel, the welders were equipped with individual samplers of WF nanofractions, as well as cassette filters for evaluation of the total number of particles. Concentration of manganese for both the welding processes varied in the range of 2.8–199, nickel — 10–51, chromium — 40–105 mg/m^3. Concentration of hexavalent chromium varied in the range of 0.5–1.3 mg/m^3 [9]. As regards the fraction of manganese, chromium and nickel in particles of nanosized fractions relative to their content in WF, it is as follows: in welding of low-carbon steel manganese fraction was equal to 10–56 %, and in welding of stainless steel manganese fraction was 59, that of nickel was 64 and that of chromium was 90 %. These results are indicative of the fact that the vast majority of chromium, manganese and nickel are present in particles of nanosized fractions smaller than 300 nm [9].

Nanoparticle emissions in working zone air during welding operations can be assessed also using stationary instruments, which record in real time the total number of particles from 1 up to 200 nm and their size distribution. In particular, diffusion aerosol spectrometer DAS-2702 was used to obtain data on dynamics of changes in time of the number of WFSC particles in different ranges of their dimensions from 1 up to 100 nm, after welding with electrodes with rutile and carbonate-fluorite type of coating. It was found that nanoparticle concentration in working zone air depends on welding electrode grade and diameter, as well as distance from the welding zone (particle concentration decreases with greater distance from the sampling point to the welding zone). It was also established that in the production premises where welding operations are performed all the time, WF nanoparticles can stay in the air medium for a long time after the operations are stopped [10].

Kind of welding consumable, particle size and time after impact are important factors in formation of free radicals and deposition of particles, which should be taken into account when developing protection strategies [2]. Animal studies showed that WF is removed from the body in three stages. At the first stage, alveoli and airways are cleared with the help of mucus, which then penetrates into the alimentary tract and is quickly removed with semi-clearance period of one day. At the second stage, the process runs slower, semi-clearance period is up to 7 days. At the third clearance stage, clearance of the lungs proceeds slower and is more complex: semi-clearance period can be up to several weeks. At this stage, removal of individual particles is associated with their ability to dissolve in tissues and with continuous clearance of the lungs by macrophages [11].

It is remarkable that in vivo experiment to study long-term presence and deposition of metals in the lungs, as well as inflammatory potential after inhalation

priming of laboratory animals (rats) with WF, metals detected in the lungs were removed at different times. Priming was performed with WF (57 % Fe, 20 % Cr, 14 % Mn, 9 % Ni), which forms in stainless steel welding and WF (83 % Fe, 15 % Mn), which forms in low-carbon steel welding. So, potentially more toxic chromium and manganese were removed from the lugs faster than iron, probably, owing to their movement from the respiratory tract to other tissues [12].

It should be noted that the consequence of welding processes, generating aerosols containing such toxic metals as hexavalent chromium, manganese and nickel, is lung tissue damage and inflammation and lung tumors in animal experiments. Manganese presence in WF increases the risk of undesirable neurological responses, such as Parkinson disease, etc. [13]. There are data on manganese nanoparticle involvement in development of manganese-induced Parkinsonism in welders, because of its ability to penetrate into the brain through olfactory nerve [7]. In its turn, chromium and nickel presence can cause damage and inflammatory processes in the lungs, tumors, immune disorders and systemic toxicity. Nickel can cause malignant neoplasms in the lungs [13]. Despite the fact that in the USA the permissible exposure limit in the workplace was lowered (from 0.05 to 0.005 mg/m^3, that, by the way, is 2 times lower than in Ukraine), in practice it is not always possible to protect welders who often have to work in closed confined space, and exhaust ventilation can be ineffective here [13]. It is known [13] that this gave rise to the initiative of minimizing potentially hazardous components in welding consumables through development of new consumables with lower Cr (VI) and Mn content.

WF potential hazards are traditionally assessed using both toxicological methods in vivo (on laboratory animals), and adequate short-term tests in vitro (when experiments are performed «in vitro» — outside the living organism). Express-methods in vitro allow determination of WF toxicity in a relatively short time, thus saving time and reducing the number of laboratory animals used in experiment. However, these methods are not mutually exclusive. Express-methods in vitro are required for screening assessment of WF toxicity, providing preliminary information on potential hazard of a welding consumable and maximum rational planning of experimental studies during in vivo tests.

Specifics of biological impact of WF containing different quantities of manganese, iron, chromium, nickel and silicon in WFSC, were précised earlier. The connection of WF cytotoxic effect with WFSC initial composition, their solubility in biological solutions of the body, and biosphere simulator solution was established. The extent and nature of WFSC combined impact are enhanced at increase of the content of potassium, silicon, fluorine, sodium and calcium (in decreasing order of harmful effect) [14]. In vitro studies of cell culture showed that soluble particles, formed in manual arc welding of stainless steel, are more toxic than WF particles, forming in gas-shielded arc welding of stainless and low-carbon steel [15].

The role of WFSC soluble and insoluble components containing hexavalent chromium [16–20] was also studied. In particular, it was established that WFSC forming in coated electrode manual arc welding is more toxic, and has a transforming effect on laboratory animal cells, that was associated with the presence of hexavalent chromium in WFSC, while the contribution of other components, namely trivalent chromium, fluorides, nickel and manganese is small. Insoluble components containing hexavalent chromium have a more toxic and transforming effect on fibroblasts of hamster kidneys than hexavalent chromium.

Here mitotic delay cannot be attributed only to hexavalent chromium concentration, it can be also affected by other components of WFSC [20].

Now it seems clear that a combination of in vitro and in vivo methods provides the most complete information not only about WF potential hazard, but also about the specifics of biological effects of its components. In particular, assessment of pulmonary toxicity of fumes formed by Ni–Cu-containing electrodes (Ni–Cu WF) used as substitutes in Ar and CO_2 welding of stainless steel in experiments in vitro (culture of rat pulmonary macrophages in the doze of 0.05 and 0.25 mg/ml) and in vivo (intratracheal and intraperitoneal priming of laboratory animals in the dozes of 0.5 and 2 mg per rat demonstrated persistent damage and inflammation of lung tissue, as well as direct damaging action of pulmonary macrophages. Despite the fact that all the three aerosols (Ni–Cu WF, as well as aerosols, formed in stainless and low-carbon steel welding) reduced macrophage viability in the high dose (0.25 mg/ml) and had no significant effect in the low dose (0.05 mg/l), after 24 h Ni–Cu WF caused macrophage death in the low dose (0.05 mg/ml), i.e. demonstrated higher cytotoxicity compared to fumes generated in welding stainless and low-carbon steel. Thus, despite chromium reduction, considerable levels of nickel, copper and other potentially hazardous metals (titanium, aluminium) can enhance WF cytotoxic action [13].

Similar results were obtained when studying cytotoxic effects of Ni- and Cu-based welding consumable and two well-studied WF, formed in gas-shielded arc welding of stainless and low-carbon steel [21]. While WF formed in stainless and low-carbon steel

welding lead to increased production of free radicals, compared to Ni–Cu-containing material, the fumes from this new consumable were more toxic, including cell death and causing mytochondrial dysfunction in low doses (0.05 mg/ml).

Thus, despite the fact that toxic cell reactions in response to WF effect largely depend on metal composition, recent results of in vitro and in vivo studies convincingly show that reduction of hexavalent chromium and manganese content in welding consumable implies higher concentration of other metals, and, therefore, does not guarantee welder's safety.

In conclusion, it should be noted that prediction of harmful effects on the body by controlling the working conditions with application of modern hygienic approaches, and a complex approach to performance of toxicological studies of welding consumables (including new, potentially less toxic ones) in vivo and in vitro experiments have an important role in the search of effective methods of prevention of WF toxic component formation, and, accordingly, prevention of professional diseases. It is of certain interest to develop not only informative, but also less labour-consuming and expensive express-methods of screening assessment of toxicity of WF formed in different welding processes that will allow evaluation of cumulative effect from the impact of the totality of toxicants present in WFSC, including unidentified components. In its turn, substantiated and rational application of modern methods of WF toxicological-hygienic studies will contribute to a deeper understanding of processes, proceeding in the air of working zone in welding, and in biological media, as well as development of safer welding consumables and minimizing professional risk for welding profession members, respectively.

1. Levchenko, O.G. (2010) *Occupational safety in welding productio*n: Tutorial. Kyiv: Osnova.
2. Leonard, S.S., Chen, B.T., Stone, S.G. et al. (2010) Comparison of stainless and mild steel welding fumes in generation of reactive oxygen species. *Part Fibre Toxicol*., Nov. 3.
3. Gorban, L.M., Timoshina, D.P. (2004) Factors of professional risk of workers of modern welding production and ways for optimizing of their labor conditions. In: *Proc. of 24th Congress of Hygienists of Ukraine on Hygienic Sci. and Practice at the Boundary of Centuries*, Vol. 2, 69–71.
4. Kusraeva, Z.S. (2011) *Assessment of professional risk in modern methods of electric arc welding and cutting of metals*: Syn. of Thesis for Cand. of Medical Sci. Degree. St.-Petersburg.
5. Zheng, W., Antonini, J.M., Lin, Y.C. et al. (2015) Cardiovascular effects in rats after intratracheal instillation of metal welding particles. *Inhal Toxicol*., 27(**1**), 45–53.
6. Oberdoerster, G. (2010) Safety assessment for nanotechnology and nanomedicine: Concepts of nanotoxicology. *J. Int. Med*., 267(**1**), 89–105.
7. Elder, A., Gelein, R., Silva, V. et al. (2006) Translocation of inhaled ultrafine manganese oxide particles to the central nervous system. *Environ. Health Perspect*., 114(**8**), 1172–1178.
8. Stepanyuk, S.M., Pokhodnya, I.K., Yavdoshchin, I.R. (2012) Study of morphology, chemical composition and dispersion of particles of Ts3A welding electrodes with different types of coatings. In: *Proc. of 2nd All-Ukrainian Sci.-Techn. Conf. of Junior Sci. and Students* (Ukraine, Koblevo, 4–8 Sept. 2012).
9. Cena, L.G., Chisholm, W.P., Keane, M.J. et al. (2015) A field study on the respiratory deposition of the nano-sized fraction of mild and stainless steel welding fume metals. *J. Occup. Environ. Hyg*., 12(**10**), 721–728.
10. Demetska, O.V., Leonenko, O.B., Tkachenko, T.Yu. et al. (2012) Dynamics of concentration of ultradispersed particles in manual welding with electrodes. *Ukr. Zhurnal z Medycyny Pratsi*, **1**, 3–7.
11. James, M., Antonini, J.M. (2003) Health effects of welding. *Critical Rev. in Toxicology*, 33(**1**), 61–103.
12. Antonini, J.M., Roberts, J.R., Stone, S. et al. (2011) Persistence of deposited metals in the lungs after stainless steel and mild steel welding fume inhalation in rats. *Arch. Toxicol*., 85(**5**), 487–498.
13. Antonini, J.M., Badding, M.A., Meighan, T.G. et al. (2014) Evaluation of the pulmonary toxicity of a fume generated from a nickel-, copper-based electrode to be used as a substitute in stainless steel welding. *Environ. Health Insights*, 15(**8**), 11–20.
14. Pokhodnya, I.K., Suprun, S.A., Onoprienko, E.N. (1983) Occupational hygiene. *Respubl. Mezhved. Sbornik Zdorovie*, Issue 19, 37–43.
15. Antonini, J.M., Lawryk, N.J., Krishna Murthy, G.G. et al. (1999) Effect of welding fume solubility on lung macrophage viability and function in vitro. *J. Toxicol. Environ. Health*, **58**, 343–363.
16. Maxild, J., Andersen, M., Kiel, P. et al. (1978) Mutagenicity of fume particles from metal arc welding on stainless steel in the salmonella/microsome test. *Mutat. Res*., **56**, 235–243.
17. Baker, R.S.U., Arlauskas, A., Tandon, R.K. et al. (1986) Toxic and genotoxic action of electric arc welding fumes on cultured mammalian cells. *J. Appl. Toxicol*., **6**, 357–362.
18. Biggart, N.W., Rinehart, R.R., Verfaille, J. (1987) Evidence for the presence of mutagenic compounds other than chromium in particles from mild steel welding. *Mutat. Res*., **180**, 55–65.
19. Elias, Z., Poirot, O., Baruthio, F. et al. (1991) Role of solubilized chromium in the induction of morphological transformation of Syrian hamster embryo (SHE) cells by particulate chromium (VI) compounds. *Carcinogenesis*, **12**, 1811–1816.
20. Hansen, K., Stern, R.M., Fletcher, A. et al. (1985) Nickel and chromium compounds and welding fumes in mammalian cell transformation bioassay in vitro. In: *Biological effects and health hazards of welding fumes and gases*, 305–310. Amsterdam: Elsevier Press.
21. Badding, M.A., Fix, N.R., Antonini, J.M. et al. (2014) A comparison of cytotoxicity and oxidative stress from welding fumes generated with a new nickel-, copper-based consumable versus mild and stainless steel-based welding in RAW 264.7 mouse macrophages. *PLOS ONE*, 9(**6**), 11–20.

Received 10.03.2016

COMPANY «FRONIUS UKRAINE» IS 25 YEARS IN UKRAINE

In June, 2016 Company «Fronius Ukraine» celebrated its 25-year anniversary. In 1991 the joint Ukrainian-Austrian enterprise «Fronius–Fakel», a subsidiary of the global famous Austrian company «Fronius International GmbH», was founded. «Fronius–Fakel» (A.I. Komisar, Director General) produced welding equipment according to the Austrian technology. Mobility, reliability, appropriate design, excellent welding characteristics allowed widely applying the «Fronius» equipment in many branches of industry, agricultural production and consumer services.

Meeting of Mr. G. Fronius with Prof. B.E. Paton on the eve of opening of the Joint Venture «Fronius–Fakel» in Ukraine

«Fronius International» was founded in 1945 by the Austrian Günter Fronius in Pettenbach (Austria) and is one among the world leaders and the developer of welding technologies (more information about «Fronius International» can be found on the site: www.fronius.ua). The Ukrainian subsidiaries «Fronius International» — «Fronius–Fakel» and its successor «Fronius Ukraine», officially registered in 2005, followed the similar strategies in the development of innovative welding technologies.

Today «Fronius International» has three divisions (Perfect Welding, Perfect Charging, Solar Energy), which specialize in welding equipment, systems for battery charging and solar electronics.

The Perfect Welding division is developing the innovative welding technologies and brings them to readiness for implementation into production. They include systems for electric arc and resistance spot welding together with the corresponding proposal of services. More than 40,570 high-tech welding systems for manual, automatic and robotic use were introduced and successfully applied at many large and small enterprises in Ukraine. The nuclear power engineering, aviation, automobile industry, shipbuilding, railroad cars building, agricultural machinery, construction, production of metal structures, production of robots are the main branches of industry on which «Fronius» is focused.

Solemn ceremony of opening of the Joint Venture «Fronius–Fakel» (1991)

The problem of robotization, which is very relevant for the Ukrainian economy, occupies a special place. Here «Fronius Ukraine» offers unique solutions on the basis of the well-known systems TPS (TransPulsSynergic) and TPS/i (TransProcessSolution) for im-

«Fronius Ukraine» division in Knyazhichi (Kiev region)

provement of quality and efficiency. Namely, due to such properties and the presence of guaranteed and highly-professional technical and service support, the overwhelming majority of robotic systems in Ukraine are equipped with «Fronius» welding systems.

«Fronius Ukraine» always keeps pace with the times and provides users with a wide range of services, training and seminars, packages of technical service, commissioning, retrofitting of the system, rent, calibration, welding tests, demonstration systems, repair services and many other. «Fronius» pays a considerable attention to the maintenance and service. The department of the national and technical support provides a comprehensive operational consultation support of the users of the «Fronius» equipment due to the presence of highly-qualified personnel, among which five international welding engineers (IWE), experts in different processes and directions. In the «Fronius Ukraine» Technological Center, the total area of which is 800 m^2, there is a showroom with a full line of «Fronius» products (more than 30 demonstration systems), special rooms for presentations, a large park of rental equipment, testing stands for diagnostics, calibration and service maintenance for high-frequency welding systems, completed stands for training the practical skills of welding and the laboratory for automated welding. Almost every year at the national Product Launch the «Fronius Ukraine» announces 5–10 new developments in the field of MIG, TIG, MMA welding and new welding technologies and processes such as PMC, LSC, PMC MIX, CMT Twin and other.

During the last 25 years the motto «Customer is on focus» of «Fronius Ukraine» has not changed and we are confidently pacing into the century of digital revolution. Every week we announce the latest solutions in the field of welding in the social networks (www.facebook.com/FroniusUkraine). Due to our teams on sales and service (there are three of them in the part of the company, locating in the village Knyazhichi, in the cities Stryj and Dnepr), we are always ready to help a customer to solve his problems.

Technological Centre of «Fronius Ukraine»

Company «Fronius Ukraine» expresses its gratitude to all those who have chosen and successfully apply the «Fronius» equipment. We hope and are almost sure that the Ukrainian economy, having armed with innovative technologies and equipment, will become one of the most advanced and competitive in the world.

We congratulate the specialists and partners with the 25-year anniversary! We wish them further successes, expansion of partner contacts, useful cooperation, new achievements and prosperity.

E.O. Paton Electric Welding Institute,
Editorial Board of «The Paton Welding Journal»